Bianca Höller, BSc

Experimental Determination of Thermodynamic Parameters for the Characterisation of Phase-Change-Materials

MASTER'S THESIS

to achieve the university degree of

Diplom-Ingenieurin

Master's degree programme: Chemical and Process Engineering

submitted to

Graz University of Technology

Supervisor

Ao.Univ.-Prof. Dipl.-Ing. Dr.techn. Raimund Almbauer

Institut für Verbrennungskraftmaschinen und Thermodynamik

Second supervisor
Dipl.-Ing. Dr.techn. Martin Heimel

Graz, June 2016

Vorwort

Die vorliegende Masterarbeit ist im Rahmen des Abschlusses meines Studiums Verfahrenstechnik an der Technischen Universität Graz entstanden. Im Zeitraum September 2015 bis April 2016 habe ich mich der Datenaufbereitung und dem Verfassen dieser Arbeit gewidmet.

Ich habe meine Arbeit am Institut für Verbrennungskraftmaschinen und Thermodynamik verfasst. An dieser Stelle möchte ich mich beim Institutsvorstand Herrn Univ.-Prof. Dipl.-Ing. Dr. techn. Helmut Eichlseder für diese Möglichkeit bedanken.

Ein besonderer Dank gilt meinem betreuenden Professor Ao. Univ.-Prof. Dipl.-Ing. Dr. techn. Raimund Almbauer für seine fachliche Unterstützung und instruktiven Inputs während meiner Arbeit.

Ich möchte diese Gelegenheit auch nutzen, um mich bei meinem Zweitbetreuer Dipl.-Ing. Dr. techn. Martin Heimel für seine ausgiebige Unterstützung zu bedanken. Vielen Dank für Zeit und Mühen, die du in meine Arbeit investiert hast. Du hast meine Fragen immer geduldig und ausführlich beantwortet.

Mein Dank gilt auch Mario Hainschitz und der Firma Research Center Pharmaceutical Engieering (RCE) für die Möglichkeit der Differential Scanning Calorimetry Messungen.

Ein herzlicher Dank gilt meinem Freund Martin Landfahrer. Dein guter Rat und lieben Worte haben mir immer geholfen. Außerdem möchte ich mich bei meinem Vater und meiner Oma bedanken, die mich während des Studiums so herzlich unterstützt haben.

Eidesstattliche Erklärung

Ich erkläre an Eides statt, dass ich die vorliegende Arbeit selbstständig verfasst, andere als die angegebenen Quellen/Hilfsmittel nicht benutzt und die den benutzten Quellen wörtlich und inhaltlich entnommene Stellen als solche kenntlich gemacht habe

Statutory Declaration

I declare that I have authored this thesis independently, that I have not used other than the declared sources / resources and that I have explicitly marked all material which has been quoted either literally or by content from the used sources.

…… ……..

date (signature)

Kurzfassung

Das Ziel dieser Masterarbeit war es, ein bestehendes Phase-Change Material (PCM), beziehungsweise eine Mischung dieses Materials mit anderen Medien hinsichtlich Wärmeleitfähigkeit, spezifische Wärmekapazität und latenter Wärmemenge experimentell zu untersuchen. Außerdem wurde die Phasenwechseltemperatur bestimmt. Das pulverförmige, mikroverkapselte PCM wurde zum einen mit Wärmeleitpaste und zum anderen mit Motoröl SAE 0W-30 gemischt.

Die Versuchsanordnung bestand aus einer Stahlhohlkugel, in deren Mitte eine kleinere Kugel angebracht wurde, welche als Wärmequelle diente. In bestimmten Abständen wurden Thermoelemente angebracht um ein Temperaturprofil zu messen. Um die notwendigen Parameter bestimmen zu können, wurde dementsprechend ein Modell in MATLAB programmiert. Dieses bestimmt die gesuchten Parameter durch Kurvenanpassung an die Messdaten. Die erhaltenen Daten werden abschließend in eine Kühlkreislaufsimulation eingebracht.

Abstract

The aim of this master thesis was the experimental examination of a phase-change material (PCM) mixed with other media in terms of thermal conductivity, specific heat capacity and specific latent heat. In addition, the phase change temperature was determined. The powdery, microencapsulated PCM was mixed on the one hand with heat conducting paste and on the other hand with engine oil SAE 0W-30.

The experimental setup consisted of a hollow steel sphere and a smaller one in the middle, which served as a heat source. At certain intervals, thermocouples are attached to measure a temperature profile. In order to determine the necessary parameters, a model in MATLAB was created. Thereby the parameters are defined by curve fitting to the measured data. The obtained data are finally incorporated into a refrigeration circuit simulation.

Contents

1 Introduction 1
2 Theoretical Background 3
2.1 Latent Heat 3
2.2 Phase-Change Materials 3
2.2.1 Solid-Liquid Phase-Change 4
2.2.2 Encapsulated Paraffin 4
2.3 Enhancement of Energy Efficiency of Refrigerating Systems 5
2.4 Experiment Design 7
2.4.1 Spherical Model 7
2.4.1.1 Theoretical Fundamentals of Spherical Model 7
2.4.1.2 Evaluation of the Measured Data 14
2.4.2 Differential Scanning Calorimetry (DSC) 15
2.4.2.1 Derivation of Mathematical Treatment 16
2.4.2.2 Measurement and Evaluation Procedure 18
2.4.2.3 Heat Capacity Measurement 18
2.4.2.4 Temperature-Modulated Differential Scanning Calorimetry 19
2.5 Plausibility Check of the Calculation Model and Parameter Variation 19
2.5.1 Sphere Cooled down without Interior Heat Source 19
2.5.2 Sphere Heated from the Inside at Ambient Temperature of -30 [°C] 31
2.5.3 Parameter Adjustment 47
3 Experimental Studies 49
3.1 Calibration of the Thermocouples 49
3.2 Density Measurements 51
3.3 Differential Scanning Calorimetry (DSC) – Measurements 52
3.4 Sphere Measurement Setup– Measurements 52
3.4.1 Heat Conducting Paste as Mixing Component 52
3.4.2 Engine Oil as Mixing Component 55
3.4.3 Engine Oil and Aluminium Powder as Mixing Component 56
4 Results and Discussion 58
4.1 Density-Measurement 58
4.2 Temperature-Modulated Differential Scanning Calorimetry 59
4.3 Evaluation of the Experimental Data 62
4.3.1 Heat Conducting Paste as Mixing Component 62
4.3.1.1 0 [wt%] Phase-Change Material and 100 [wt%] Heat Conducting Paste 62
4.3.1.2 10 [wt%] Phase-Change Material and 90 [wt%] Heat Conducting Paste 66
4.3.2 Oil as Mixing Component 70

4.3.2.1 55 [wt%] Phase-Change Material and 45 [wt%] Oil 70
4.3.2.2 44 [wt%] Phase-Change Material, 36 [wt%] Oil and 20 [wt%] Aluminium Powder 75
4.4 Summary of the Results and Discussion 79
4.4.1 Specific Heat Capacity 79
4.4.2 Thermal Conductivity 80
4.4.3 Phase Change Temperature Range, Subcooling and Hysteresis 80
4.4.4 Melting Enthalpy 82
4.4.5 Heat Transfer Coefficient 83
4.5 Measurement Uncertainties 84
4.5.1 Density Measurements 84
4.5.2 Temperature in the Sphere and Ambient Temperature 85
4.5.3 Distance of the Measurement Points 87
4.5.4 Heating Power 88
4.5.5 Diameter of the Sphere 88
4.5.6 Heat Transfer Coefficient 89
4.6 Optimization of the Measurement Procedure 89
4.7 Effects on Refrigeration Circuit 90
5 Conclusion 93
6 References 94
7 Appendix 95
7.1 List of Equipment 95
7.2 Differential Scanning Calorimetry Heat Capacity Measurement Results 96
7.3 List of Figures 98
7.4 List of Tables 101

List of Abbreviations

Latin Abbreviations

A	m²	cross sectional area
C	J/K	heat capacity
c	J/(kg·K)	specific heat capacity (in some references it is indicated as *cp*)
D	m	diameter
E_a	J	external energy
h_{melt}	J/kg	specific melting enthalpy
L	m	length, thickness
m	kg	mass
P_{el}	W	electrical power
$\dot{q}$	W/m^2	heat flux
q_{rev}	J/kg	reversible heat
Q	J	heat
$\dot{Q}$	W	heat flow
r	m	radius
R	K/W	therminal resistance
t	s	time
T	K	thermodynamic temperature
U	J	internal energy
W	J	work

Greek Abbreviations

α	W/(m²·K)	heat transfer coefficient
β	1/K	volume expansion coefficient (isobaric)
κ	m^2/s	thermal diffusivity
λ	W/(m·K)	thermal conductivity
ν	m^2/s	kinematic viscosity
ρ	kg/m³	density

Indices

l	liquid
s	solid
I, II	melting temperature range

1 Introduction

In the course of this master thesis, a phase-change material was examined in terms of thermal conductivity, specific heat capacity, specific latent heat and phase change temperature. The phase-change material is a microencapsulated paraffin blend and is intended for the use in refrigerating systems to increase the time averaged evaporating temperature. Thereby, the energy consumption may be reduced.

The necessary parameters are determined by means of curve fitting to measured data. Therefore, a model of sphere, where one-dimensional, transient heat conduction in radial direction is considered, is created in the programming environment MATLAB. The model consists of a hollow steel sphere and a smaller one in the middle, which serves as a heat source. The sphere is filled with the examined material and is divided in several layers. First, the model provides information about the measurement setup. For that, the parameters are assessed from the literature. Thereafter, the test rig is built. Then the measurement results are read into MATLAB and the parameters are determined due to adjustment of the theoretical curve to the measuring data.

The thesis is divided in three sections, the theoretical background, the experimental studies and the results and discussion. The theoretical background deals with the description of phase-change materials and their impact on cooling circuits. It also includes the theoretical fundamentals of the sphere model created in MATLAB and its plausibility check, which demonstrates the best procedure to adjust the parameters to the measured data. Moreover, a part of the investigated mixtures is also examined with a differential scanning calorimetry (DSC). The theory of this measurement procedure is described in this chapter as well.

The chapter “experimental studies” deals with the calibration of the thermocouples and the description of the density measurement. Furthermore, the measurements with the differential scanning calorimeter, which are carried out by the company RCE, are briefly described. The main part of this chapter is the description of the measurement process using the developed spherical test rig. First, the phase-change material is mixed with heat conducting paste and filled in the steel sphere with an outer diameter of 150 [mm]. Then the phase-change material is mixed with engine oil. For this a larger sphere is used, having an outer diameter of 200 [mm]. Afterwards, aluminium powder is added to the mixture with oil and a further measurement is started.

The chapter “results and discussion” includes the results of the density measurements and the measured curve by the temperature-modulated differential scanning calorimeter. Moreover, the results of the parameter adjustment are demonstrated in this chapter. A further part of this chapter is the determination and the impact of the measurement uncertainties. Thereby, the maximal errors of the constraints like density, position of the thermocouples or temperature

are found out. The values of the measurement uncertainties are introduced into the curve fitting to find out its influence on the investigated parameters.
In addition, the resulted values of thermal conductivity, specific heat capacity and melting enthalpy are introduced into an available refrigeration circuit simulation, where the impact on the energy consumption of the simulated freezer is observed.

2 Theoretical Background

The increasing demand of energy is becoming a grand challenge for the engineering community. The thermal energy storage is an important option to fulfil the rising request. Latent heat and sensible heat are two possible forms for thermal energy storage. Sensible heat storage is based on the change of temperature in a material during the process of storing and releasing heat. The amount of heat that can be stored depends on the specific heat capacity, the change in temperature and the mass of the medium [1].

Besides the thermal energy storage there are other energy storage methods like mechanical energy, thermochemical and electrical storage that can be stored through batteries for instance. The first one includes gravitational energy storage or compressed air energy storage. Thermochemical energy storage is based on a reversible chemical reaction in which energy is absorbed and released in breaking and reforming molecular connection [2].

This thesis deals with latent heat storage, also called phase-change storage, therefore the other kinds of storage will not be examined in more detail.

2.1 Latent Heat

As already mentioned, thermal energy can be stored in the form of latent heat. Thereby energy is stored during phase change under almost unchanged temperature. Latent heat storage is a very efficient method for storing energy because of a high storage density and it offers a nearly isotherm mode of operation between charging and discharging [1].

This form of thermal energy storage depends on the storage materials called phase-change materials. Thereby the material undergoes a solid to solid, solid to liquid, liquid to gas or solid to gas phase change or the reserve during the energy transfer process [1].

2.2 Phase-Change Materials

Phase-change materials absorb energy during the heating process, whereby a phase change takes place. During a cooling process the energy is released and the phase changes to the previous one. Phase-change materials absorb a high amount of heat during the melting process [3]. With regard to the mode of phase transition, solid-gas and liquid-gas phase transition effect a large volume change. For this reason, phase-change materials, which show a solid-solid or solid-liquid transformation, are more suitable for thermal energy storage systems. However, the heat of transition is lower than that of solid-gas and liquid-gas phase-change materials. Materials with a solid-solid phase transition, which change from one crystalline form to another, offer a smaller heat of transition than the liquid-solid phase-change materials [1].

2.2.1 Solid-Liquid Phase-Change

Solid-liquid phase change materials can store a relative high amount of heat. If the pressure is not changed substantially because of the volume change, which is usually less than 10 [%], the heat storage as latent heat occurs at a constant temperature [4].

The suitability of the phase-change material for a specific application depends on the desired temperature level and gradient. The melting and solidification temperature of the material must be between the absorbing and releasing temperature [5]. Depending on its phase change temperature, materials are used for maintaining low temperatures in air conditioning, for solar heating and for refrigeration for example [6].

Phase-change materials for solid-liquid phase transition can be classified in two categories, inorganic, including hydrated salts and organic, which includes paraffins or fatty acids. Depending on the several requirements, a suitable material has to be chosen for a good performance. As mentioned above the phase-change temperature plays an important role in the selection. Furthermore the energy stored per volume is significant. The behaviour of the material must not be changed after several thermal cycles; therefore a high stability is an important parameter. Another essential parameter is the thermal conductivity with regard to the heat transfer or charging and discharging power [5].

2.2.2 Encapsulated Paraffin

The phase-change material, which is examined in the course of this work, is a microencapsulated paraffin blend. Mixed with heat-conducting paste, it is intended for the use in refrigerating systems.

Paraffins are saturated hydrocarbons with the general formula C_nH_{2n+2}. They are often used as solid-liquid phase-change materials because of their beneficial properties like a high heat storage capacity over a small temperature range, non-toxic and environmentally compatible [1]. A mixture of paraffins is usually used because pure alkanes are very expensive. Moreover, it is possible to get phase-change materials with different melting temperatures because of mixing alkanes with various chain lengths [4]. Hence, paraffins can be used for several applications because of the variety of the phase-change temperature. Some paraffin organics are suitable for cold storage applications because of their low melting temperature [7].

Furthermore paraffin waxes show little or no supercooling during crystallisation and usually non-corrosiveness. They are chemically inert, stable and demonstrate no phase segregation after repeatedly freeze-melt cycles. The melting enthalpy does not degrade consequently [2].

Paraffins have a low thermal conductivity, which reduces the heat transfer during the charging and discharging process. In many cases, solid-liquid phase-change materials are encapsulated to increase the heat-transfer area. Further reasons of the encapsulation are to hold the liquid phase and to obviate contact of the phase-change material with the environment. The integration into other materials is still possible [4]. The capsule stays solid regardless the phase-change material is liquid or solid.

Encapsulations can be classified into macro- and micro-encapsulations. Macro-encapsulation is primary done to prevent leakage. Thereby the phase-change materials are filled into containers with a size range between some millilitres and some litres. In the course of a micro-encapsulation, solid or liquid particles with a size between 1 [µm] and 1000 [µm] are encapsulated with a solid shell, which has to be compatible with the phase-change material [4].

There are various methods of micro-encapsulation like spray drying, fluid bed coating, coacervation or interfacial polymerisation. Spray drying is a mechanical method, whereby the core material is dispersed into a concentrated solution of wall material. The resulted emulsion is atomized and dried with a heated gas. The yielded dried capsules are collected at the bottom of the drying chamber. Solid particles can be encapsulated with the fluid bed coating. Thereby the core material is fluidized by air from the bottom. The particles are covered with the liquid wall material by means of a nozzle. Then the cover of the particles is solidified by cooling or solvent vaporization. The operation is repeated until the desired thickness of the wall is reached [8].

Complex coacervation is a chemical technique to encapsulate a core material. Thereby the core material is dispersed into an aqueous gelatine solution. Then gum Arabic is added and a liquid complex coacervate is formed by adjusting the concentration and pH. The process is ended by hardening and separating the microcapsules [4]. Interfacial polymerisation is a further chemical technique whereby the wall is formed by polymerisation of monomers at the surface of core material. A solution of monomer and core material is dispersed in an aqueous phase. Then a reactant is added and a polymerization takes place at the surface of the core droplets or particles and forms the capsule wall [8].

The encapsulated paraffin blend [MPCM-10D] used for the examination is produced by the company “microtek laboratories”. The capsule wall consists of an inert and very stable polymer. The mean particle size is between 17 µm and 20 µm. The content of the phase change material in capsule amounts 85 - 90 [wt%] [8].

2.3 Enhancement of Energy Efficiency of Refrigerating Systems

The energy efficiency for a refrigeration process is determined by the difference of condensation and evaporation temperature. Through the use of phase-change materials this temperature-difference can be decreased and thereby the energy consumption may be reduced. A study of the University of Paderborn shows, that the addition of phase-change materials located on the evaporator results in reduction of energy consumption of 12 [%] [9]. Figure 1 shows the refrigerant cycle by means of a T,s-diagram [10].

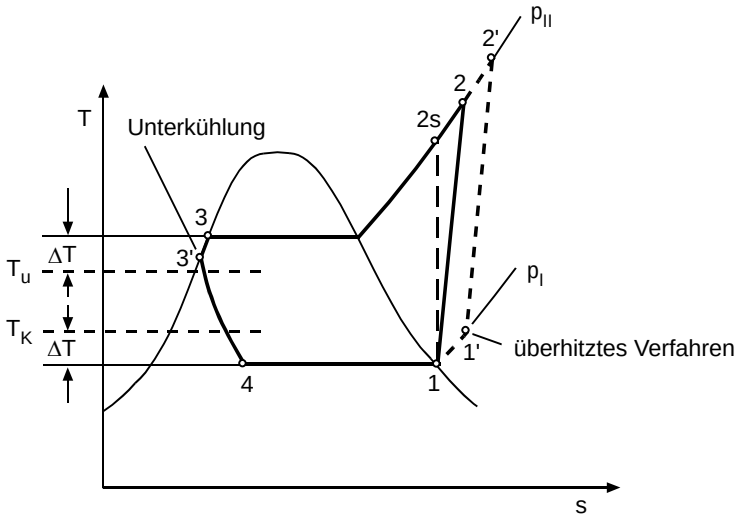

Figure 1 T,s-digram of a simplified refrigerant cycle. T_u = ambient temperature, T_K = temperature of cold store; Unterkühlung = subcooling, überhitztes Verfahren = superheated process

The change of state 1 – 2s constitutes the isentropic compression. The compressor does not work frictionless by which the amount of heat to be dissipated increases. For operational reasons the condition of output of the evaporator is ideally superheated (1' – 2'). The heat transfer performed by the condenser is represented by the change of state 2 – 3. The refrigerant is cooled as close as possible to the ambient temperature. The condition of the input at the adiabatic throttle is sub cooled. The amount of heat, which is absorbed by the evaporator (4 -1') is the cooling capacity of the system.

Conventional household refrigerators use a compressor in on/off mode. Due to this cyclic operation and the use of phase-change material the evaporation temperature may be increased and the condensation temperature may be decreased which result in a lower work input. Thus the energy consumption can be reduced.

During the on-mode, phase-change material, which encases the condenser tube, stores one part of the condensation heat. The other part of the heat is released to ambient. During off-time, the stored heat still can be released to the environment. The ongoing heat transfer results in a reduction of the heat transfer during the on-mode. Thus the condensation temperature and pressure can be lower [11].

The encapsulated paraffin blend which is estimated in the course of this work, is intended to be located on the evaporator coil and should increase consequently the evaporation temperature. During the off-mode, the phase-change material stores the heat from the cabinet, until the melting process is completed. During the on mode the stored heat energy of the phase-change material is transferred to the refrigerant [12].

Due to the enhancement of the heat transfer because of the phase-change material, the evaporation temperature and, coupled with this, the pressure in the evaporation increase. This results in a decrease of energy consumption.

Furthermore, the addition of phase-change materials has an impact on the working time of the refrigerating systems. Studies from Azzouz et al. conducted in 2007 show that the on-cycle of

the refrigerator with phase-change material is three times longer and the off-cycle is seven times longer than of the refrigerator without one. This effect can additionally lead to further increase in the efficiency of the system.

The knowledge of the most important parameters of the phase-change material is relevant to investigate its use in refrigerator systems. The phase-change temperature range and the energy stored per volume are essential for suitable application of the material. Specific heat capacity is also determined in the course of this work and specifies the heat amount which is necessary to raise the temperature of a kilogram by one Kelvin. It is usually denoted as c [J/kg·K].

Another fundamental parameter is the thermal conductivity, which is very low of paraffin [1]. Thermal conductivity characterises the capability of a substance to transport heat energy by conduction, which means energy transport by a temperature gradient. Thermal conductivity is in general a function of temperature and is measured in Watts per meter Kelvin. It is denoted as λ. Generally the thermal conductivity of the solid phase is higher than of the liquid one [13]. Thermal conductivity is an essential parameter for a good performance. By means of a heat-conducting paste, the phase-change material will be fixed on the evaporator coil. Furthermore, the heat-conducting paste may slightly increase the thermal conductivity of the paraffin blend and may prevent airspaces which are a perfect insulation. The thermal conductivity has to be high enough to ensure a sufficient charging and discharging power. In the course of this work, these parameters are investigated.

2.4 Experiment Design

2.4.1 Spherical Model

For the determination of the parameters thermal conductivity, specific heat capacity, specific melting enthalpy and melting temperature range a model of a sphere is programmed. One-dimensional, transient heat conduction in radial direction is considered. The advantage of a model in the form of a sphere is the assumption of heat conduction in one direction without deflections.

2.4.1.1 Theoretical Fundamentals of Spherical Model

First, the spherical model is created in MATLAB. A sphere made out of steel is filled with a mixture of phase-change material and a mixing component. The sphere is cooled from the outside and can be heated from the inside by a small steel sphere at the same time until a constant temperature profile is reached. Thermocouples are placed at defined positions to measure the temperature.

The model divides the content into several layers. The equation for the heat flux $\dot{q}$ [W/m^2] according to the law of Fourier is given by equation 1 [13]:

$$\dot{q} = -\lambda \frac{dT}{dr} \quad \text{(Eq. 1)}$$

The heat flux is proportional to the temperature gradient and to the thermal conductivity of the material. The cross-sectional area depends on the radius. Thus the heat flux is not constant because of the area variation in direction of the heat flow [13].

The surface of the sphere is inserted as cross-section area [14]:

$$\dot{Q} = A * \dot{q} = -\lambda * 4 * \pi * r^2 * \frac{dT}{dr} \quad \text{(Eq. 2)}$$

The heat flow is constant for given surface temperature, geometry and material properties [14]:

$$\dot{Q} = \lambda * 4 * \pi * \frac{(T_{layerI} - T_{layerII})}{\left(\frac{1}{r_{layerI}} - \frac{1}{r_{layerII}}\right)} \quad \text{(Eq. 3)}$$

Figure 2 shows a sketch of the described model. The blue dots represent the thermocouples. The grey outside and inner circles constitute the steel spheres.

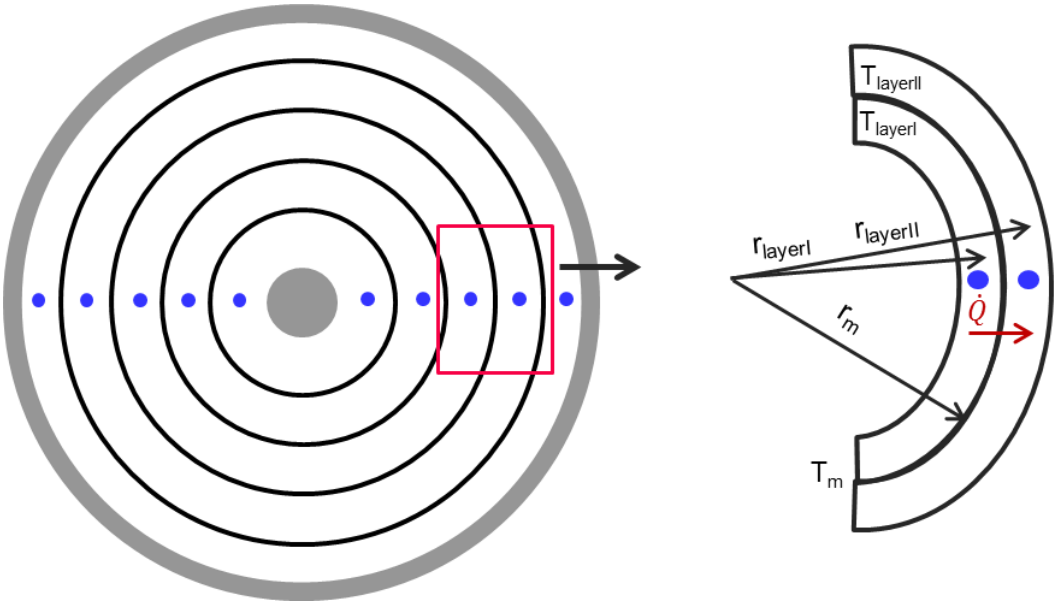

Figure 2 Sketch of the spherical model

The temperatures T_{layerI} and $T_{layerII}$ [K] constitute the temperatures of the particular phase-change material layer respectively. r_{layerI} and $r_{layerII}$ [m] constitute the averaged radius of the phase-change layers.

The temperatures of the separate layers vary, because of the different distance from the internal heat source respectively from the external surface. Therefore, the melting temperature may be reached and phase change occurs in one layer, while it is not the case in the adjacent layer. For this reason, the thermal conductivity λ [W/m^2·K] and the specific heat capacity c [J/kg·K] of the adjacent layers can be different because of the occurring phase change. For this purpose, the determination of the heat flow between two layers must be divided at the border. However, it is assumed that the thermal conductivity and the specific heat capacity are constant in each single layer:

$$\dot{Q} = \lambda_1 * 4 * \pi * \frac{(T_{layerI} - T_m)}{\left(\frac{1}{r_{layerI}} - \frac{1}{r_m}\right)} = \lambda_2 * 4 * \pi * \frac{(T_m - T_{layerII})}{\left(\frac{1}{r_m} - \frac{1}{r_{layerII}}\right)} \qquad \text{(Eq. 4)}$$

T_m [K] and r_m [m] represent the temperature and the radius of the border of two layers.

The heat flows are splitted up into $\dot{Q}_{\text{right}}$ and $\dot{Q}_{\text{left}}$ as shown in Figure 3.

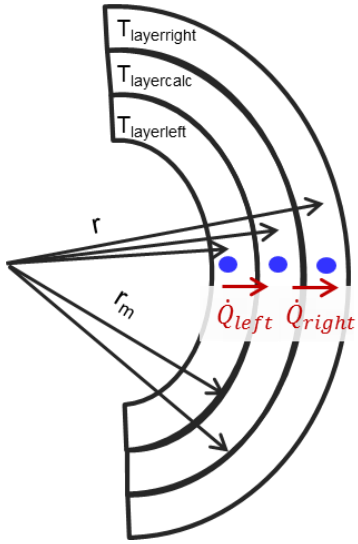

Figure 3 Sketch of the spherical model including $\dot{\boldsymbol{Q}}_{\text{right}}$ and $\dot{\boldsymbol{Q}}_{\text{left}}$

After eliminating of T_m, the heat flow of the left side can be expressed as:

$$\dot{Q}_{left} = \frac{\frac{\lambda_{left} * 4 * \pi}{\left(\frac{1}{r_{layerleft}} - \frac{1}{r_{ml}}\right)} * \frac{\lambda_{calc} * 4 * \pi}{\left(\frac{1}{r_{ml}} - \frac{1}{r_{layercalc}}\right)}}{\frac{\lambda_{left} * 4 * \pi}{\left(\frac{1}{r_{layerleft}} - \frac{1}{r_{ml}}\right)} + \frac{\lambda_{calc} * 4 * \pi}{\left(\frac{1}{r_{ml}} - \frac{1}{r_{layercalc}}\right)}} * (T_{layerleft} - T_{layercalcprev}) \qquad \text{(Eq. 5)}$$

r_{ml} [m] constitutes the radius of the border with the left layer of the calculated one. $T_{layercalcrev}$ [K] is the temperature of the calculated layer and $T_{layerleft}$ [K] is the temperature of the layer on the left side of the calculated one. $r_{layercalc}$ [m] is the averaged radius of the calculated layer and $r_{layerleft}$ [m] is the averaged radius of the left layer of the calculated one.

The heat flow of the right, $\dot{Q}_{right}$, side is given as:

$$\dot{Q}_{right} = \frac{\frac{\lambda_{calc} * 4 * \pi}{\left(\frac{1}{r_{layercalc}} - \frac{1}{r_{mr}}\right)} * \frac{\lambda_{right} * 4 * \pi}{\left(\frac{1}{r_{mr}} - \frac{1}{r_{layerright}}\right)}}{\frac{\lambda_{calc} * 4 * \pi}{\left(\frac{1}{r_{layercalc}} - \frac{1}{r_{mr}}\right)} + \frac{\lambda_{right} * 4 * \pi}{\left(\frac{1}{r_{mr}} - \frac{1}{r_{layerright}}\right)}} * (T_{layercalcprev} - T_{layerright}) \qquad \text{(Eq. 6)}$$

r_{mr} [m] constitutes the radius of the border with the right layer of the calculated one. $T_{layerright}$ [K] is the temperature of the layer on the right side of the calculated one. $r_{layerright}$ [m] is the averaged radius of the right layer of the calculated one.

The changes of the temperatures in the layers are determined from the energy balance equation [10]:

$$dQ_a + dW = dU + dE_a \qquad \text{(Eq. 7)}$$

dW [J] denotes the work and is an energy transported through a system boundary. dU [J] and dE_a [J] are the change of internal and external energy of the system. dW and dE_a are zero in this case. This results in following equation [10]:

$$dU = dQ_a \qquad \text{(Eq. 8)}$$

The specific heat capacity, denoted as c [J/kg·K], specifies the heat amount which is necessary to raise the temperature of a kilogram by one Kelvin [10]:

$$c = \frac{dq_{rev}}{dT} \qquad \text{(Eq. 9)}$$

For solid and liquid bodies, the thermal expansion is generally very small and can be neglected. The correlation $dq_{rev} = du + pdv$, with $dv <<$ results in following equation [10]:

$$c = \frac{du}{dT} \quad \text{(Eq. 10)}$$

Inserted in equation 8 results the following correlation:

$$c * m * dT = dQ_a \quad \text{(Eq. 11)}$$

or based on quasi-stationary states:

$$c * m * \frac{dT}{dt} = \frac{dQ_a}{dt} = \dot{Q}_a(t) \quad \text{(Eq. 12)}$$

$\dot{Q}_a(t)$ is time-dependent. Considering the spherical model following correlation results. The heat flows of both sides are totalled and add to the temperature $T_{layercalcrev}$ [K] of the layer to calculate the temperature of the layer after the time step:

$$\frac{c * m * (T_{layercalcnew} - T_{layercalcprev})}{\Delta t} = \dot{Q}_{left} + \dot{Q}_{right} \quad \text{(Eq. 13)}$$

or

$$T_{layercalcnew} = \frac{(\dot{Q}_{left} + \dot{Q}_{right}) * \Delta t}{m * c} + T_{layercalcprev} \quad \text{(Eq. 14)}$$

m [kg] and *c* [J/kg·K] are the mass and the specific heat capacity of the current layer. The time step of the calculation is *Δt* [s]. $T_{layercalcnew}$ [K] is the determined temperature of the layer after the time step. For the determinations, performed in the course of this work, the time step amounts 5 [s]. The duration of the experiments, carried out later, amounts about a day.

The thermal conductivity and the specific heat capacity are assumed to be constant at the solid phase and at the liquid phase, but different for both phases.

Figure 4 shows the temperature dependence of the thermal conductivity and specific heat capacity during a melting process [4]:

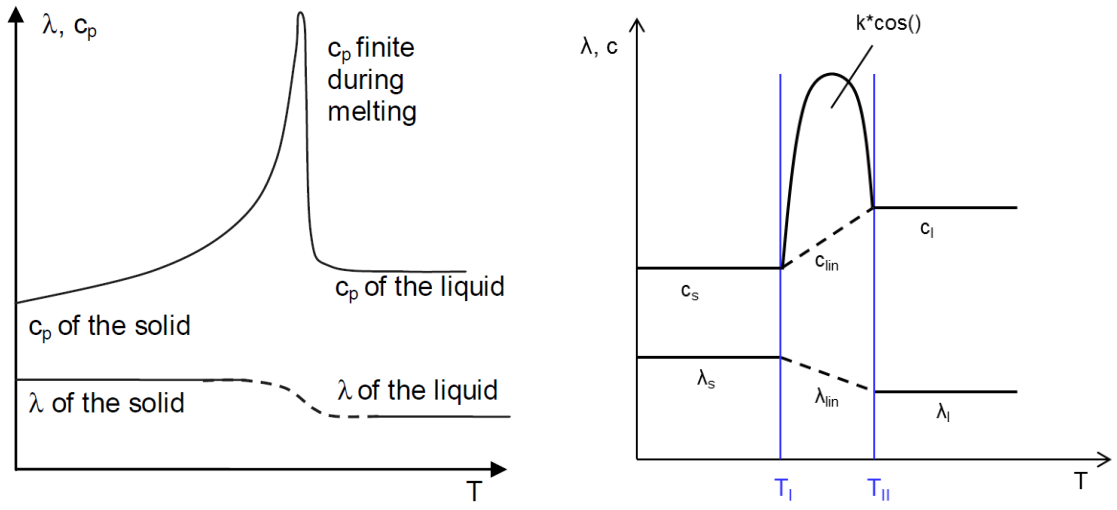

Figure 4 Relationship between thermal conductivity & specific heat capacity and temperature during a melting process [6]. Right: simplification in the model

The values of the thermal conductivity during the phase change are calculated by linear interpolation.

The specific heat capacity increases strongly during the melting process because the heat is absorbed without changes in temperature for the ideal case or only small changes in temperature for the real case. For the determination of the specific heat capacity during the phase change following available equation is used:

$$c = c_{lin} + k * \cos\left(\frac{\pi * (T - T_{mean})}{T_{diff}}\right) \quad \text{(Eq. 15)}$$

c_{lin} [J/kg·K] is the value of the specific heat capacity at the current temperature T calculated by linear interpolation. T_{mean} [K] is the average temperature and T_{diff} [K] the difference of the phase change temperature range. k is a coefficient that is computed as follows, whereby h_{melt} [J/kg] constitutes the melting enthalpy:

$$k = \frac{h_{melt} * \pi}{2 * T_{diff}} \quad \text{(Eq. 16)}$$

For the calculation of the internal layer the heat flow of the left side is replaced by the electric power input P_{el} [W] which is introduced by a smaller steel sphere including a small bulb.

The steel sphere, assumed as the outmost layer of the sphere, is surrounded by air. Therefore the heat flow on the right side is replaced by the heat flow $\dot{Q}_u$ [W] which is computed as [14]:

$$\dot{Q}_u = \propto * A * (T_u - T_{layercalcprev}) = \propto * 4 * \pi * {r_{layercalcout}}^2 * (T_u - T_{layercalcprev}) \quad \text{(Eq. 17)}$$

$r_{layercalcout}$[m] is the outer radius of the steel sphere. $\propto$ [W/m^2·K] is a proportional factor and called heat transfer coefficient. It is a function of the flow state and the physical properties of the fluid [13]. The temperature gradient in the steel sphere is negligible compared to the temperature difference between surface and ambient temperature if the Biot-number is smaller than 1. The Biot-number is defined as [13]:

$$Bi = \frac{\propto * L}{\lambda_{Sphere}} \quad \text{(Eq. 18)}$$

α [W/m^2·K] is the heat transfer coefficient, λ_{Sphere} [W/m·K] is the thermal conductivity of the sphere and L [m] constitutes the thickness of the sphere.

The heat transfer coefficient in the case of free convection is determined as follows. For the determination of the dimensionless parameters the material values at the temperature T_{Ref} [K] are used. T_{Sphere} [K] and T_∞ [K] are the temperature of the sphere surface and the temperature of the surrounding air [15]:

$$T_{Ref} = \frac{T_{Sphere} + T_\infty}{2} \quad \text{(Eq. 19)}$$

The Rayleigh number *Ra*, the Prandtl number *Pr* and the Nusselt number *Nu* are defined as [15]:

$$Ra = \frac{\beta * g * \Delta T * D^3}{v * \kappa} \quad \text{(Eq. 20)}$$

$$Pr = \frac{v}{\kappa} \quad \text{(Eq. 21)}$$

$$Nu = \frac{\propto * D}{\lambda_{Fluid}} \quad \text{(Eq. 22)}$$

β [1/K] is the isobaric expansion coefficient, g is the gravitational acceleration and amounts 9.81 [m/s^2] and ΔT is the temperature difference between the sphere surface and the

surrounding fluid. ν [m^2/s] constitutes the kinematic viscosity, κ [m^2/s] is the thermal diffusivity and λ [W/m·K] is the thermal conductivity of the surrounding fluid. *D* [m] constitutes the diameter of the sphere [15].

In the case of free convection around spheres the Nusselt number *Nu* can be described approximately as [15]:

$$Nu = 0.56 \left[\left(\frac{Pr}{0.846 + Pr}\right) Ra\right]^{\frac{1}{4}} + 2 \qquad \text{(Eq. 23)}$$

After computation of the Nusselt number, the heat transfer coefficient α can be determined with equation 22.

The model delivers information about the experimental design and the course of the experiment. Furthermore the suitable size of the external and the interior steel sphere can be chosen. The model shows the maximum temperatures that are reached in the sphere and the duration until a constant temperature profile is achieved.

The model also demonstrates the degree of the influence of the heat transfer coefficient and the thermal conductivity of the steel sphere to the reached temperatures of the mixture inside the sphere.

2.4.1.2 Evaluation of the Measured Data

The spherical model has two necessities during this work. First it provides information about the measurement setup and the heating power. For this the value of the heat transfer coefficient is determined from equation 22 and the values of thermal conductivity and specific heat capacity are assessed from the literature. Afterwards the experiments were performed, the measurement results are read in and the parameters are determined by adaption. The temperature of the thermocouples is interpolated between the theoretical layers to compare it with the measurement results. Thus the values of the thermal conductivity, the heat transfer coefficient and the specific heat capacity or melting enthalpy can be determined due to adjustment of the theoretical curve to the measurement data.

The minimizing of the absolute value is done by the MATLAB-function *fminsearch*. Thereby the values of the parameters are varied till the minimum of the function, which returns a scalar, is found. The parameters are introduced to the function as a vector. The scalar is the absolute value of the resulted temperatures. Furthermore the maximal number of iterations must be defined.

The results of the minimum search must be checked for plausibility. The optimum has to be found within a meaningful parameter range. For that reason the appropriate selection of the initial values is essential.

2.4.2 Differential Scanning Calorimetry (DSC)

The phase-change onset temperature, the energy stored per volume and the specific heat capacity are determined by differential scanning calorimetry. It is an analytical tool, where a temperature range is scanned. The calorimeters have two crucible positions. In addition to the crucible, filled with the phase-change material, an empty crucible acting as a reference is mounted. The heat stored in the phase-change material sample is determined by the difference in the signal of both samples [4].

DSC can be divided in two working principles, power compensating calorimeters and heat exchanging calorimeters. Power compensating calorimeters work with electrical heaters to compensate the temperature difference between the two samples during the temperature program [4].

The calorimeter used in the course of this thesis is a heat exchanging calorimeter. The difference in the heat exchanged between sample and ambient and reference and ambient is determined. For this, a thermal resistance, constructed as disk-type is used, where the heat flow is measured through the disc-shape support [4]. Figure 5 shows a heat exchanging calorimeter with a disc-type measuring system, where S and R constitute the sample and reference crucible [16]:

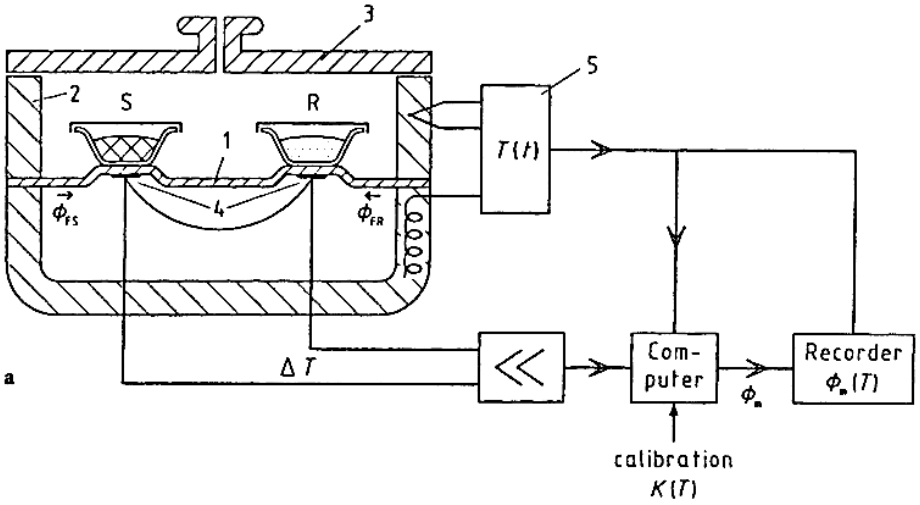

Figure 5 Heat-exchanging calorimeter. 1 disk-support, 2 oven, 3 cover, 4 thermocouples, 5 temperature controller and programming device

Temperature sensors are integrated in the disk. During heating, the heat goes through the disk to the samples. The differential temperature signal of the sample and reference sample is constant when the same heat flows into both. If a sample transition occurs, a differential signal in the form of a peak in the curve is recorded [16].

During phase transition, the temperature difference between sample and reference is not constant in time.

2.4.2.1 Derivation of Mathematical Treatment

The following equations describe the theoretical fundamentals of differential scanning calorimeters which are represented by a simple model shown in Figure 6 [16]:

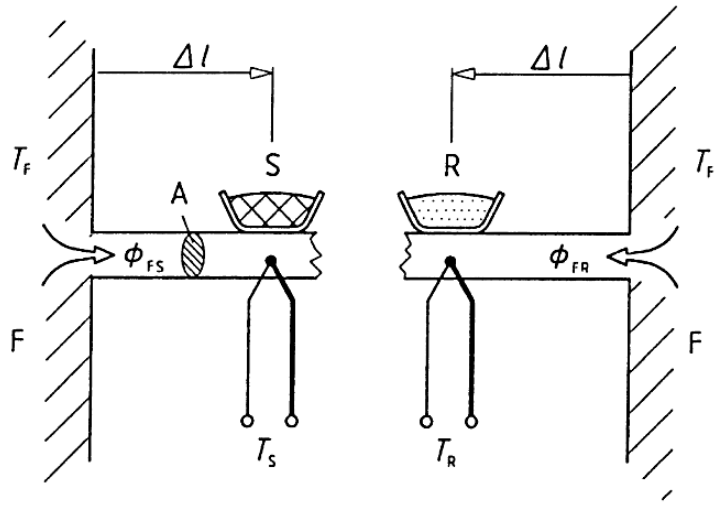

Figure 6 Simple model of the DSC to describe its functional principle

$\dot{Q}_{F-S}$ and $\dot{Q}_{F-R}$ [W] are the heat flows from the furnace to the sample and from the furnace to the reference.

The amount of the heat flow is proportional to the temperature difference, where the thermal conductivity is the proportionality factor [16]:

$$\frac{\dot{Q}_{F-S}}{A} = -\lambda \frac{(T_S - T_F)}{\Delta l} \quad \text{and} \quad \frac{\dot{Q}_{F-R}}{A} = -\lambda \frac{(T_R - T_F)}{\Delta l} \qquad \text{(Eq. 24)}$$

A [m^2], λ [$W/m \cdot K$] and Δl [m] are given by the properties of the heat conduction path and can be summarized to the global resistance *R* [K/W]. Because of the symmetry they have the same value for both sides. The value of *R* is determined by calibration.

$\dot{Q}_r$ [W] is the heat flow which occurs inside the sample. It is the energy which represents the energy absorption or release inside the sample due to phase transition. The heat capacity of the sample C_s [J/K] is determined as [16]:

$$C_S \frac{dT_S}{dt} = \dot{Q}_{F-S} - \dot{Q}_r \qquad \text{(Eq. 25)}$$

Thereby the heat is released when $\dot{Q}_r$ shows a negative value. With the measured signal $\Delta T = (T_S - T_R)$ the equation can be written as [16]:

$$C_S\left[\frac{dT_R}{dt}+\frac{d\Delta T}{dt}\right]=\dot{Q}_{F-S}-\dot{Q}_r \quad \text{(Eq. 26)}$$

The heat capacity of the reference can be determined as follows, whereby $\dot{Q}_r = 0$ applies [16]:

$$C_R\frac{dT_R}{dt}=\dot{Q}_{F-R} \quad \text{(Eq. 27)}$$

The difference of both equations results [16]:

$$\dot{Q}_{F-S}-\dot{Q}_{F-R}=(C_S-C_R)\frac{dT_R}{dt}+C_S\frac{d\Delta T}{dt}+\dot{Q}_r \quad \text{(Eq. 28)}$$

When the heat flows are replaced by equation 24 and the global resistance is inserted the following results from equation 21 [16]:

$$\dot{Q}_r=-\frac{\Delta T(t)}{R}-(C_S-C_R)\frac{dT_R}{dt}-C_S\frac{d\Delta T(t)}{dt} \quad \text{(Eq. 29)}$$

The measured signal ΔT, obtained as electric voltage, is not proportional to the heat flow released or absorbed inside the sample. The signal is not equal to zero even if $\dot{Q}_r$ is zero and steady-state conditions are assumed. It has the value $-R*\beta*(C_S-C_R)$, with $\beta=dT_R/dt$.

This value constitutes the curve before and after a peak and is parallel to the abscissa if the parameters are constant and is called baseline. In the real case they are not constant thus the baseline is not parallel to the abscissa.

For the determination of the total heat of transition Q_r [J] charged/discharged in the sample the following equation is valid, where t_1 and t_2 are the beginning and end of the peak in the curve [16]:

$$Q_r=\int_{t1}^{t2}\dot{Q}_r\,dt \quad \text{(Eq. 30)}$$

2.4.2.2 Measurement and Evaluation Procedure

According to Figure 5 the measured heat flow depending on the temperature, is the signal output of the differential scanning calorimeter and accessible to the user. The measured heat flow rate is internally in the software of the calorimeter assigned to the measured signal ΔT.

In practice, first a zero curve is defined, whereby both crucibles are empty. The line shows the thermal behaviour of the measuring system itself and effects of possible asymmetries.

The baseline is the measured curve caused by the difference of heat capacities on the sample and the reference. There are no reactions and transition in the sample. The zero line is added to the baseline. If transition occurs the baseline is interpolated to connect the measured curve before and after the peak.

A peak appears in the measured curve when a temperature difference between sample and reference takes place due to a reaction or a transition inside the sample [16].

The desired information about latent heat or phase transition range can be obtained from only a qualitative evaluation of the differential scanning calorimeter curves.

2.4.2.3 Heat Capacity Measurement

The measurement of the specific heat capacity of a sample can be determined by calibration with a *c*-standard. The measurement consists of three steps. The first one is performed with an empty reference ($C_{R,cr}$ [J/K]) and an empty sample crucible ($C_{S,cr}$). Then the *c*-standard is put into the sample crucible ($C_{S,St}$) because of asymmetries [4]:

$$\Delta T_{empty} = R * \beta\left(C_{S,cr} - C_{R,cr}\right), \quad \text{(Eq. 31)}$$

$$\Delta T_{standard} = R * \beta\left(C_{S,cr} + C_{S,st} - C_{R,cr}\right), \quad \text{(Eq. 32)}$$

$$\Delta T_{sample} = R * \beta\left(C_{S,cr} + C_{S,sa} - C_{R,cr}\right) \quad \text{(Eq. 33)}$$

R [K/W] is the terminal resistance and β [K/s] is the heating rate. Afterwards the sample is put into the sample crucible ($C_{S,sa}$) and the following summarized equation results [4]:

$$\frac{\Delta T_{sample} - \Delta T_{empty}}{\Delta T_{standard} - \Delta T_{empty}} = \frac{c_{sample} * m_{sample}}{c_{standard} * m_{standard}} \quad \text{(Eq. 34)}$$

The specific heat capacity can then be determined. In the course of this work, the heat capacity of some sample mixtures is examined with differential scanning calorimetry. The software is unsuitable for measurement within the indicated temperature range from -20 [°C] to 100 [°C]. It stopped the measurement at about -15 [°C]. The measurement results are not described in detail and are found attached to this work.

2.4.2.4 Temperature-Modulated Differential Scanning Calorimetry

The evaluation of the DSC results is difficult because of the various transformations occurring during heating. By means of the temperature-modulated differential scanning calorimetry thermodynamic and kinetic events can be distinguished.

The temperature profile is usually overlaid by a sinusoidal disturbance impact. The sample temperature is still increased but the heating rate is non-linear. The form of the DSC curve in raw data is oscillated, which is separated into two components.

This results in three curves, the total, reversing and non-reversing curve. The total curve delivers the same information as the curve from the conventional differential-scanning calorimeter. The reversing curve shows phenomena like glass transition. The non-reversing curve is determined by subtracting the reversing curve from the total curve and shows crystallization, for example [17].

2.5 Plausibility Check of the Calculation Model and Parameter Variation

Before starting with the evaluation of the measurement data a plausibility check of the model is carried out to exclude programming errors. Thereby the parameters are varied and the results are compared. Another reason for this check is to find out the best procedure to adjust the parameters to the measured data.

2.5.1 Sphere Cooled down without Interior Heat Source

For the first check the interior heat source is off and the sphere with a diameter of 0.15 [m] is cooled down to -30 [°C]. The starting temperature T_0 of the sphere is 25 [°C] and the check is performed with four theoretical layers, additionally one layer for the interior sphere and one layer for the hollow steel sphere. The table below shows the values of the parameters during the check.

ϱ [kg/m^3]	c_s [J/kg·K]	c_l [J/kg·K]	λ_s [W/ m·K]	λ_l [W/ m·K]	h_{melt} [J/kg]	α [W/ m^2·K]	T_I [°C]	T_{II} [°C]
1000	1000	1300	1	0.7	20000	5	-20	-15

Table 1 Values of the parameters during the plausibility check of the sphere cooled down without interior heat source

ϱ is the density of the content and c_s is the specific heat capacity of the solid phase and c_l of the liquid one. λ_s and λ_l constitute the thermal conductivity of the solid and the liquid phase,

h_{melt} is the melting enthalpy and α is the heat transfer coefficient. T_I and T_{II} represent the phase change temperature range.

Figure 7 shows the temperature profiles of all calculated layers.

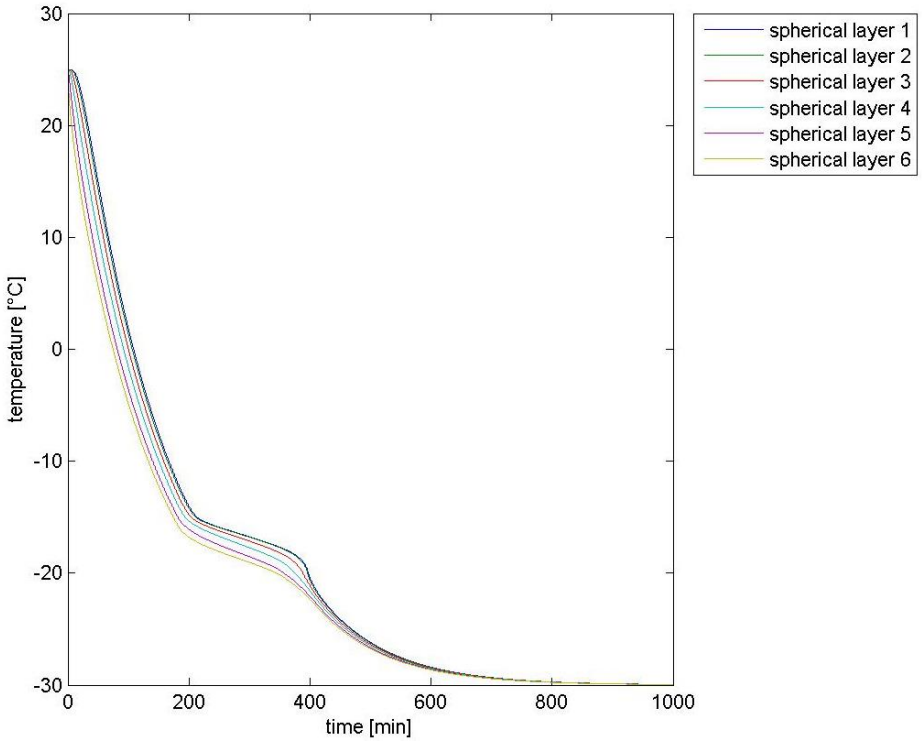

Figure 7 Transient temperatures at six positions cooled down from 25 [°C] to -30 [°C]

Spherical layer 1 and 6 represent the steel spheres of the model. Spherical layer 1 is the steel sphere inside and spherical layer 6 is the outer hollow steel sphere. Spherical layers 2 till 5 are the layers of the filled sample material containing phase-change material from the inside to the outside.

Figure 8 Temperature profile over the averaged radii of all six layers cooled down from 25 [°C] to -30 [°C]

Figure 8 shows the temperature profile over the averaged radii of the layers recorded every 100 minutes over 1000 minutes.

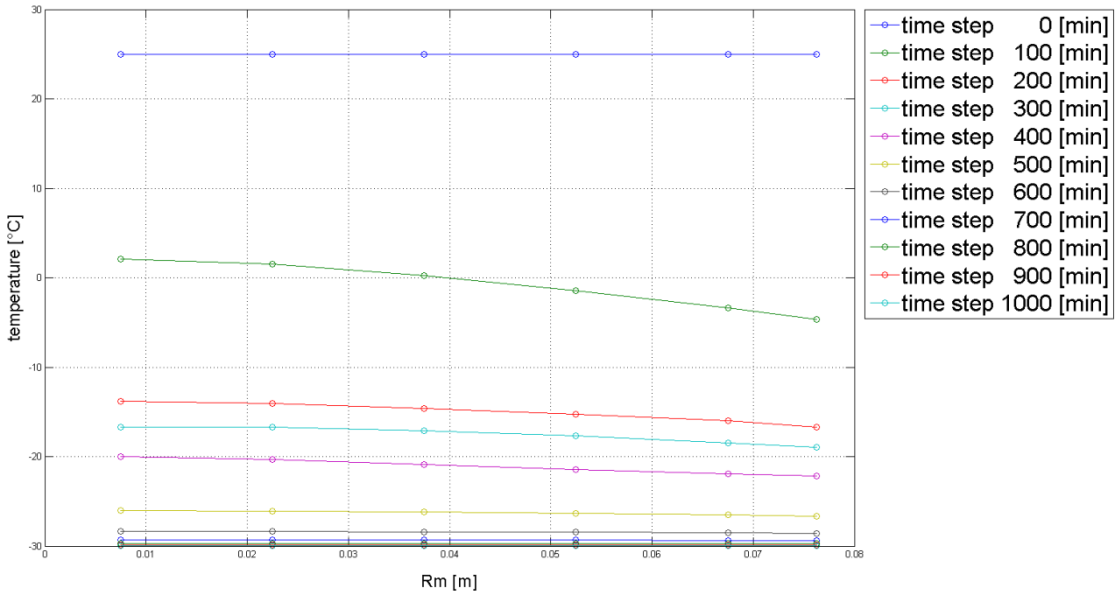

Figure 8 Temperature profile over the averaged radii of all six layers cooled down from 25 [°C] to -30 [°C]

The small circles represent the averaged radius of each layer, whereby the two outer circles on both sides mark the averaged radii of the steel spheres. The outer layers cool down first. Furthermore, a smaller radial temperature gradient between the sphere and the air leads to a decreased heat transport.

Variation of Specific Heat Capacity

Specific heat capacity c [J/kg·K] specifies the heat amount which is necessary to change the temperature of a kilogram by one Kelvin. Thus, a higher value of c leads to a lower heating or cooling rate of the object. The specific heat capacities of the solid and of the liquid phase are changed to find its influences to the temperature profile.

First, the values for c_s are varied from 900 to 2000 [J/kg·K] and for the comparison spherical layer 3 is selected. Figure 9 shows the temperature profile of the third theoretical layer of the sphere cooled down to -30 [°C].

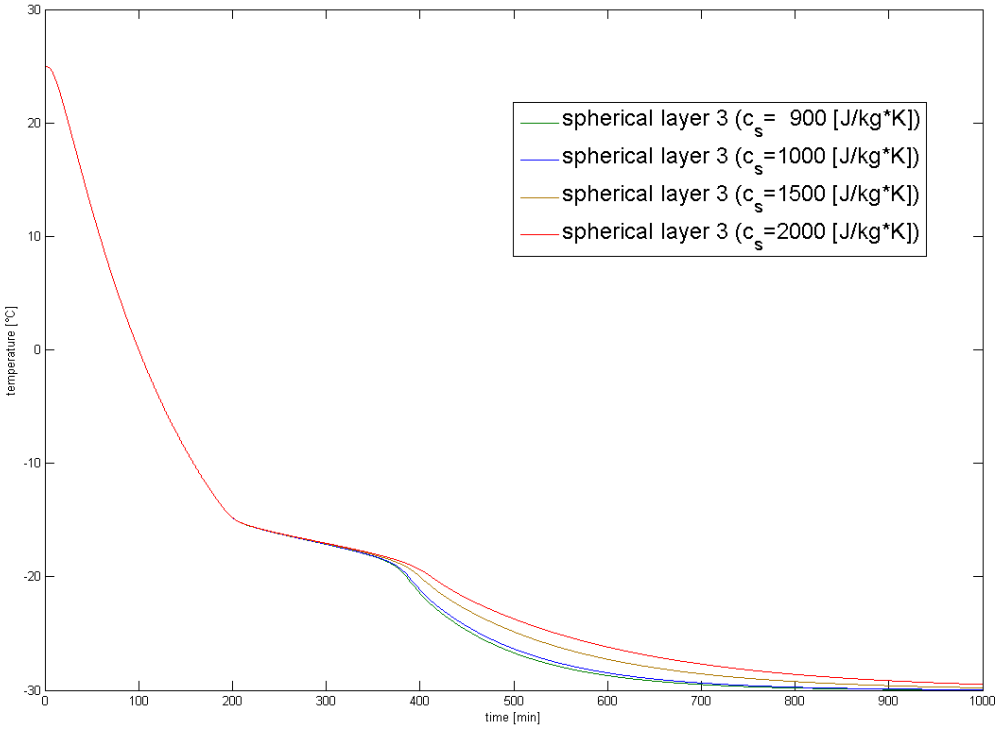

Figure 9 Transient temperatures at third position cooled down from 25 [°C] to -30 [°C] with varied specific heat capacity of the solid phase

It can be seen that the higher the values of the c_s are, the flatter is the curve. The ambient temperature of -30 [°C] is reached later with higher values of the specific heat capacity. The diagram also shows that the value of the heat capacity of the solid phase has no influence on the value of the liquid phase.

Figure 10 shows the zoom of the temperature profile within the indicated phase-change temperature range:

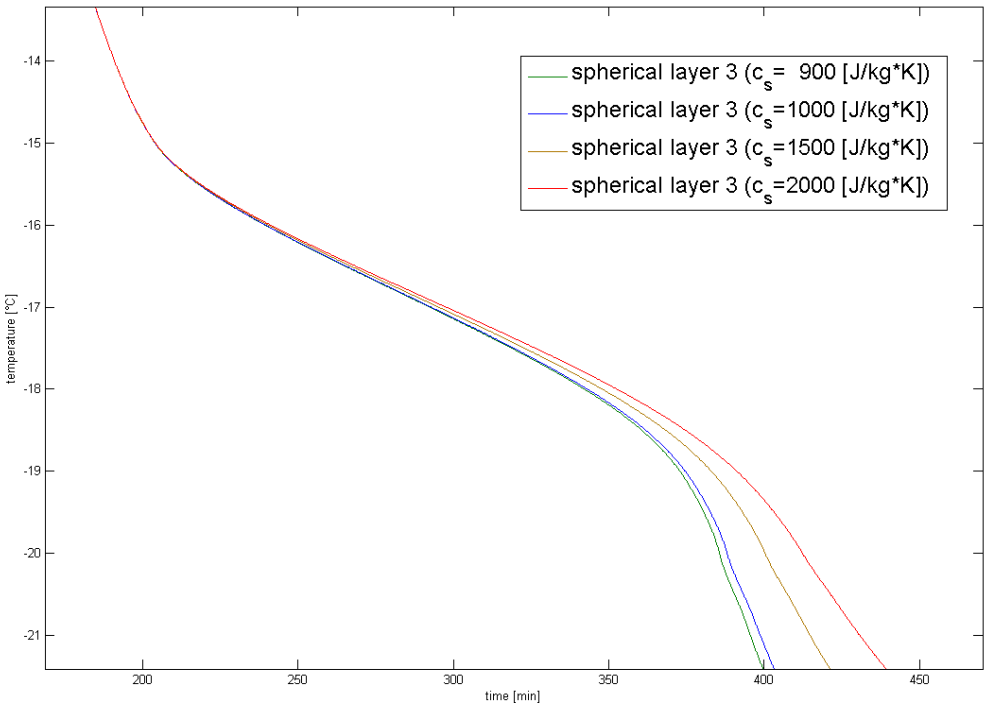

Figure 10 Zoom of the transient temperatures at third position cooled down from 25 [°C] to -30 [°C] with varied specific heat capacity for the solid phase

It shows that the specific heat capacity of the solid phase influences slightly the temperature development within the temperature range of the phase change, as well.

Next, the value of the specific heat capacity of the liquid phase is varied between 900 and 2000 [J/kg·K]. Thereby the value of c_s is set to 1000 [J/kg·K] again. Figure 11 shows the temperature profile of the third theoretical layer of the sphere with varied c_l, cooled down to -30 [°C]:

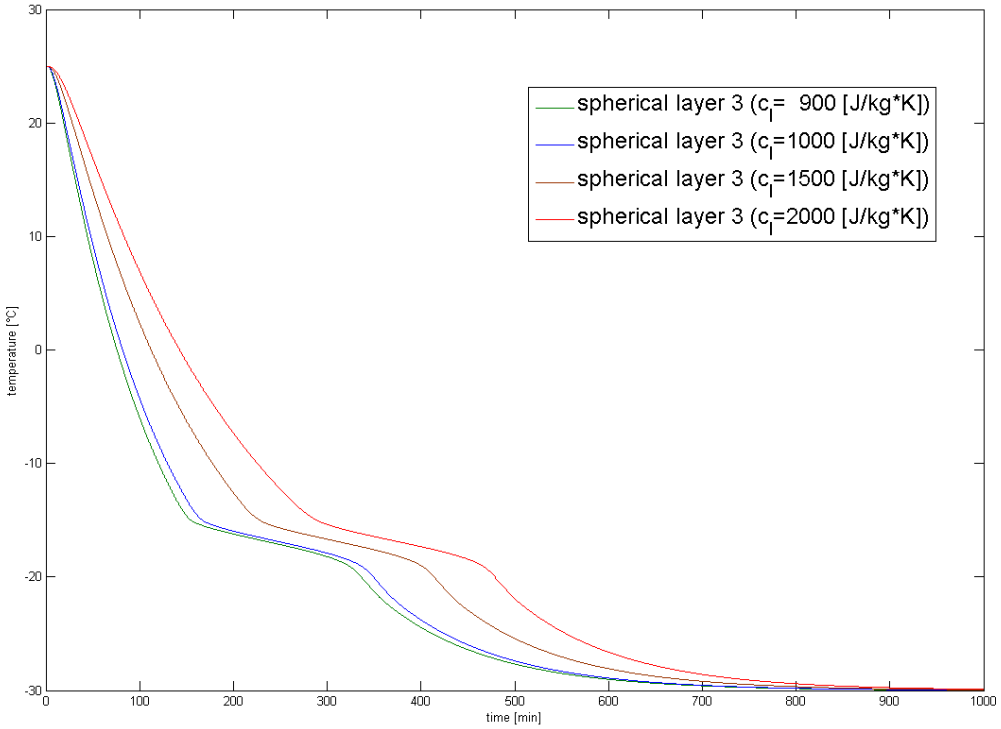

Figure 11 Transient temperatures at third position cooled down from 25 [°C] to -30 [°C] with varied specific heat capacity for the liquid phase

The diagram shows that a lower value of c_l results in a steeper curve. The value of the specific heat capacity of the liquid phase influences the beginning of the phase change and consequently the end of the change, as well.

c_l also affects slightly the temperature development within the temperature range of the phase change. At 16 [°C] the difference of time between the curve c_l =2000 [J/kg·K] and c_l =1500 [J/kg·K] amounts 62.5 minutes and at -19 [°C] it amounts 64.8 minutes.

Variation of Thermal Conductivity

Next, the values of the thermal conductivity of the solid and of the liquid phase are changed to find its influences to the temperature profile. Thermal conductivity characterises the ability of a substance to transport heat energy by conduction. The higher λ is, the better is the transmission of heat energy or the faster are the temperature differences balanced in this case.

Figure 12 shows the temperature profile of spherical layer 3 of the content with varied thermal conductivity of the solid phase between 0.4 and 1.0 [W/kg·K].

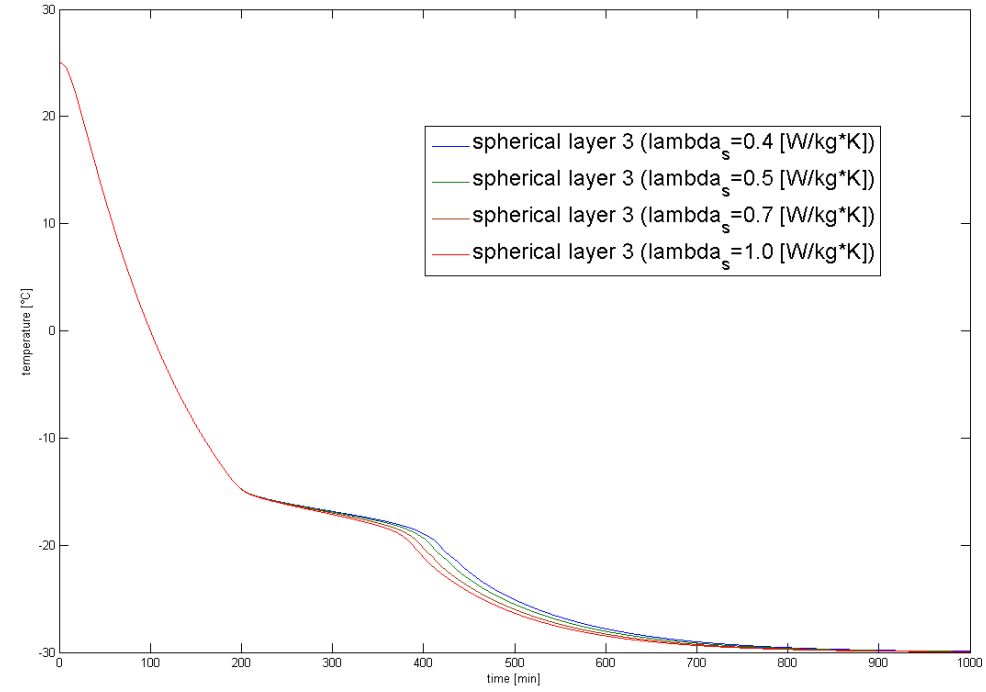

Figure 12 Transient temperatures at third position cooled down from 25 [°C] to -30 [°C] with varied thermal conductivity for the solid phase

It can be seen that the curve with the highest thermal conductivity reaches the ambient temperature of -30 [°C] first. Figure 13 shows the magnification of the temperature profile within the indicated phase-change temperature range:

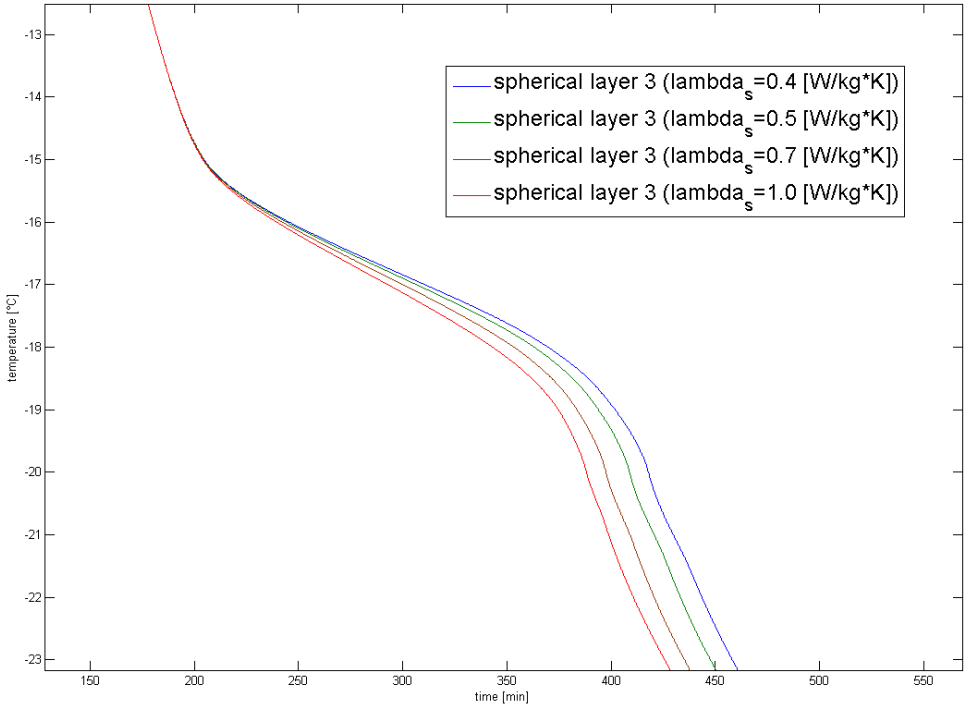

Figure 13 Magnification of the transient temperatures at third position cooled down from 25 [°C] to -30 [°C] with varied thermal conductivity for the solid phase

It shows that the thermal conductivity of the solid phase influences the temperature development within the temperature range of the phase change as well. A higher value of λ_s results in an increased heat conduction.

Next, the value of the thermal conductivity of the liquid phase is varied between 0.4 and 1.2 [W/kg·K], shown in Figure 14. Thereby the value of λ_s is set to 1 [W/m·K] again.

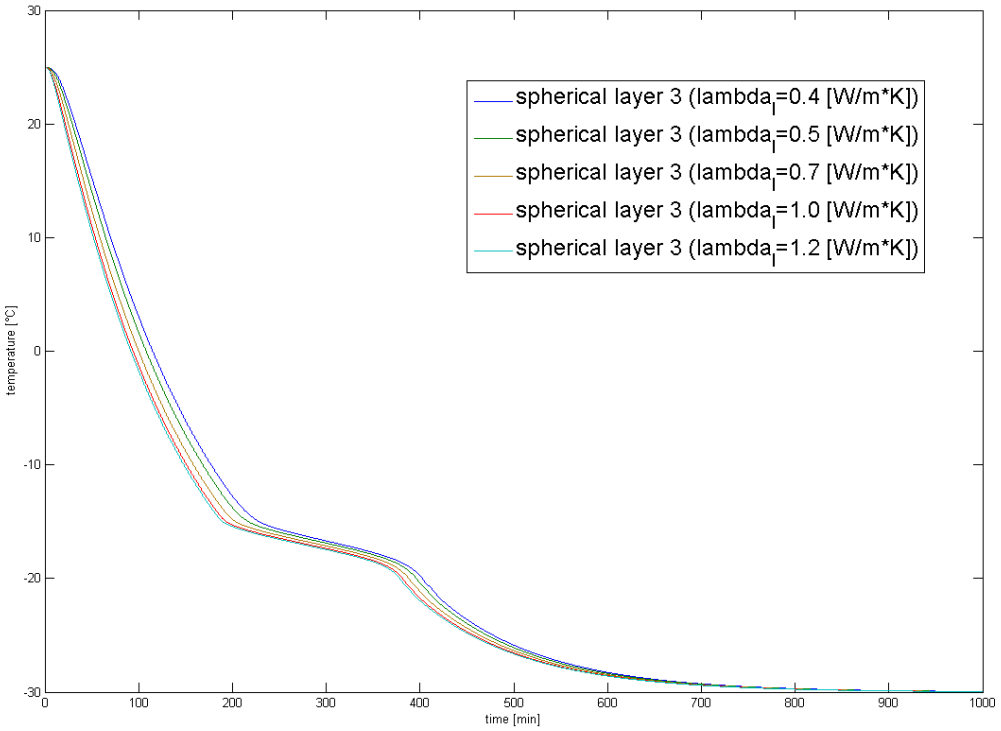

Figure 14 Transient temperatures at third position cooled down from 25 [°C] to -30 [°C] with varied thermal conductivity for the liquid phase

The diagram shows that a higher value of λ_l results in a steeper curve. The value of the thermal conductivity of the liquid phase influences the beginning of the phase change and consequently the end of the change as well. For example the curve with λ_l is 0.4 [W/m·K] reaches the initial phase change temperature after 228.8 minutes, the curve with a thermal conductivity of 1 [W/m·K] reaches the temperature already after 193.8 minutes.

Variation of Melting Enthalpy

Next, the value of the melting enthalpy is varied to find its influence to the temperature profile. An increase of the melting enthalpy should result in a later achievement of the end of the phase change temperature. It is the quantity of energy, which is necessary to change the state from a solid to a liquid. The quantity of the solidification enthalpy is the same.

Figure 15 shows the temperature profile of spherical layer 3 of the mixture with varied specific melting enthalpy between 15000 and 200000 [J/kg]:

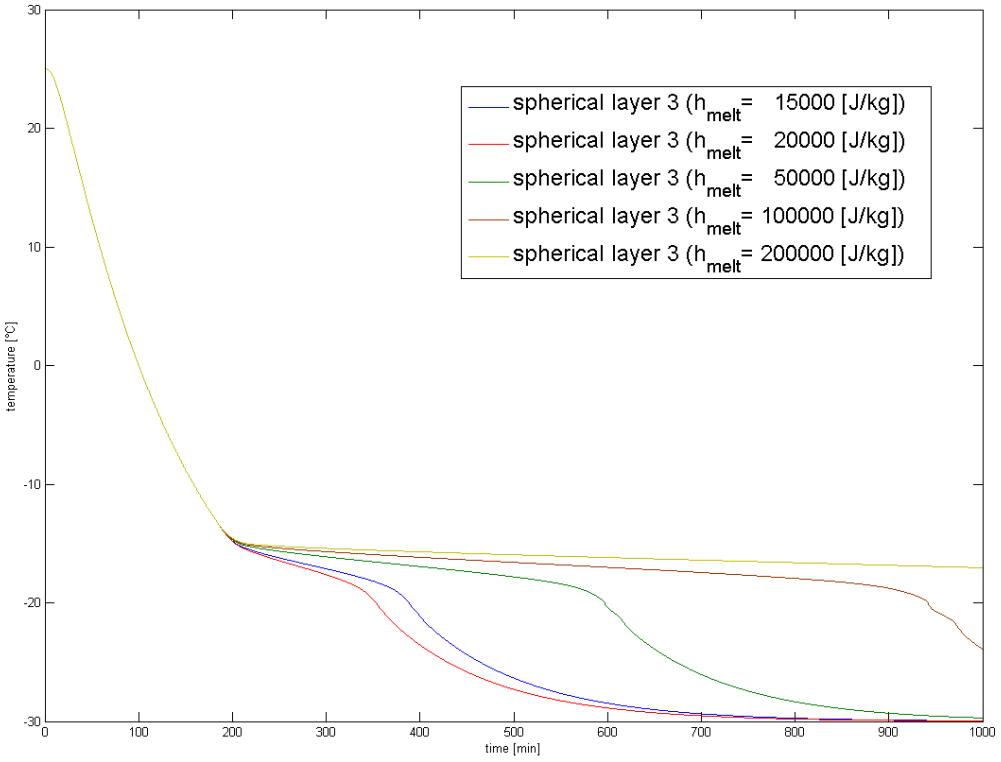

Figure 15 Transient temperatures at third position cooled down from 25 [°C] to -30 [°C] with varied specific melting enthalpy

It shows that the melting enthalpy has a large influence on the time when the end of the phase change temperature is reached. The end of the phase transition of the curve with a melting enthalpy of 200000 [J/kg] is out of the specified time range.

Figure 16 shows the temperature profile of all six layers with a melting enthalpy of 20000 [J/kg]:

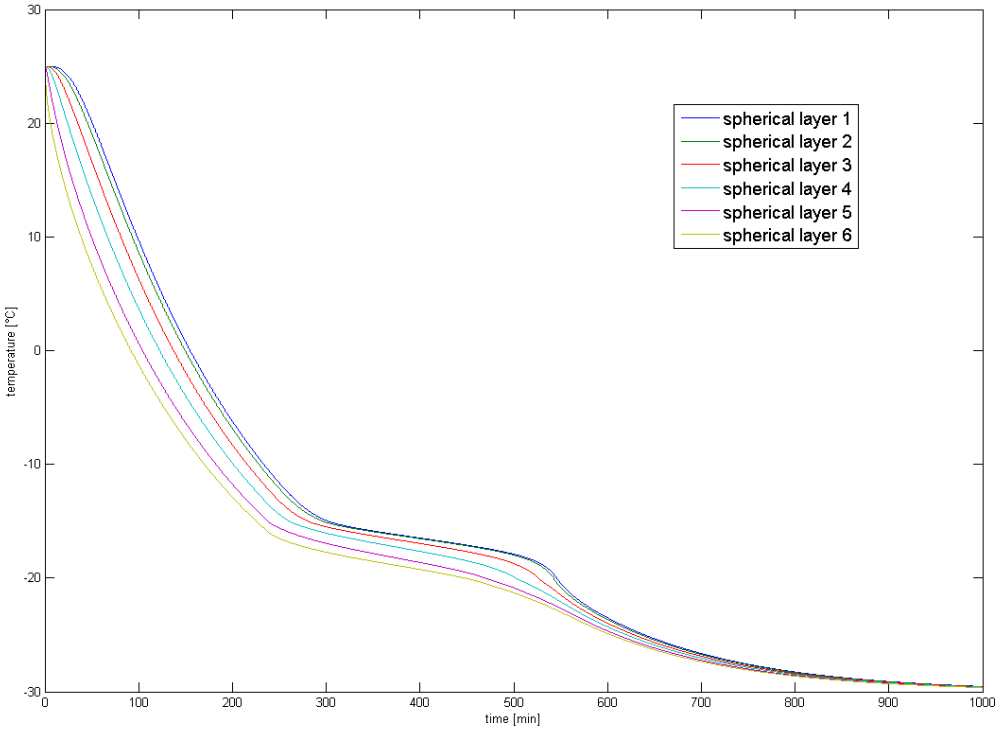

Figure 16 Transient temperatures at six positions cooled down from 25 [°C] to -30 [°C] with a specific melting enthalpy of 20000 [J/kg]

The phase transition shows up more significant in the inner layers because of the lower mass, which can be seen in the shape of the temperature curve of spherical layer 1 between 300 and approximate 550 minutes.

Variation of Heat Transfer Coefficient

The value of heat transfer coefficient α is varied to find its influence on the temperature profile. A higher α means a better heat transfer between the sphere and the ambient air and thus a constant ambient temperature should be reached earlier. Figure 17 shows the temperature profile of spherical layer 3 of the mixture with varied heat transfer coefficient between 2 and 10 [W/ m^2·K].

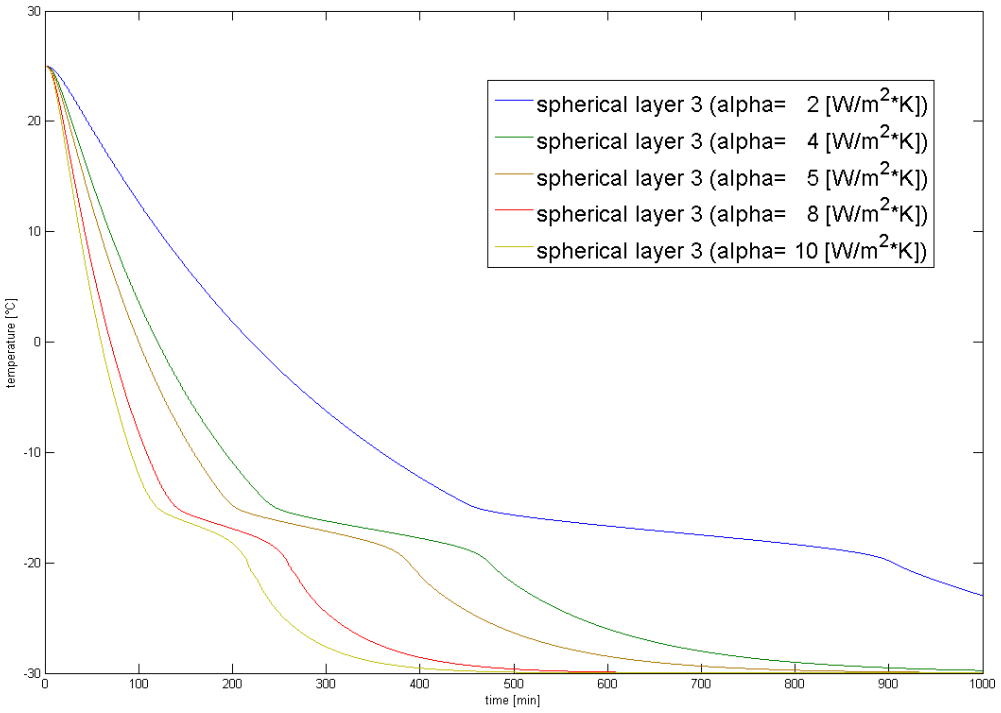

Figure 17 Transient temperatures at third position cooled down from 25 [°C] to -30 [°C] with varied heat transfer coefficient

The diagram shows that a higher heat transfer coefficient results in a steeper curve and the constant ambient temperature is reached earlier. It has also a large influence on the duration of the phase transition. A higher value of α reduces the time of the phase transition.

Variation of density of the sample material

The density ρ is varied to find its influence on the temperature profile. Due to the conservation of energy, it is expected, that the density has a similar influence as the specific heat capacity of the mixture.

$$\dot{Q} = \rho * V * cp * \frac{dT(t)}{dt} \qquad \text{(Eq. 35)}$$

Thereby V [kg/m^3] is the volume of the respective layer.

Figure 18 shows the temperature profile of spherical layer 3 of the mixture with varied density values:

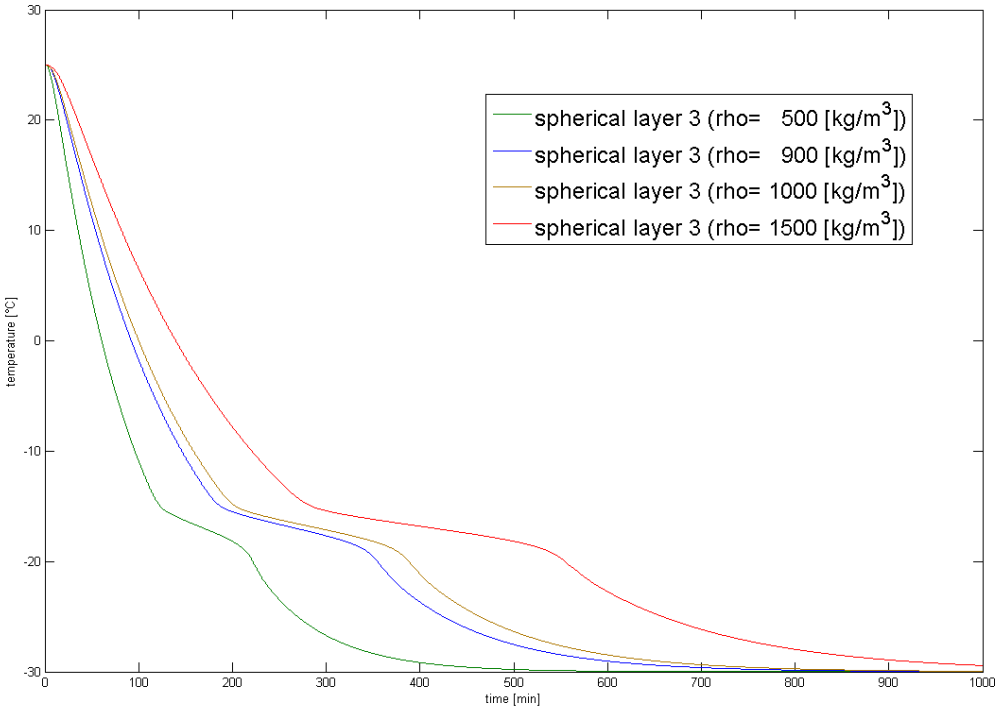

Figure 18 Transient temperatures at third position cooled down from 25 [°C] to -30 [°C] with varied density

The diagram shows, that a lower density results in a steeper curve and thus the ambient temperature is reached earlier. It has also an influence on the duration of the phase transition.

Variation of thermal conductivity, specific heat capacity and density of the outer and inner steel sphere

The values of the thermal conductivity, specific heat capacity and density of the steel spheres are varied to find their influence to the temperature profile.

Figure 19 shows the influence of the specific heat capacity of the steel sphere inside and outside:

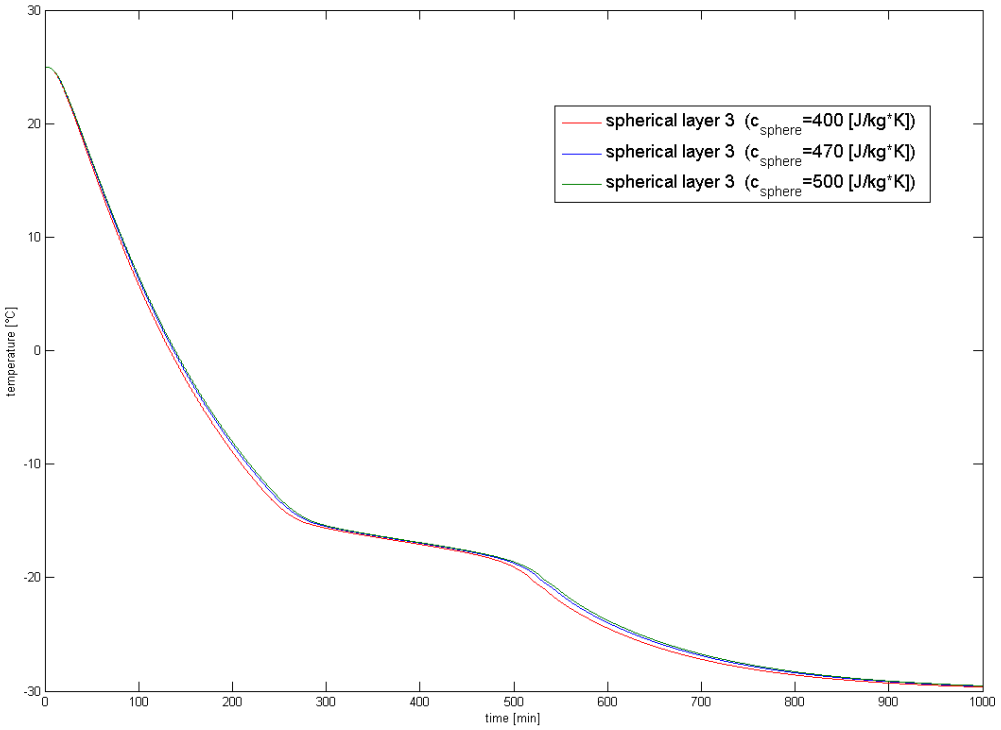

Figure 19 Transient temperatures at third position cooled down from 25 [°C] to -30 [°C] with varied specific heat capacity of the steel sphere

The diagram shows that a lower value of *c* results in an earlier achievement of the ambient temperature. A difference of 100 [J/kg·K] results in a maximal temperature difference of 1 [K]. The influence of the density is similar to *c*. The variation of the thermal conductivity shows no appreciable effect. The material values of the steel spheres are taken from the literature. *c* amounts 477 [J/ kg·K], λ is 50 [W/m·K] and ϑ amounts 8000 [kg/m^3] [18].

2.5.2 Sphere Heated from the Inside at Ambient Temperature of -30 [°C]

The second plausibility check is done by heating the sphere with a diameter of 0.15 [m] inside. The ambient and initial temperature of the sphere amounts -30 [°C]. The check is performed with twenty-five theoretical layers, additionally one layer for the interior sphere and one layer for the hollow steel sphere. The diameter of the interior sphere amounts 0.03 [m]. The table below shows the values of the parameters during the check.

ϑ [kg/m^3]	c_s [J/kg·K]	c_l [J/kg·K]	λ_s [W/ m·K]	λ_l [W/ m·K]	h_{melt} [J/kg]	α [W/ m^2·K]	T_I [°C]	T_{II} [°C]
1000	1000	1300	1	0.7	20000	5	-20	-15

Table 2 Values of the parameters during the plausibility check of the sphere heated from the inside at an ambient temperature of -30 [°C]

ϱ is the density of the sample material and c_s is the specific heat capacity of the solid phase and c_l of the liquid one. λ_s and λ_l constitute the thermal conductivity of the solid and the liquid phase, h_{melt} is the specific melting enthalpy and α is the heat transfer coefficient. T_I and T_{II} represent the phase change temperature range.

Figure 20 shows the temperature profiles of all 27 calculated layers.

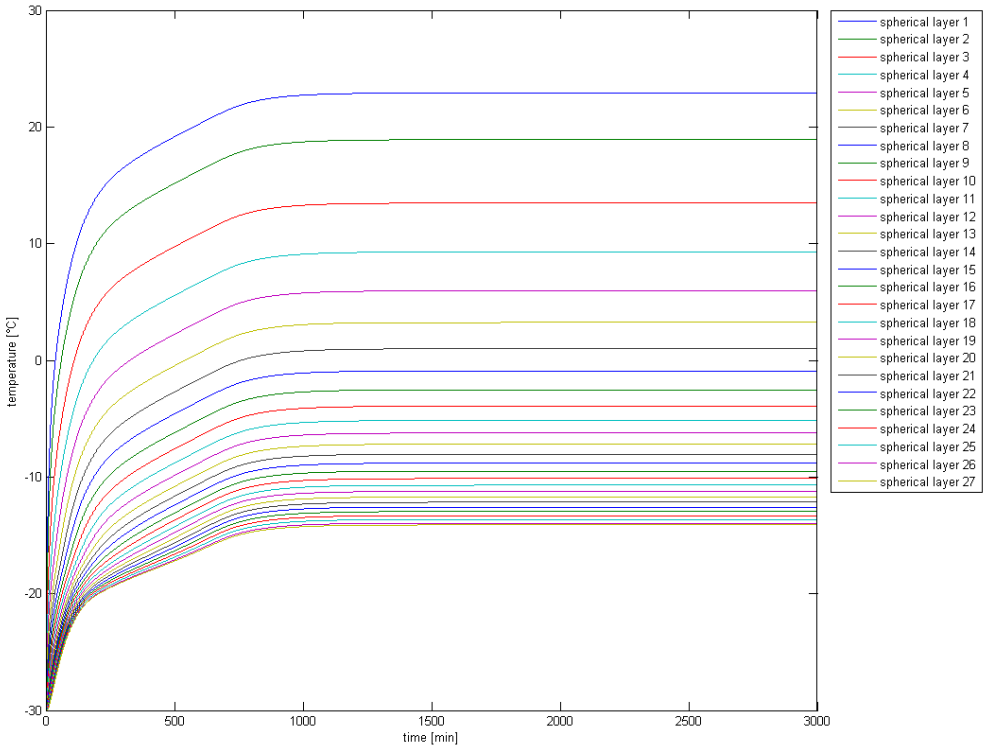

Figure 20 Temperatures at twenty-seven positions heated with 6 Watt from the inside at an ambient temperature of −30 [°C]

Spherical layer 1 and 27 represent the steel spheres of the model. Spherical layer 1 is the steel sphere inside and spherical layer 27 is the outer hollow steel sphere. Spherical layers 2 till 26 are the layers of the filled sample material containing phase-change material from the inside to the outside.

Figure 21 shows the temperature profile over the averaged radii of the layers recorded every 200 minutes over 3000 minutes.

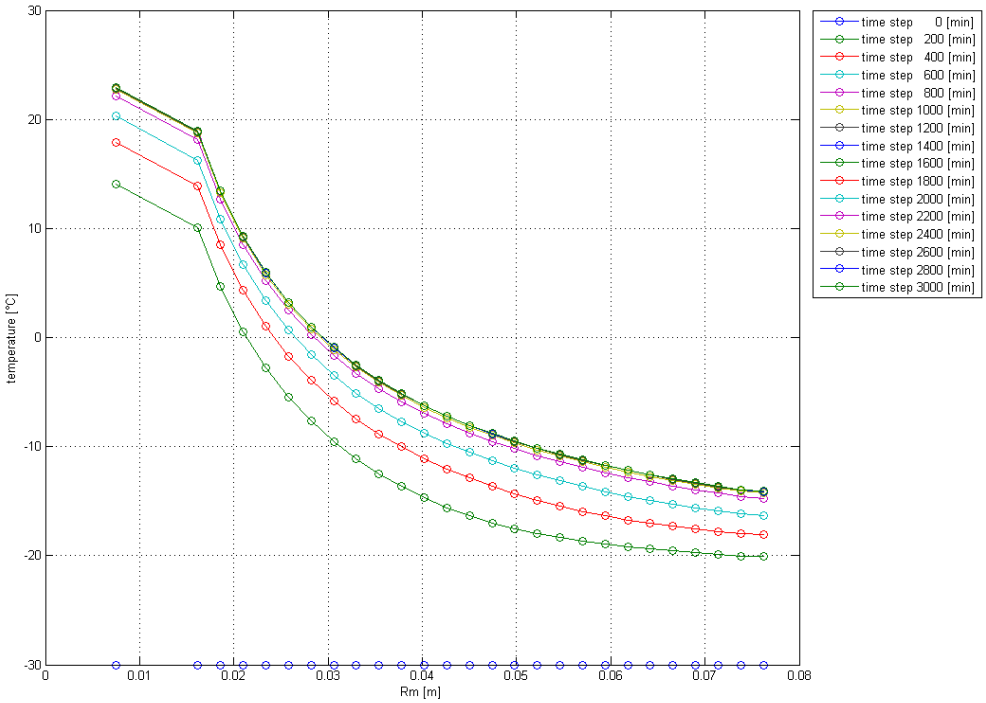

Figure 21 Temperature profile over the averaged radii of all twenty-seven layers heated with 6 Watt from the inside at an ambient temperature of -30 [°C]

The small circles represent the averaged radius of each layer, whereby the two outer circles on both sides mark the radii of the steel spheres. The temperature of the layers is higher, the closer the layers are to the interior steel sphere, which serves as the heat source.

Variation of Specific Heat Capacity

The specific heat capacities of the solid and of the liquid phase are varied to find their influences on the temperature profile. The heating power P_{el} is 6 Watt.

The values for c_s are varied between 900 and 2000 [J/kg·K]. For the comparison spherical layer 3, 7 and 20 are selected and shown in Figure 22.

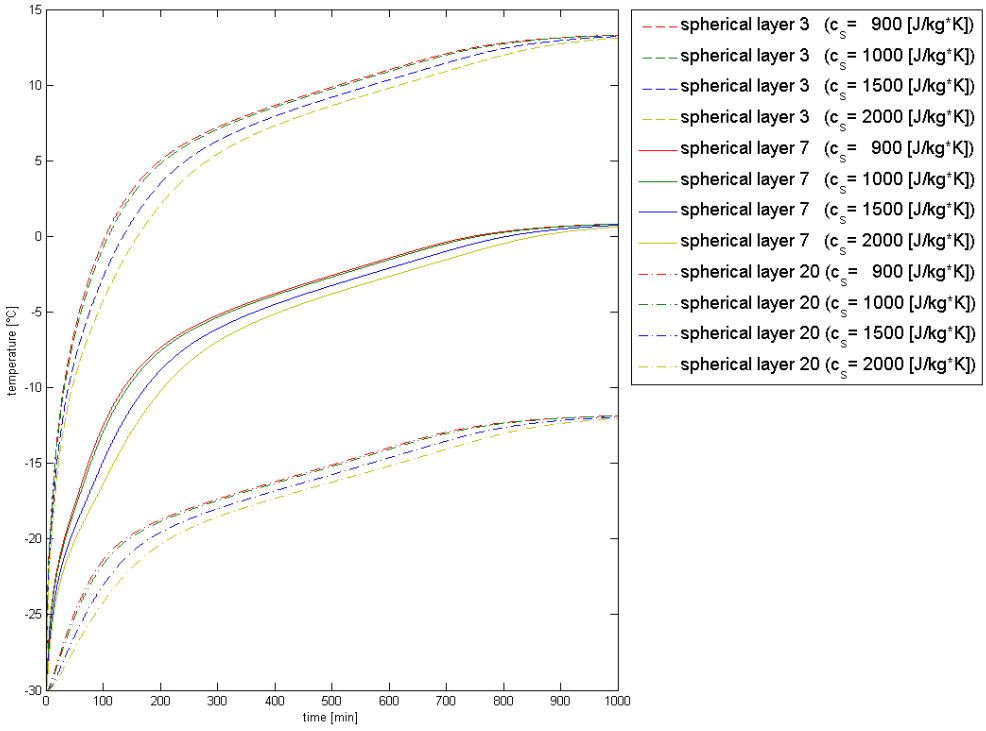

Figure 22 Temperatures at third, seventh and twentieth position heated with 6 Watt from the inside at an ambient temperature of -30 [°C] with varied specific heat capacity for the solid phase

It can be seen that the higher the values of the c_s are, the flatter is the curve and the later a constant temperature is reached. The influence of c_s on the phase transition is recognizable in the outer layers because of its higher mass. The temperature development of each layer is influenced by the others. This results in such a temporal behaviour of the influence of the specific heat capacity of the solid phase.

Next, the value of the specific heat capacity of the liquid phase is varied. Thereby the value of c_s is set to 1000 [J/kg·K] again. Figure 23 shows the temperature profile of the third, seventh and twentieth theoretical layer of the sphere with varied c_l between 900 and 2000 [J/kg·K]. The heating power amounts 6 Watt.

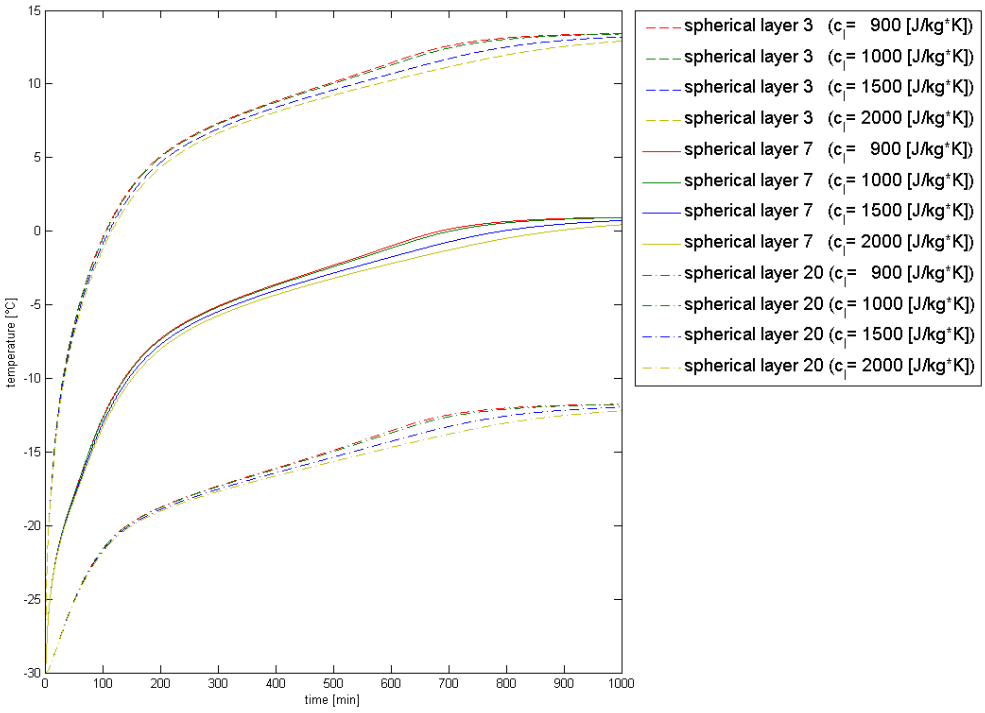

Figure 23 Temperatures at third, seventh and twentieth position heated with 6 Watt from the inside at an ambient temperature of -30 [°C] with varied specific heat capacity for the liquid phase.

This diagram shows again that the higher the values of the $c_{l,}$ are the flatter is the curve and the later a constant temperature is reached. The temporal behaviour of the influence of the specific heat capacity of the liquid phase is the same as of the solid phase.

The heat capacity of both phases has no influence on the value of the temperatures of sphere in the steady state. It affects the duration of its achievement.

Variation of Thermal Conductivity

Next, the values of the thermal conductivity of the solid and of the liquid phase are varied to find their influences on the temperature profile. Figure 24 shows the temperature profile of spherical layer 3, 7 and 20 of the sample material with varied thermal conductivity of the solid phase between 0.4 and 1.2 [W/m·K].

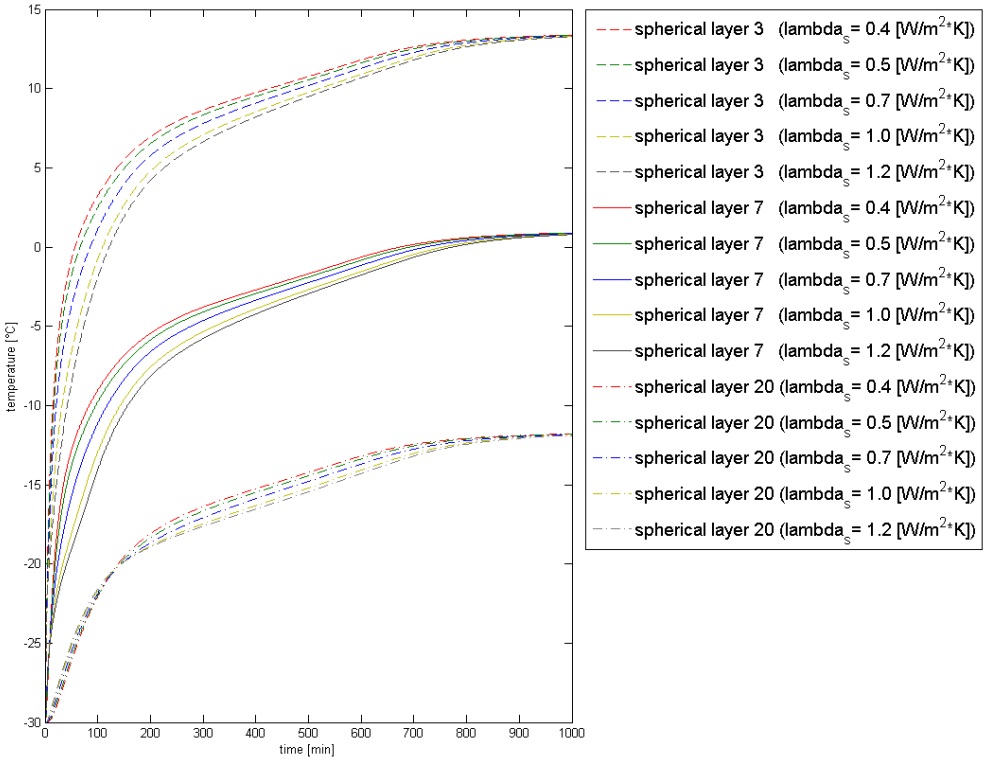

Figure 24 Temperatures at third, seventh and twentieth position heated with 6 Watt from the inside at an ambient temperature of -30 [°C] with varied thermal conductivity for the solid phase.

As expected, a higher value of the thermal conductivity results in a flatter curve. After the phase transition, the curves reach almost the same temperature because of the same value of $\lambda_{l.}$

Figure 25 shows the temperature profile with a heating power of 2 Watt and a calculation time of 3000 minutes. Phase change occurs only in the first layers within the indicated thermal conductivity range of 0.4 – 1.2 [W/m·K].

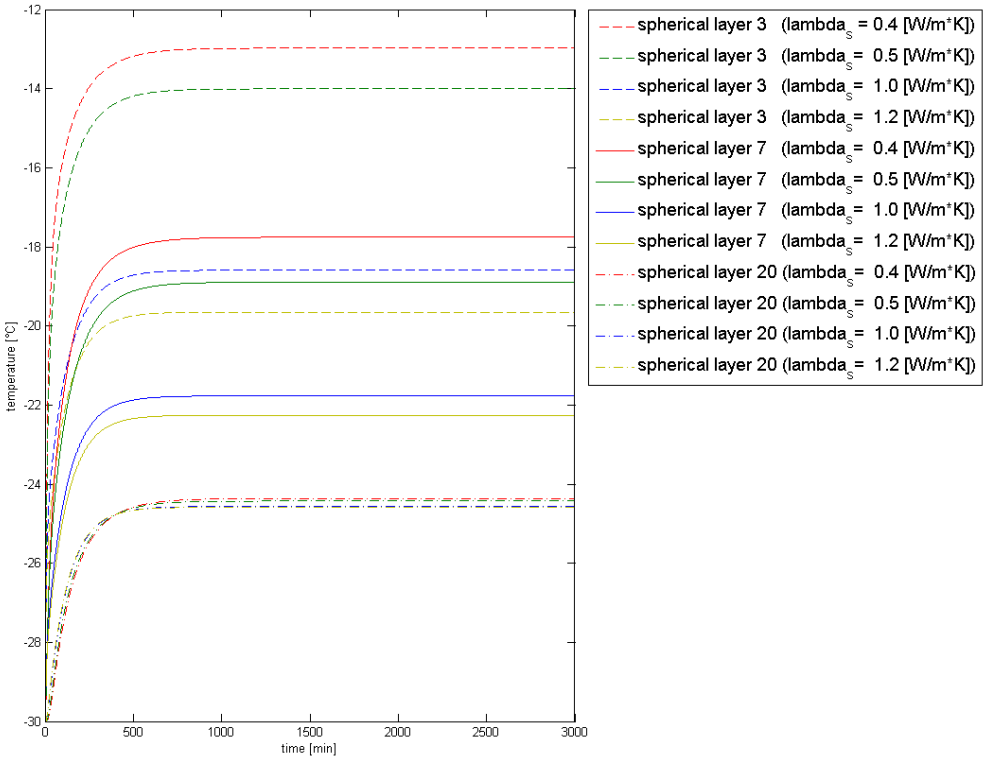

Figure 25 Temperatures at third, seventh and twentieth position heated with 2 Watt from the inside at an ambient temperature of -30 [°C] with varied thermal conductivity for the solid phase.

This diagram shows that a higher value of λ_s results in a lower temperature in the spheres at steady state. A higher thermal conductivity entails a smaller temperature difference:

$$\dot{Q} = A * q = \ - \ \lambda * 4 * \pi * r^2 * \frac{dT}{dr} \qquad \text{(Eq. 36)}$$

Furthermore it can be seen that with increasing radius the temperature gradient in given constant heat power becomes smaller. This also can be explained with equation 36. The equation is satisfied if the temperature difference becomes smaller with a larger transfer surface.

Figure 26 shows the temperature profile of spherical layer 3, 7 and 20 of the content with varied thermal conductivity between 0.4 and 1.2 [W/m·K] of the liquid phase. λ of the solid phase is set to 1.0 [W/m·K] again:

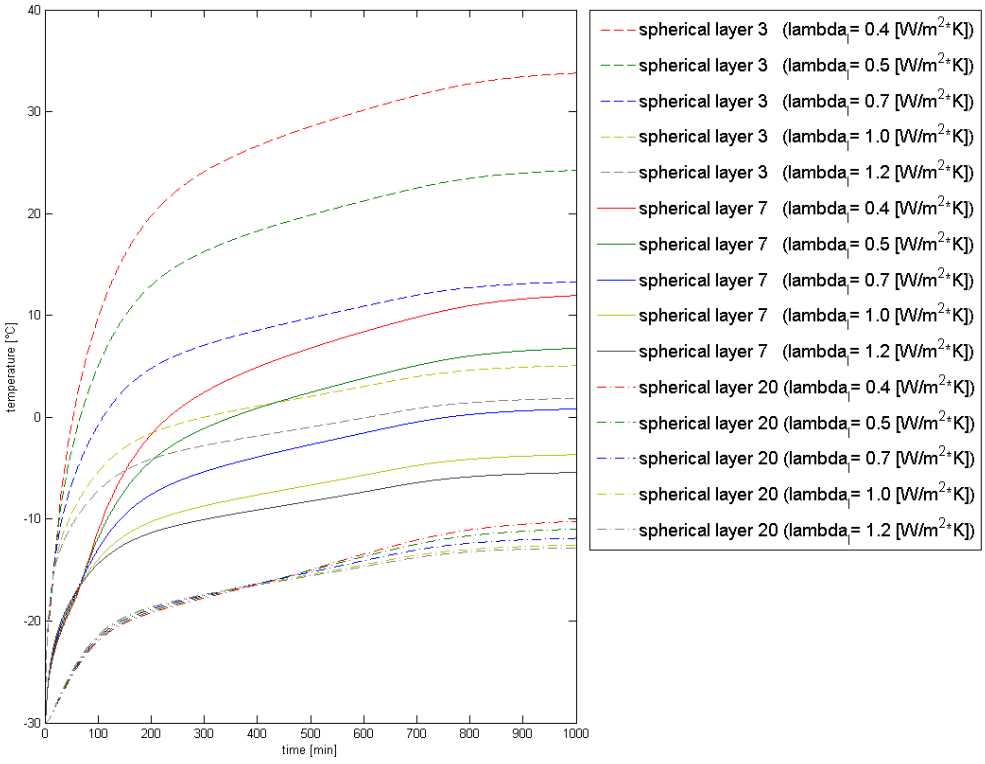

Figure 26 Temperatures at third, seventh and twentieth position heated with 6 Watt from the inside at an ambient temperature of -30 [°C] with varied thermal conductivity for the liquid phase.

This diagram shows that equation 36 is also valid for the thermal conductivity of the liquid phase. A higher transfer surface entails to a smaller temperature difference and a higher thermal conductivity results in lower temperatures in the spheres.

The thermal conductivity has no effect on the steady state temperature of the outer steel sphere. Figure 27 shows the temperature profile with varied values of λ_l, whereby the calculation time is set to 3000 minutes:

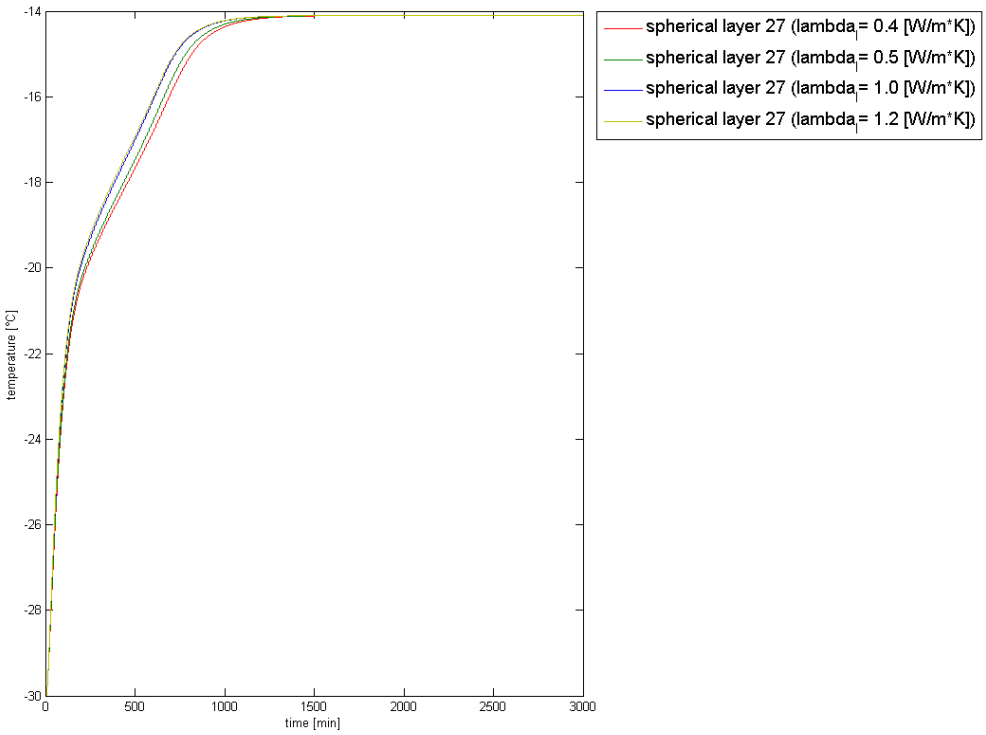

Figure 27 Temperatures at twenty-seventh position (outer steel sphere) heated with 6 Watt from the inside at an ambient temperature of -30 [°C] with varied thermal conductivity for the liquid phase.

Variation of Melting Enthalpy

Next, the value of the specific melting enthalpy is varied to find its influence on the temperature profile. The calculation time amounts 3000 minutes. Figure 28 shows the temperature profile of spherical layer 3, 7 and 20 of the mixture with varied specific melting enthalpy between 20000 and 100000 [J/kg]. The sphere is heated with 6 Watt again.

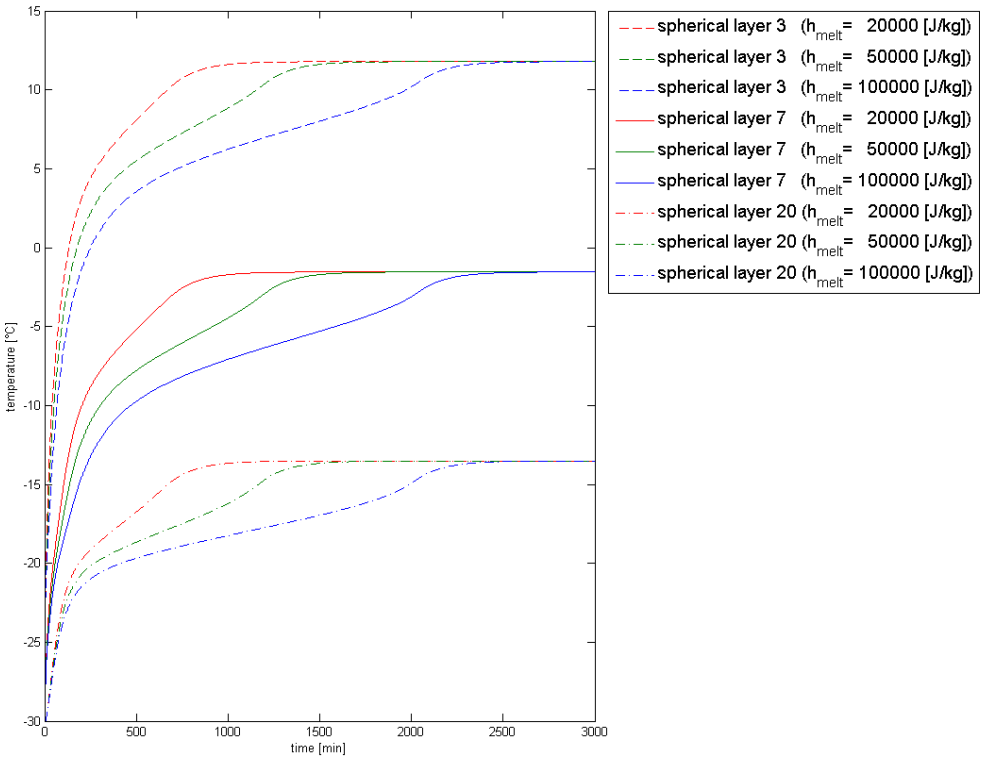

Figure 28 Temperatures at third, seventh and twentieth position heated with 6 Watt from the inside at an ambient temperature of -30 [°C] with varied specific melting enthalpy.

The value of the melting enthalpy has no influence on the value of the temperature of the steady state. However it affects the duration of the phase change process.

Variation of Heat Transfer Coefficient

The value of heat transfer coefficient α is varied to find its influence on the temperature profile. Figure 29 shows the temperature profile of spherical layer 3, 7 and 20 of the filled mixture with varied heat transfer coefficient.

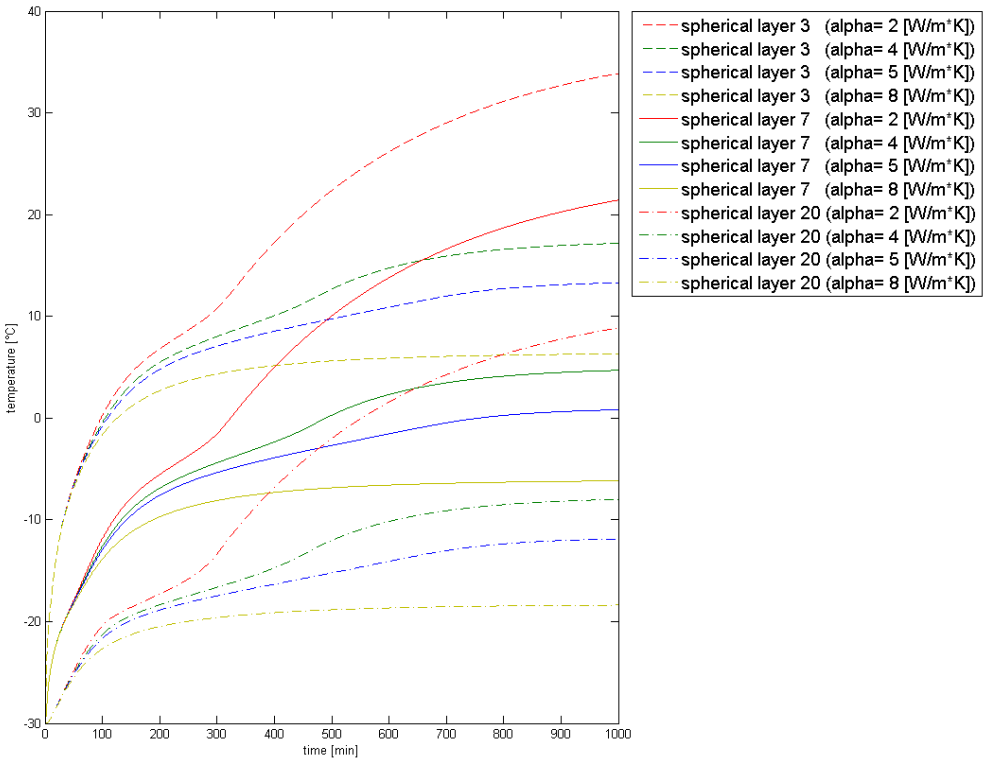

Figure 29 Temperatures at third, seventh and twentieth position heated with 6 Watt from the inside at an ambient temperature of -30 [°C] with varied heat transfer coefficient.

The diagram shows that a lower heat transfer coefficient results in a later achievement of a steady state. Furthermore the temperatures in the sphere are higher if the heat transfer coefficient is smaller which shows following equation:

$$\dot{Q}_u = \propto * A * \left(T_u - T_{steelsphere}\right) \qquad \text{(Eq. 37)}$$

T_u is the ambient temperature and $T_{steelsphere}$ is the temperature of the outer steel sphere, also indicated as spherical layer 27 in this case. In contrast to the thermal conductivity, the heat transfer coefficient affects the steady state temperature of the outer steel sphere. Figure 30 shows the temperature profile of the outer steel sphere with varied values of α, whereby the calculation time is set to 3000 minutes.

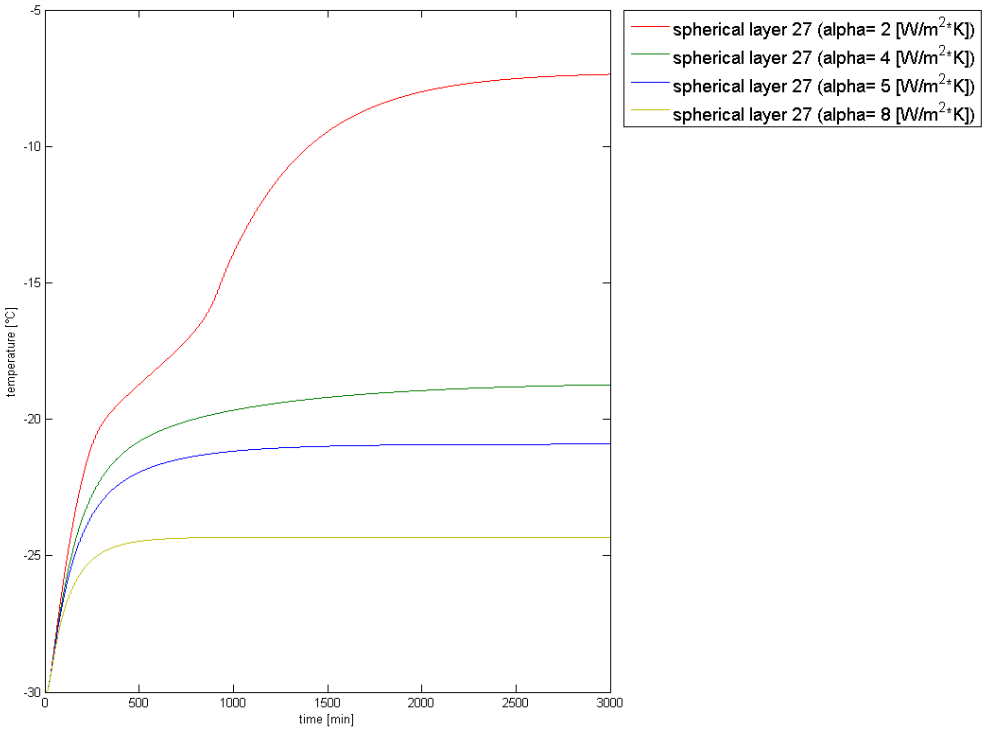

Figure 30 Temperatures at twenty-seventh position (outer steel sphere) heated with 6 Watt from the inside at an ambient temperature of -30 [°C] with varied heat transfer coefficient.

Variation of Density of the Sample Material

The value of density ϱ is varied to find its influence on the temperature profile. Figure 31 shows the temperature profile of spherical layer 3, 7 and 20 of the mixture with varied density between 500 and 1500 [kg/m^3]:

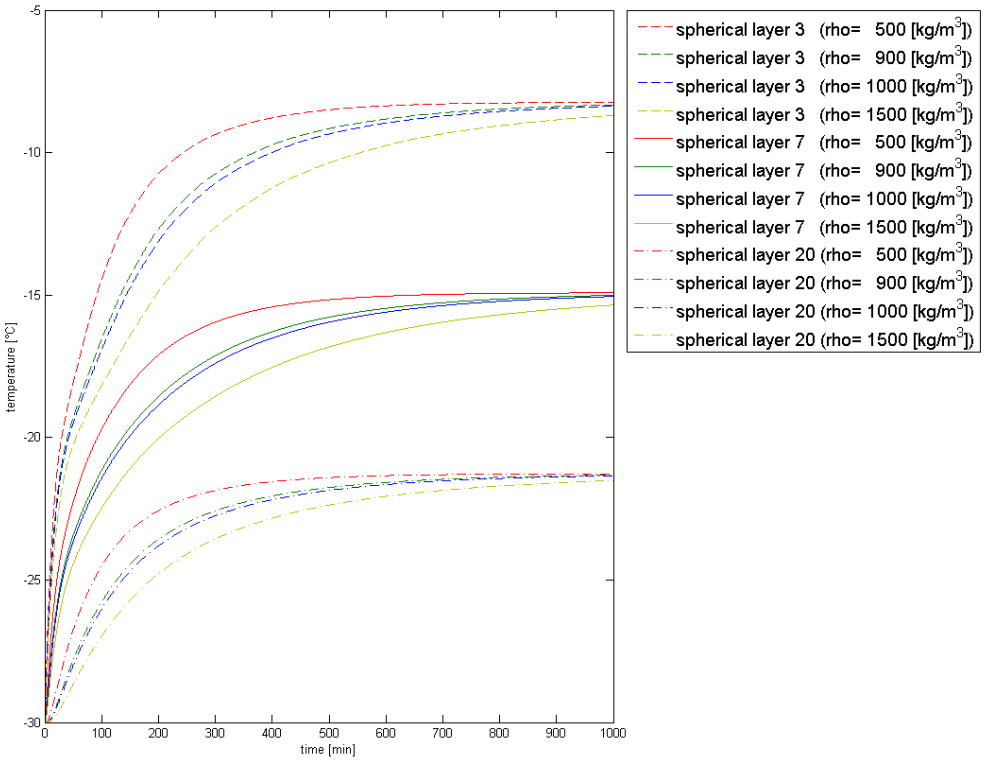

Figure 31 Temperatures at third, seventh and twentieth position heated with 6 Watt from the inside at an ambient temperature of -30 [°C] with density.

The temperature profile shows that a lower density of the content results in steeper curve and the steady state is reached earlier.

First Law of Thermodynamics

The system boundary is set around the sphere. In accordance to the following formula, the electrically introduced heat power must be the same as the amount of heat transferred to the ambient air after achievement of a steady state.

$$dU = dQ \qquad \text{(Eq. 38)}$$

$$U_2 - U_1 = (T_2 - T_1) * c * m = \int (\dot{Q}_u + P_{el}) * \mathrm{dt} \qquad \text{(Eq. 39)}$$

dU [J] is the change of internal energy of the system and is zero at a steady state. Furthermore all terms as a function of time can also be set to zero at a steady state. This results in:

$$-\dot{Q}_u = P_{el} \qquad \text{(Eq. 40)}$$

P_{el} [W] constitutes the introduced heat and $\dot{Q}_u$ [W] is the heat transferred to the ambient. The heat power P_{el} and the calculation time are varied. This check is performed with twenty theoretical layers, additionally one layer for the interior sphere and one layer for the hollow steel sphere. The table below shows the results of $\dot{Q}_u$:

P_{el} [W]	Calculation time [min]	$\dot{Q}_u$ [W]
4.000	1000	-3.891
4.000	1500	-3.963
4.000	2000	-3.987
4.000	3000	-3.998
4.000	4000	-4.000
4.000	5000	-4.000
4.000	5500	-4.000
9.000	1000	-8.980
9.000	1500	-8.999
9.000	2000	-9.000

Table 3 Results of the heat transferred to the ambient with varied calculation time and heating power

It can be seen, that after a certain calculation time, a steady state is reached and the equation 40 is satisfied. The time of the achievement of steady state conditions depends on the heating power and on the presence of a phase transition. Table 4 shows the results of $\dot{Q}_u$ after 3000 minutes with varied heating power:

P_{el} [W]	Calculation time [min]	$\dot{Q}_u$ [W]
10	3000	-10.0000
9	3000	-9.0000
6	3000	-6.0000
5	3000	-4.9996
4	3000	-3.9983
3	3000	-3.0000
1	3000	-1.0000

Table 4 Results of the heat transferred to the ambient with varied heating power

Figure 32 shows the temperature profile of the eleventh layer, which is situated centrally, with varied heating power.

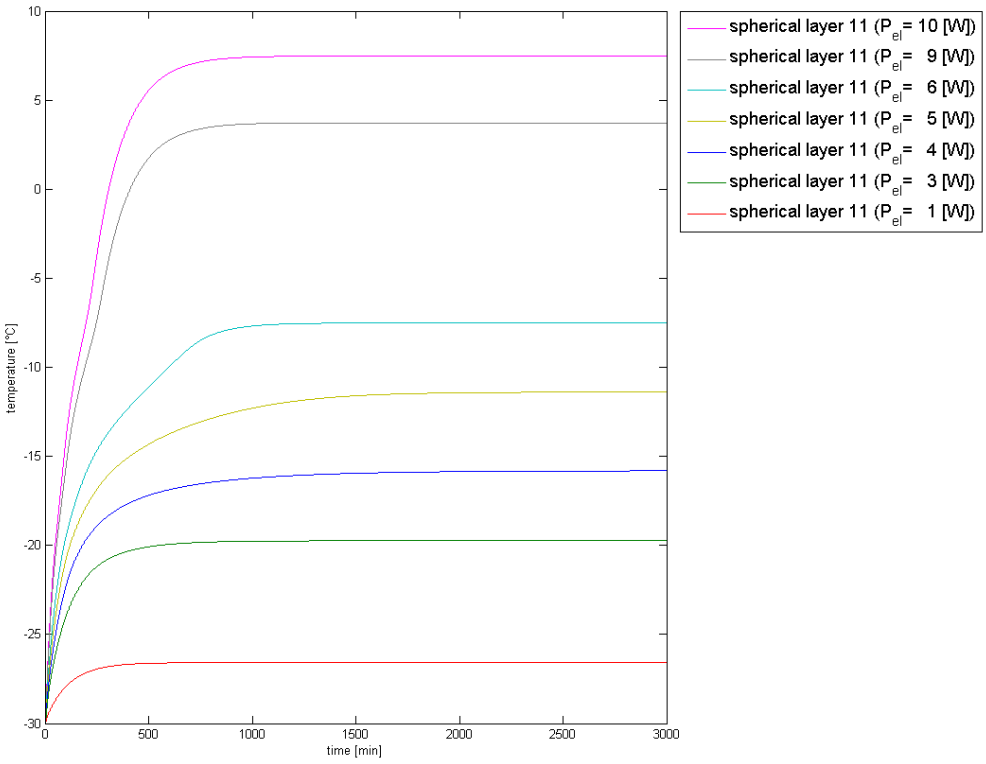

Figure 32 Temperatures at eleventh positions heated with varied heating power from the inside at an ambient temperature of -30 [°C]

The curves with a heating power of 4 and 5 Watt need longer to achieve a steady state because the phase transition which occurs between -15 and -20 [°C] influences the temporal development of the temperature profile. There is no phase change in the layers of the sphere heated with 1 Watt. In the sphere heated with 3 Watt phase transition occurs only in the first ten layers which amounts only about 25 [%] of the total mass of the content. The mass of these layers is too small to influence the result of $\dot{Q}_u$ [W] after 3000 minutes.

In all spherical layers in the spheres heated with 4 and 5 Watt, phase transition occurs. That's why a steady state is not reached after a calculation time of 3000 minutes. In the spheres heated with 6, 9 and 10 Watt phase change occurs in all layers as well, but the heating rate is high enough to reach a steady state after the indicated calculation time. Figure 33 shows the mass distribution of the sphere divided into 20 layers.

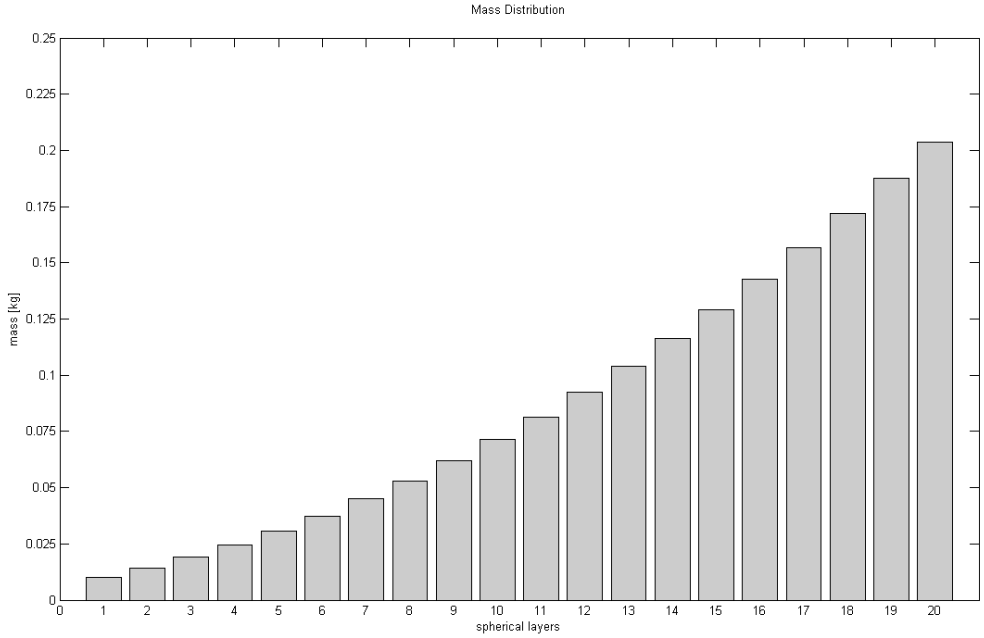

Figure 33 Mass distribution of the content of the sphere divided into 20 layers

The most obvious phase transition can be recognized on the temperature profile of the runs heated with 9 and 10 Watt. The reason for that is the high heating rate, which causes a rapid phase change especially in the outer layers which have a higher mass. Figure 34 shows the temperature profile of all twenty-two layers heated from the inside with 9 Watt at an ambient temperature of -30 [°C].

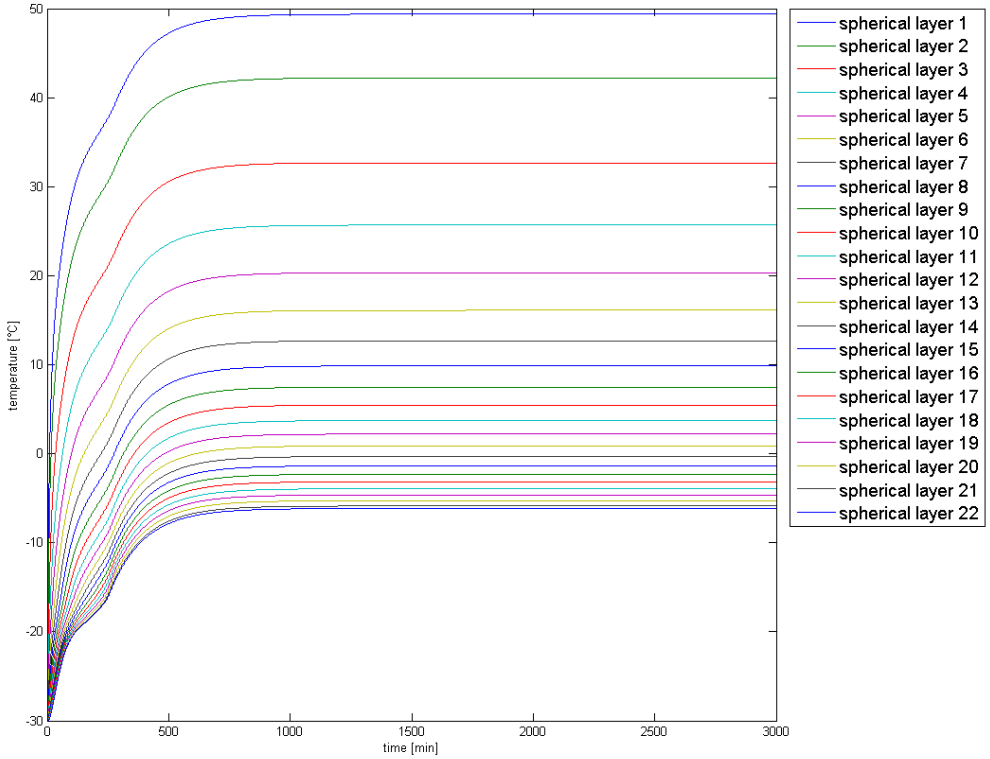

Figure 34 Temperatures at twenty-two positions heated with 9 Watt from the inside at an ambient temperature of -30 [°C]

2.5.3 Parameter Adjustment

In the course of the plausibility check two different experiments are simulated. First, the sphere is cooled down to -30 [°C] without interior heat source. Then the sphere is heated from the inside at an ambient temperature of -30 [°C].

Thereby, the parameters specific heat capacity, thermal conductivity, specific melting enthalpy and heat transfer coefficient are varied. In addition to the exclusion of programming errors, another key reason for the variation of the parameters is the finding of the best procedure to adjust the parameters to the measured data. The test rigs are created similar to the simulated one. As already mentioned the measurement results are read into MATLAB and the parameters are determined due to adjustment of the theoretical curve to the measuring data.

Specific Heat Capacity

The effect of c_l on the temperature profile getting from the simulated experiment, where the sphere is cooled down to -30 [°C] without interior heat source is stronger. Thereby the maximal temperature difference of the curves of the third layer with a c_l of 900 and 2000 [J/kg·K] amounts about 9 [°C]. The maximal difference of the same curves performed with the same sphere heated from the inside with 6 Watt at an ambient temperature of -30 [°C] amounts only about 3 [°C].

For that reason the specific heat capacity of both phases is adjusted to the measurement results getting from the test rig where the sphere is cooled down to -30 [°C] without interior heat source.

Thermal Conductivity

The effect of the thermal conductivity on the temperature profile getting from the simulated experiment, where the sphere is heated from the inside at an ambient temperature of -30 [°C], is stronger. It shows that the thermal conductivity has a great impact on the steady state temperature in the sphere. The maximal temperature difference of the simulated curves of the third layer with λ_l of 0.4 and 1.2 [W/m·K], heated with 6 Watt at an ambient temperature of -30 [°C] amounts over 30 [°C]. The maximal difference of the same curves of the runs cooled down to -30 [°C] without heat source is only about 3 [°C].

Heat Transfer Coefficient

There are three possibilities to evaluate the heat transfer coefficient. It can be determined from the Nusselt number in the case of free convection around a sphere. The solution algorithm presented in the VDI Wärmeatlas [15] is described in detail in the previous chapter. This

calculation does not include any thermal radiation and simplifies the external air flows in the cooling chamber.

Furthermore, the value of α can be calculated, using the measured surface area and ambient temperatures and the introduced heating power. The surface temperature, measured with two or three thermocouples, influences the value of α strongly. A difference of 0.5 [K] results in a deviation of α of 0.358 [W/m^2·K] considering the sphere with a diameter of 151.1 [mm]. The measured surface temperatures show higher variation than 0.5 [K].

Due to these uncertainties, the value of α is adjusted to the measurement results of the runs heated on the inside. On the one hand, the value of α influences the duration of the phase transition and on the other hand it affects the gradient of the curve. These effects can also be observed on the values of c, λ and h_{melt}. Moreover, α has an effect on the value of the temperature of the sphere when it is heated inside. Contrary to the thermal conductivity, the heat transfer coefficient has no influence on the temperature difference between the layers. The values of α determined from the measured surface are used as initial values.

Melting Enthalpy and Phase-Change Temperature Range

For the determination of the melting enthalpy and of the phase transition range, the results of the run without heat source are used. The phase change is more significant in this temperature profile, especially when a phase transition does not occur in the outer layers.

3 Experimental Studies

For the determination of the parameters thermal conductivity, specific heat capacity, specific latent heat and melting temperature range a model of a sphere is created. First the spherical model, whereby one-dimensional, transient heat conduction in radial direction is considered, is created in MATLAB to get information about the measurement setup.

This chapter describes the measurement setup and the performance of the experiments. A sphere made out of steel is filled with a mixture of phase-change material and a mixing component. To get an ambient temperature of about -30 [°C] the sphere is put into a freezer. In the middle of the sphere a further, smaller sphere made out of steel is placed. A blub is put into this sphere, which acts as a heat source.

The model, programmed in MATLAB, divides the content into several layers. To get a temperature profile of these layers, thermocouples are placed at defined positions to measure the temperature of the sample material.

Then the parameters thermal conductivity, specific heat capacity, specific latent heat, melting temperature range and heat transfer coefficient are determined by adjusting the theoretical curve to the measuring curves.

A calibration of the thermocouples is performed to eliminate measurement errors. The density measurement of the sample materials and measurements performed with differential scanning calorimetry are also described in this chapter.

3.1 Calibration of the Thermocouples

Measurement errors may occur at the thermocouple itself, at the connectors and thermocouple-wires, at the cold junction compensation and at the Data Acquisition System.

In order to eliminate these measurement errors and to perform experiments, the calibration of the thermocouples has to be accomplished. Thereby the temperature of thirty-two thermocouples of three different types is documented. Twenty-four thermocouples type T with PTFE isolation, five without isolation and three thermocouples for the surface measurement are available.

A thermostat of the company Lauda is used to achieve a desired stable temperature. The working temperature range of the thermostat is between -25 [°C] and 200 [°C]. The calibration is performed at a temperature range of -25 [°C] to 60 [°C].

First, all thermocouples are plugged in and the position of each plug is marked to maintain it during the experimentations. Then the thermocouples are fixed at the tip of the reference thermometer, which measures the temperature in the thermostat at the defined position. Figure 35 shows the setup of the calibration.

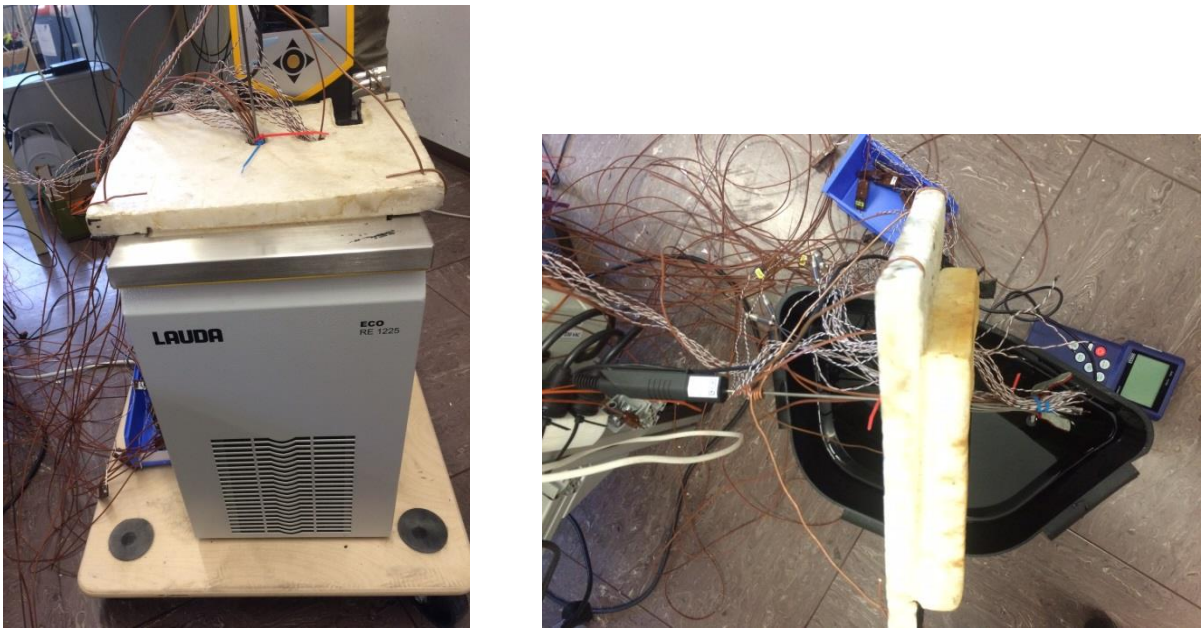

Figure 35 Left: Complete setup of the calibration. Right: Thermocouples fixed at the tip of the reference thermometer

To perform the calibration at positive temperature, water is filled into the thermostat. The first calibration is performed at 0 [°C]. After the thermometer readout shows a constant temperature, the signals of the thermocouples are recorded for a few minutes. Then the temperature of the thermostat is increased to 15 [°C] and the signals of the thermocouples are recorded again after the achievement of a constant temperature. Furthermore, the signals are recorded at 20 [°C], 60 [°C], -20 [°C] and -25 [°C]. An antifreeze agent is used to calibrate the thermocouples at sub-zero centigrade temperatures. Figure 36 shows the measured temperatures of all thermocouples at 15 [°C]:

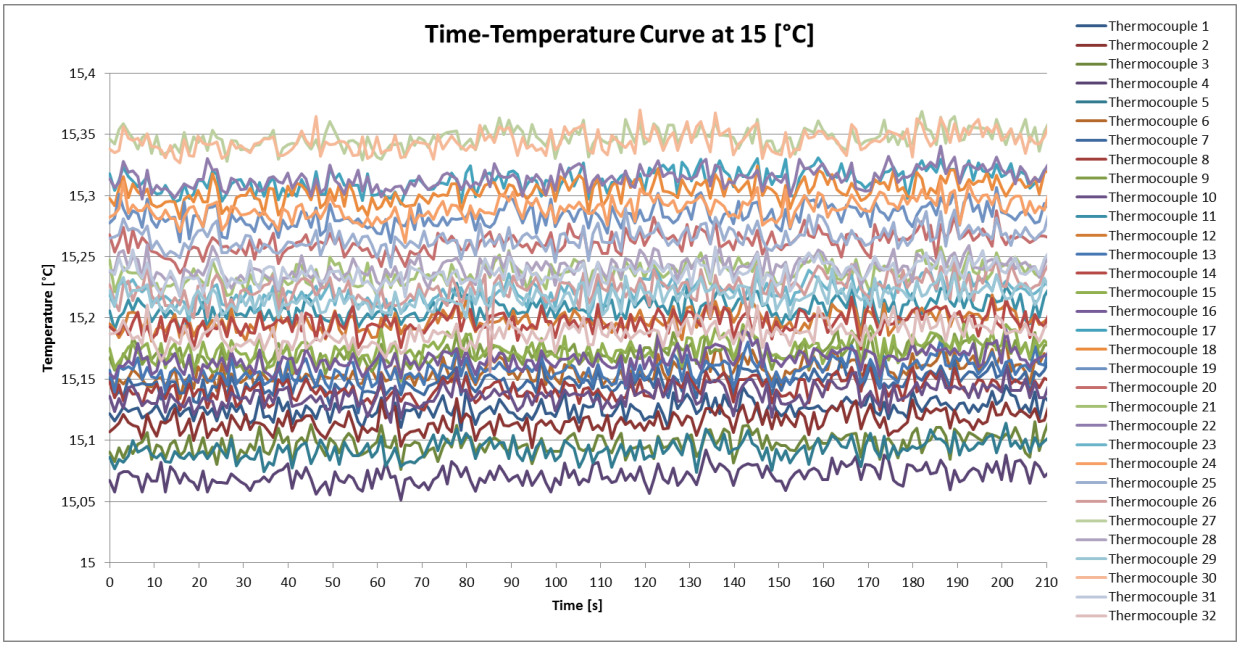

Figure 36 Measured temperatures of thirty-two thermocouples at 15 °C.

The program LabVIEW uses an internal polynomial fit to correct the temperature-voltage curve with the measured temperature of the thermometer as reference temperature. Figure 37 shows the corrected measured temperatures of all thermocouples at 15 [°C]. The slight fluctuations during the signal recording are considered as measurement noise:

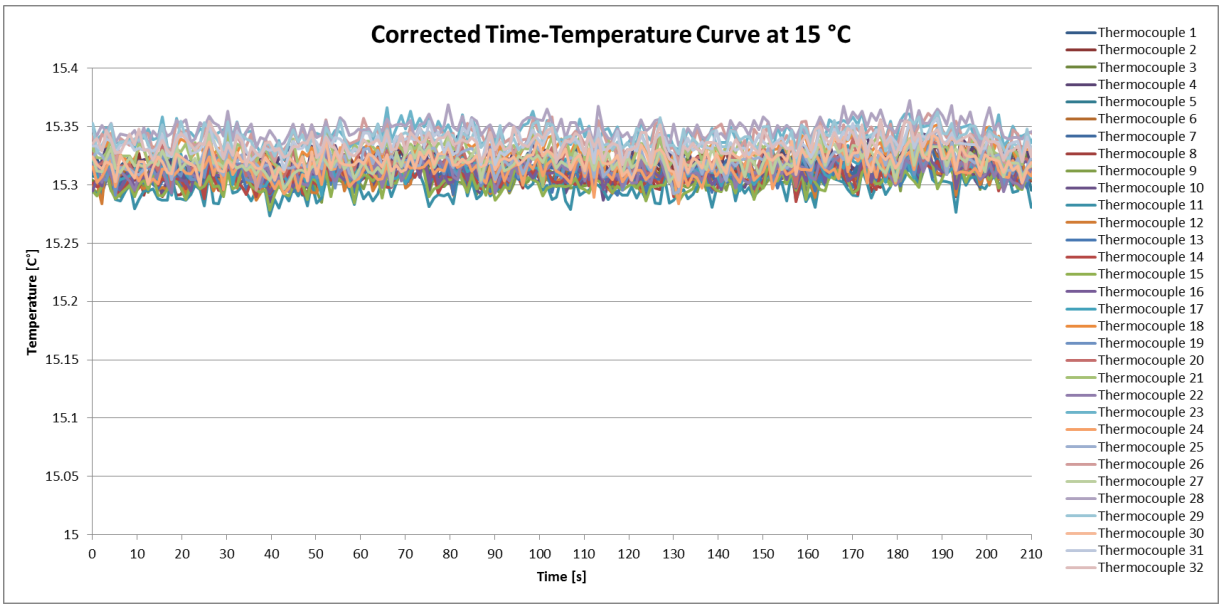

Figure 37 Measured temperatures of thirty-two thermocouples at 15°C automatic corrected by LabVIEW

For all further experiments the program delivers the corrected temperatures and need not to be converted.

3.2 Density Measurements

For the determination of the required parameters (λ, c, specific latent heat and melting temperature range), the density of the mixtures has to be found out. The density is determined by the exclusion of water in the beaker. Thereby a 50 ml beaker is used. The limit of the filling is marked. First the weight of the beaker is noted, whereby it is important that the beaker glass is clean and dry. Then the beaker is filled with water till the marking and weighed again. The temperature of the water is also measured to define its density. Afterwards the water is removed and the beaker has to be clean and dry again.

The beaker is filled with the mixture and the weight is noted. Then it is filled up to the mark with water. The density of the mixture is determined by the following formula [19]:

$$\rho_{mixture} = \left(\frac{m_2 - m_0}{(m_1 - m_0) - (m_3 - m_2)}\right) * \rho_{water} \qquad \text{(Eq. 41)}$$

m_0 is the weight of the empty beaker, m_1 the weight of the beaker filled with water, m_2 the weight of the beaker filled with the mixture and m_3 is the weight of the beaker and the mixture filled up with water till the marking. ρ_{water} constitutes the density of the water at the certain temperature. The experiment is repeated three times and the mean value is determined from the total.

3.3 Differential Scanning Calorimetry (DSC) – Measurements

First a mixture of 10 percent by weight phase-change material and 90 percent by weight heat-conducting paste was examined with the differential scanning calorimeter of the company Netzsch, provided by the company RCE.

Thereby, a total mass of 10 [g] is mixed. The components were weighted by a balance of the company Sartorius. 1.001 [g] of the phase-change material and 9.007 [g] of the heat-conducting paste are mixed and filled in a 25 [ml] beaker.

Afterwards, additional samples with 15, 5 and 0 percent by weight phase change material are investigated. The mixture with 20 percent by weight phase-change material and 80 percent by weight heat-conducting paste is too powdery and will not be examined further.

The measurements are performed with an empty reference crucible. The heating rate is 2.0 [K/min].

In addition, measurements for the determination of the heat capacity of the mixtures are performed. Thereby sapphire is used as *c*-standard.

The results of the differential scanning calorimetry are used just as indicators and comparative values.

3.4 Sphere Measurement Setup– Measurements

This section now describes the measurement setup of the spherical model and the performance of the experiment. The phase-change material is mixed on the one hand with heat conducting paste and on the other hand with engine oil SAE 0W-30. The experimental setup consists of a hollow steel sphere and a smaller one in the middle, which served as a heat source. At defined radial distances, thermocouples are attached to measure the temperature profiles (see Figure 38).

3.4.1 Heat Conducting Paste as Mixing Component

First a hollow sphere made out of steel having an inner diameter of 150 millimeters is used. A smaller hollow steel sphere with a diameter of 30 millimetres is located in the centre of the sphere in which four small bulbs connected in parallel are placed acting as a heat source.

Four thermocouples are placed at defined distances to measure the temperature of the sample material. Figure 38 shows such a setup without a filling:

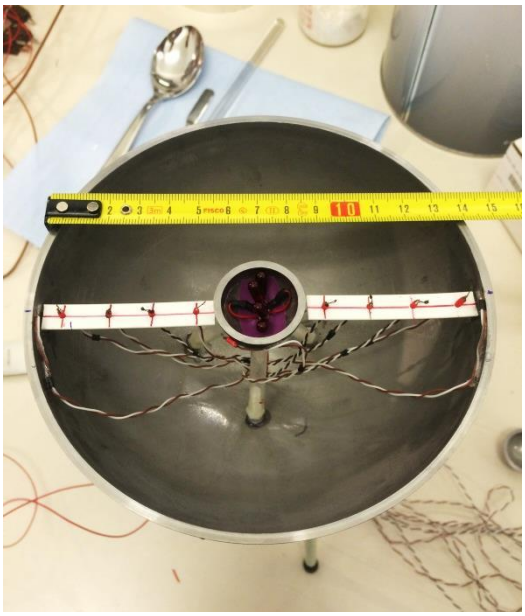

Figure 38 Setup of the lower hemisphere for the determination of the thermal conductivity and specific heat capacity

After composing the inner sphere and noting the exactly distance of the thermocouples, the sphere is filled completely with heat conducting paste, shown in Figure 39:

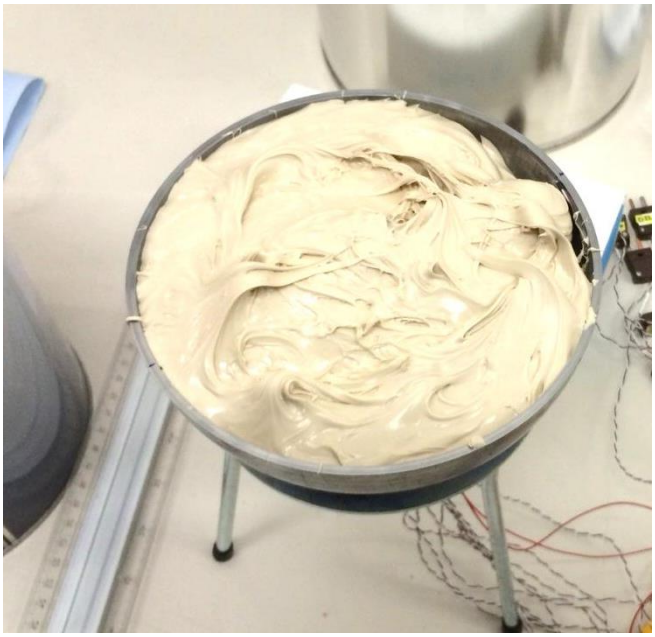

Figure 39 Lower hemisphere filled with heat conducting paste

The first measurements are performed without phase-change material. Both hemispheres are filled with the heat conducting paste, a non-Newtonian fluid. Then they were overlapped and compressed. The sphere is sealed with an aluminium tape. Additionally two thermocouples are put on the surface of the sphere.

Then the thermocouples are plugged in and the temperature measurements start. The sphere is put into a freezer which is cooled to about -32 [°C]. Another thermocouple is placed additionally into the cooling cabinet to measure the cabinet temperature at the certain position, shown in Figure 40:

Figure 40 Filled sphere put into the refrigerator and the additional thermocouple to measure the ambient temperature

The cooling process in the sphere is measured. The program LabVIEW records the temperatures every 10 seconds.

After about 17 hours the recording is stopped. Then the cables of the bulbs are connected to the power supply and additionally to a power meter and for the next measurement an electrical power of 4 Watt is set. After about 23 hours, the power is increased by 1 Watt. The power of heating is estimated with the calculation model, whereby a thermal conductivity of 0.7 [W/m·K] and a specific heat capacity of 1500 [J/kg·K] are assumed. The value of the heat transfer coefficient is determined from the Nusselt number within a temperature range of 25 and -30 [°C] and amounts 5.7 [W/m^2·K].

After the measurements are terminated, the sphere is put out of the refrigerator and is warmed up at ambient temperature for several hours. Then the upper hemisphere is taken off carefully and the heat conducting paste is removed from the top of the thermocouples. It is important not to change the position of the temperature sensors. The distance of the thermocouples is noted again. The mounting process of the upper hemisphere and the compression of both hemispheres moved the top of the thermocouples slightly.

For this purpose the construction is improved for the next measurement. The temperature sensors are fixed with a cover of hard plastic, so that only the top of the sensors sticks out. Further comparisons of the positions before and after measurements show less difference. For the evaluation of the results, the positions after the measurements, are used.

The second measurement is performed with a mixture of 10 percent by weight phase-change material and 90 percent by weight heat conducting paste. It is assumed, that the thermal conductivity of the mixture is lower than of the pure heat conducting paste. Hence, the sphere is heated first with 3.5 Watt and then the power is increased by 1 Watt.

3.4.2 Engine Oil as Mixing Component

The heat conducting paste behaves like an adhesive. Thus, it is difficult to remove the paste from the sphere and to mix it homogenously with the phase-change material. For that reason, the third measurement is performed with a mixture of engine oil SAE 0W-30 and phase-change material.

For the measurements using engine oil as mixing component, a new sphere model is constructed. The outer hollow steel sphere has an inner diameter of 200 millimetres and the hollow sphere located in the centre has an inner diameter of 50 millimetres. A small light bulb, acting as the heat source is placed inside the smaller sphere. Six thermocouples are located at defined distances between the spheres on both sides. They are fixed similarly as the previous construction.

First, the oil and the phase-change material are mixed in a beaker. To determine the parameters by means of the model it is necessary to assume that free convection is negligible. Therefore the amount of phase-change material is increased till a highly viscous mass is reached. A mixture of 55 percent by weight phase-change material and 45 percent by weight engine oil results.

For the experiment the sphere is filled with 1.845 [kg] oil and 2.256 [kg] phase-change material. Air inclusions are removed in advance with a vacuum pump. A hole is drilled at the centre of the upper hemisphere. After the exact distance of the thermocouples are noted, the hemispheres are put together and sealed with silicone and an aluminium tape. Then the sphere is filled with the mixture through the hole. The sphere is left to stand overnight.

Then, three thermocouples are put on the surface of the sphere and the whole is closed with an aluminium tape.

Then, the thermocouples are plugged in and the temperature measurements start. The sphere is put into the refrigerator with an inside temperature of about -32 [°C] again. To measure the cabinet temperature a thermocouple is placed additionally into the cooling cabinet at the certain position. The cooling process in the sphere is measured. The temperatures are recorded every 10 seconds again.

The engine oil has a very low thermal conductivity. Hence, the heating power amounts only 2.5 Watt during the first measurement. After constant temperatures are reached, the maximum temperature amounts about -5 [°C]. Hence, the heat power is increased to 4 Watt. After a

constant temperature profile is reached the power is increased again. Two further measurements with a heating power of 6 Watt and 8 Watt are performed. Thereby the small steel sphere becomes quite hot because of the low thermal conductivity.

The sphere is cooled down to about -32 [°C] again and is put out of the refrigerator. The warming-up curve to ambient temperature is measured.

Figure 41 shows the lower hemisphere after the measurements.

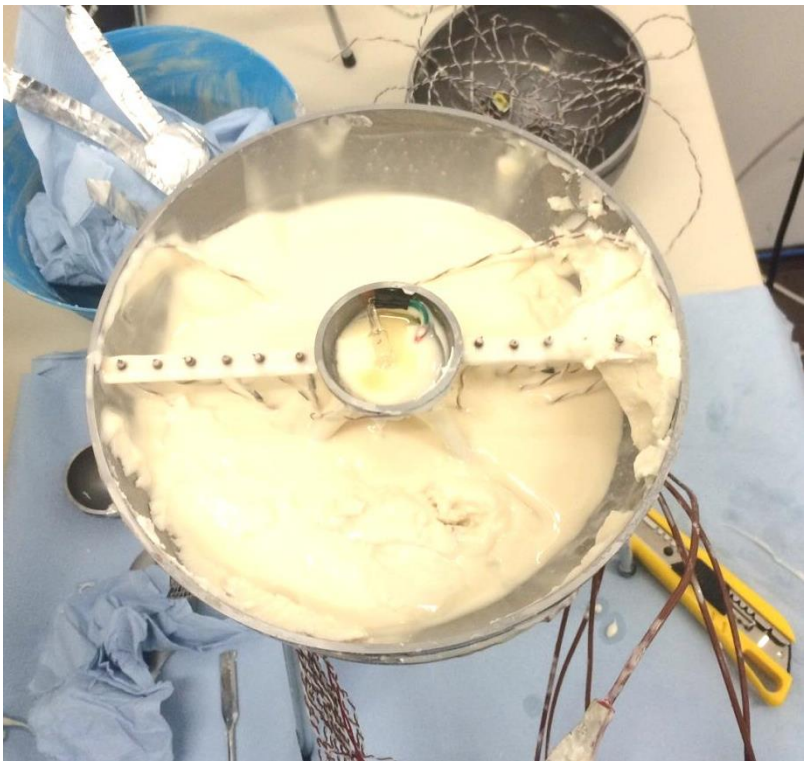

Figure 41 Lower hemisphere filled with a mixture of 55 [wt%] phase-change material and 45 [wt%] oil after the experiments

A separation of the components can be observed. An enrichment of phase change material mixed with a smaller amount of oil occurs at the outer edge, at the bottom and at the small sphere. The small sphere is filled during the measurements with the mixture. Moreover, some content leaked during the experiment. The reason for that may be the thermal expansion of the oil, which means that a part of heat transfer occurs through free convection. The calculation model is not valid if convection occurs.

3.4.3 Engine Oil and Aluminium Powder as Mixing Component

The third experiment is performed in addition to the engine oil with aluminium powder with a particle size of 55 [µm] as mixing component. The aluminium powder shall increase the thermal conductivity of the mixture. The mixture consists of 44 [wt%] phase-change material, 36 [wt%] engine oil and 20 [%] aluminium powder. Therefore 920.7 [g] aluminium powder, 2026 [g] phase-change material and 1658.5 [g] engine oil are mixed.

The experimental setup is the same as for the experiment performed with the engine oil as mixing component. A small part of the mixture is put into a beaker and is left to stand overnight. The air inclusions, which arise during the mixing, are no longer visible. Therefore the sphere is filled up and left stand overnight as well.

The sphere is cooled down to about -32 [°C] again. Then the sphere is heated with 1 Watt. The temperatures of the layers show that the heat conductivity is not as high as expected. So the heating power is increased to 8 Watt.

To recognize a phase change, the sphere is cooled down again and then heated with 10 Watt. After a constant temperature profile is reached the sphere is put out of the refrigerator and warmed up at ambient temperature.

After the end of the measurements the sphere is dismantled. A separation of the components can be observed again.

Table 5 shows the overview of the performed experiments:

Components / **Experiment**	Cooling down without interior heat source	Heated from the inside at -32 [°C] ambient temperature
Heat-conducting paste	✓	4 & 5 Watt
10 [wt%] phase-change material & 90 [wt%] heat-conducting paste	✓	3.5 & 4.5 Watt
55 [wt%] phase-change material & 45 [wt%] oil	✓	2.5, 4, 6 & 8 Watt
44 [wt%] phase-change material & 36 [wt%] oil & 20 [wt%] aluminium powder	✓	1 & 8 Watt 10 Watt

Table 5 Overview of the performed experiments

4 Results and Discussion

4.1 Density-Measurement

The results of three measurements are used to form a mean value. The values of the density of the measurements are listed in the table below:

Components	Result 1	Result 2	Result 3	Mean Value
Heat-conducting paste	1760 [kg/m^3]	1461 [kg/m^3]	1584 [kg/m^3]	**1602 [kg/m^3]**
10 [wt%] phase-change material & 90 [wt%] heat-conducting paste	1680 [kg/m^3]	1683 [kg/m^3]	1695[kg/m^3]	**1686 [kg/m^3]**
55 [wt%] phase-change material & 45 [wt%] oil	753 [kg/m^3]	849 [kg/m^3]	898 [kg/m^3]	**833 [kg/m^3]**
44 [wt%] phase-change material & 36 [wt%] oil & 20 [wt%] aluminium powder	973 [kg/m^3]	956 [kg/m^3]	931 [kg/m^3]	**953 [kg/m^3]**

Table 6 Values of the density of the mixtures

4.2 Temperature-Modulated Differential Scanning Calorimetry

The first measurement is performed with a mixture of 10 percent by weight phase-change material and 90 percent by weight heat-conducting paste. The heating rate amounts 2.0 [K/min]. Figure 42 shows the measured curve by the temperature-modulated differential scanning calorimeter.

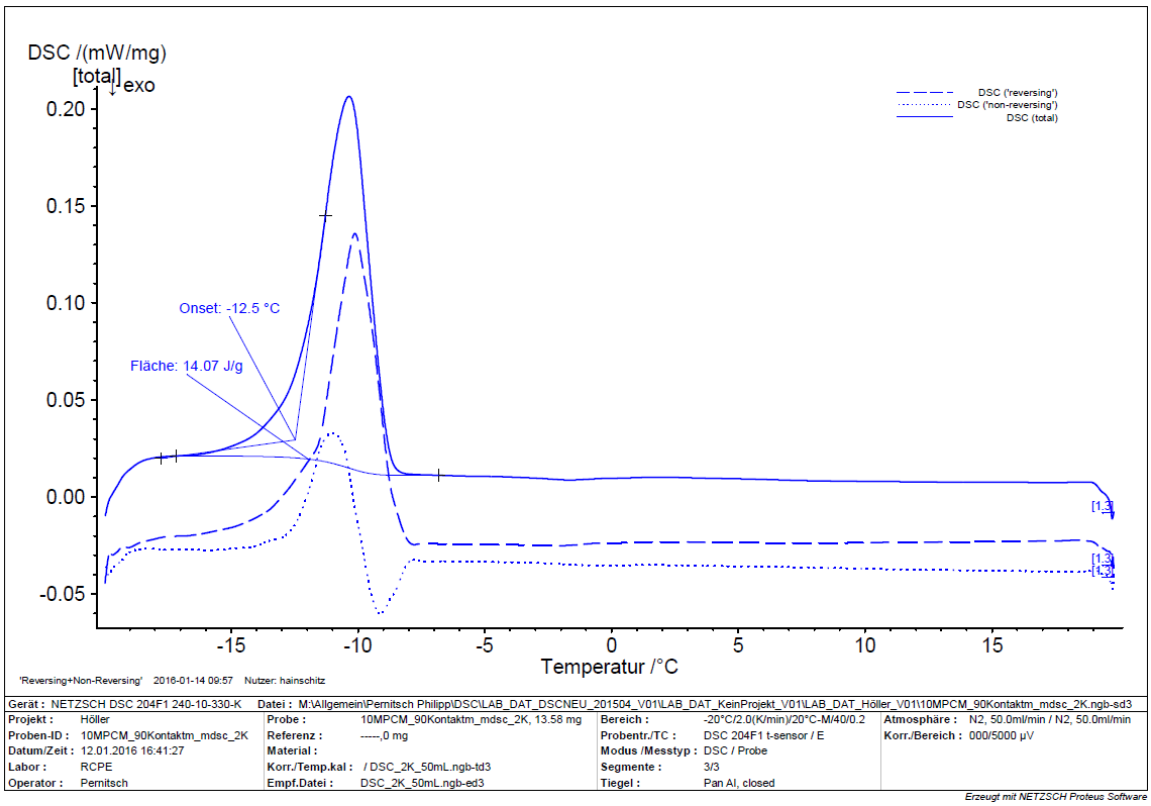

Figure 42 Temperature-modulated DSC traces at 2 [K/min] of a mixture with 10 wt% phase-change material and 90 wt% heat-conducting paste.

The measurement results in a specific melting enthalpy of 14.07 [J/g] and an onset temperature of -12.5 [°C]. The onset temperature indicates the temperature where the surface of the sample starts to change the phase. Graphically, it is the intersection of the tangent at the point of the maximum slope and the extrapolating of the baseline [16]. The scaling of the vertical axis refers to the total curve. The non-reversing curve shows an exothermic peak.

Figure 43 shows the resulted DSC curves of mixtures with 0 [wt%], 5 [wt%] and 15 [wt%] phase-change material:

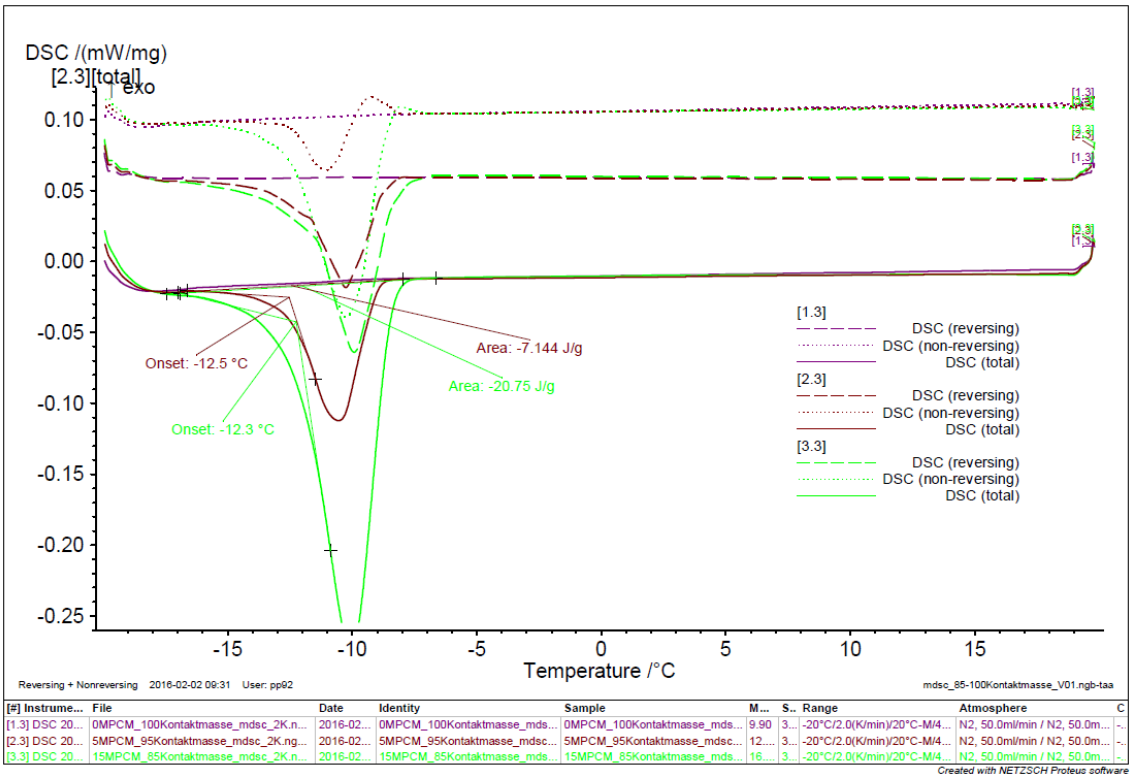

Figure 43 Temperature-modulated DSC traces at 2 [K/min] of mixtures with 0 [wt%], 5 [wt%] and 15 [wt%] phase-change material and 100 [wt%], 95 [wt%] and 85 [wt%] heat-conducting paste.

As expected, the resulted curve of the sample with 100 percent mass of the heat-conducting paste shows no phase change or rather any melting enthalpy at the measured temperature range.

The mixture of 5 [wt%] phase-change material shows a specific melting enthalpy of 7.144 [J/g] and the onset temperature is -12.5 [°C].

The onset temperature of the mixture with 15 [wt%] phase-change material is -12.3 [°C], thus it shows a deviation of 0.2 [°C] from the results of the other two sample mixtures. That can be caused by measurement errors or by a lack of thermal equilibrium in the sample. In order to be able to make precise statements, it is necessary to perform several measurements successively, but in the course of this work the results of the differential scanning calorimetry serve just as indicators and comparative values.

The specific melting enthalpy of the mixture with 15 percent by weight, amounts 20.75 [J/g].

The scaling of the vertical axis refers to the total curve and the non-reversing curve shows an exothermic peak.

The stored energy per mass has increased with increasing amount of phase-change material. Figure 44 shows the relation of the resulting specific melting enthalpy and the percentage of phase-change material:

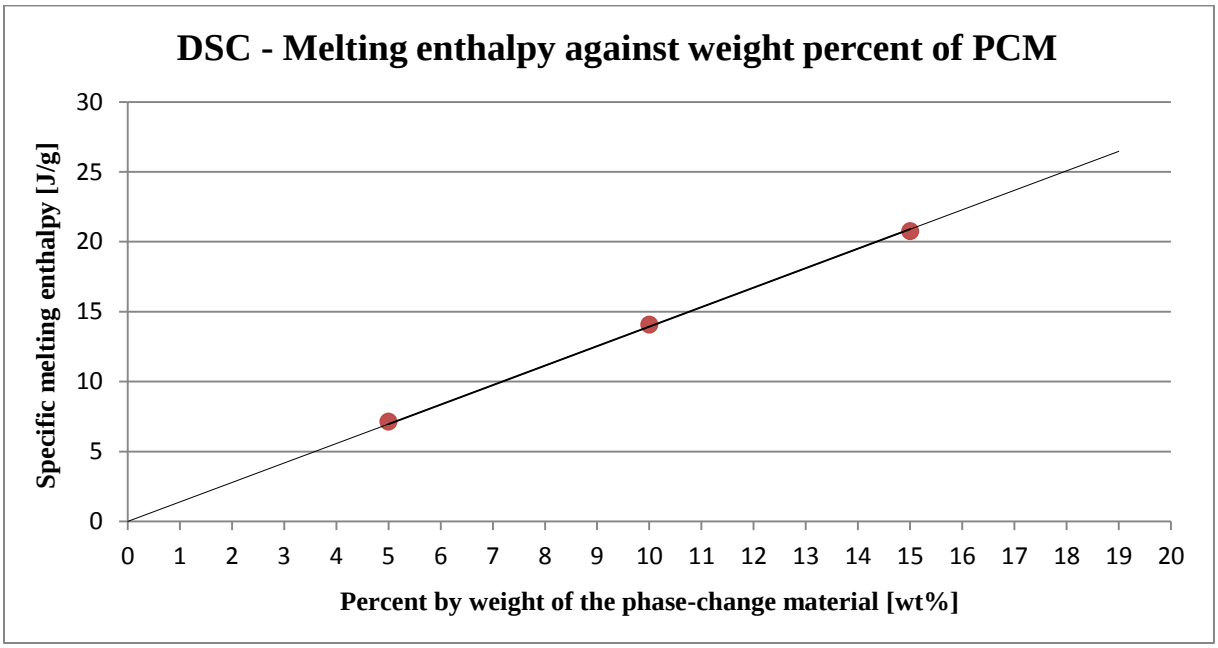

Figure 44 Relationship between the stored energy and the amount of phase-change material measured with DSC.

As expected, the diagram shows a linear relationship between the stored energy and the amount of phase-change material. The energy stored per mass increases with growing amount of phase-change material.

4.3 Evaluation of the Experimental Data

The measurement results are read in from Excel to MATLAB to start the curve-fitting procedure. Thermocouples are located at both sides of the sphere. The left side is designated as A and the right one as B. The numbering of the sensors is carried out from the inner diameter to the outer one.

4.3.1 Heat Conducting Paste as Mixing Component

4.3.1.1 0 [wt%] Phase-Change Material and 100 [wt%] Heat Conducting Paste

There is no phase change expected within the temperature range. Thus the melting enthalpy is set to zero and cannot be varied by the fitting-program. The values of the specific heat capacity, the heat transfer coefficient and the thermal conductivity are adjusted, whereby the values of the solid and liquid phases are constant as there is no phase change.

First the values of the heat transfer coefficient are determined for steady-state conditions, using the measured surface temperatures. Therefore following equation is used:

$$\dot{Q}_a = \ \propto * \pi * d^2 * \left(T_u - T_{surface}\right) = -P_{el} \qquad \text{(Eq. 42)}$$

d is the outer diameter of the sphere and amounts 151.1 [mm]. T_u [K] is the ambient temperature and $T_{surface}$ [K] is the temperature of the sphere's surface after achievement of a constant temperature distribution, which is defined as a maximal allowed temperature change of less than 0.1 [K] after an hour. The average of α is determined using the measurement data of the experiments heated with 4 and 5 [W].

The refrigerator was not opened during the increase of the heat input. Therefore, the values of α may be summarized for its determination. The table below gives the results of the heat transfer coefficient:

P_{el} [W]	T_u [°C]	$T_{surface}$ [°C]	α [W/m²·K]
4.077	-29.896	-19.546	5.508
4.077	-29.896	-20.172	5.568
4.969	-29.439	-17.332	5.722
4.969	-29.439	-18.147	6.135
Average			**5.733**

Table 7 Results of the α [W/m²·K] determined from the measured data of the sphere filled with heat conducting paste, heated with 4 and 5 [W]

The average of the thermal conductivity is determined from the measured data of the experiment heated with 4 Watt. Thereby the following equation is used [14]:

$$\dot{Q} = \lambda * 4 * \pi * \frac{(T_{layerI} - T_{layerII})}{\left(\frac{1}{r_{layerI}} - \frac{1}{r_{layerII}}\right)} \quad \text{(Eq. 43)}$$

T_{layer1} and T_{layer2} [K] are the measured temperatures and r_{layer1} and r_{layer2} [m] are the distances of the thermocouples from the center of the sphere. The table below gives the results of the thermal conductivity. The layer distance is evaluated according to the term x = $\frac{1}{r_{layer1}} - \frac{1}{r_{layer2}}$ constitutes:

P_{el} [W]	x [m^{-1}]	Temperature difference [K]	λ [W/m·K]
4.077	A 2 to 3: 22.067	5.514	1.298
	A 3 to 4: 7.649	2.776	0.894
	A 4 to 5: 4.899	1.644	0.967
	A 3 to 5: 12.548	4.420	0.921
	A 2 to 4: 34.615	8.290	1.163
	B 2 to 3: 17.365	5.251	1.073
	B 3 to 4: 8.748	2.332	1.217
	B 4 to 5: 4.484	1.233	1.180
	B 3 to 5: 13.231	3.564	1.204
	B 2 to 4: 26.112	7.583	1.117
Average:			**1.104**

Table 8 Results of λ [W/m·K] determined from the measured data of the sphere filled with pure heat conducting paste, heated with 4 [W]

Next, the value of the specific heat capacity is determined using the curve fitting of the cooling experiment without interior heating source, indicated as experiment I . λ and α are set constant. Their values are taken from table 6 and 7. Afterwards, the value of *c* is set constant during fitting the curve to results from the run heated with 4 Watt, named experiment II. The thermal conductivity and the heat transfer coefficient are adjusted. If the third decimal of the values of *c* does not change anymore, the parameters *λ* and *α* are adjusted to the curve resulted from the run heated with 4 and 5 Watt, indicated as experiment III. Table 9 shows a list of the performed experiment and the corresponding, adjusted parameters.

	Experiment	Adjusted Parameters
Experiment I	Cooling from 25 [°C] to -32[°C]	*c*
Experiment II	Heating with 4 Watt at ambient temperature of -32 [°C]	λ, α
Experiment III	Heating with 4 and 5 Watt at ambient temperature of -32 [°C]	λ, α

Table 9 List of the performed experiments with pure heat conducting paste and the corresponding, adjusted parameters.

The table below shows the trend of the results. The parameters which are adjusted in the current fitting are indicated in bold. The adjustment is finished if the third decimal points of the values of c, λ and α do not change anymore.

Number of fit-iteration	***Experiment***	***$c*10^3$ [J/kg·K]***	***λ [W/m·K]***	***α [W/ m^2·K]***
1	I	**1.300**	1.104	5.733
2	II	1.227	**1.104**	**5.733**
3	I	**1.227**	1.123	4.821
4	II	1.010	**1.123**	**4.821**
5	I	**1.010**	1.135	4.899
6	II	1.030	**1.135**	**4.899**
7	I	**1.030**	1.140	4.877
8	II	1.026	**1.140**	**4.877**
9	I	**1.026**	1.139	4.883
10	II	1.026	**1.139**	**4.883**
11	III	**1.026**	1.132	4.912
12	I	1.032	1.132	4.912
13	II	1.032	**1.132**	**4.911**
14	I	1.032	1.132	4.911

Table 10 Resulting values of specific heat capacity, thermal conductivity and of heat transfer coefficient of heat conducting paste.

The resulted values are a specific heat capacity of 1032 [J/kg·K], a thermal conductivity of 1.13 [W/m·K] and a heat transfer coefficient of 4.91 [W/m^2·K].

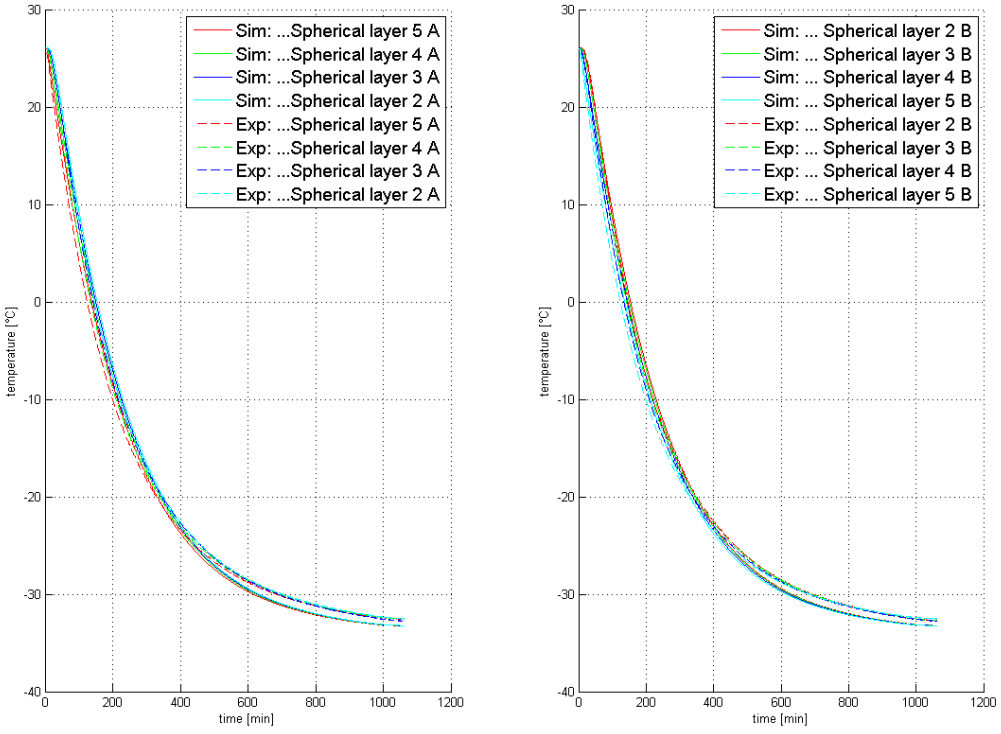

Figure 45 Measured and simulated curves of heat conducting paste cooled down to 32 [°C] without interior heat source

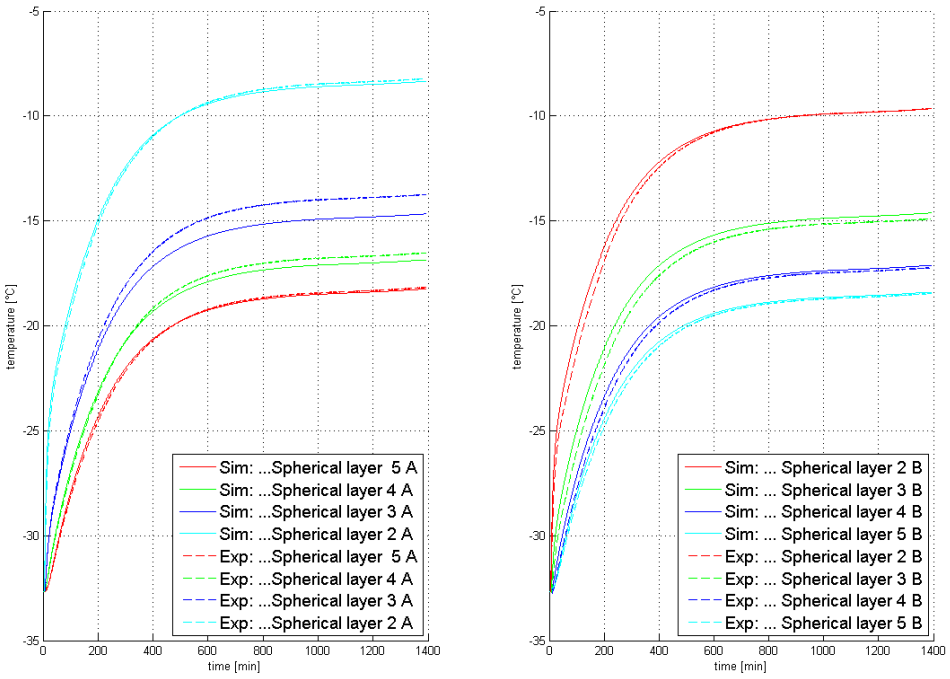

Figure 46 Measured and simulated curves of heat conducting paste cooled down to about 32 [°C] and heated with 4 Watt

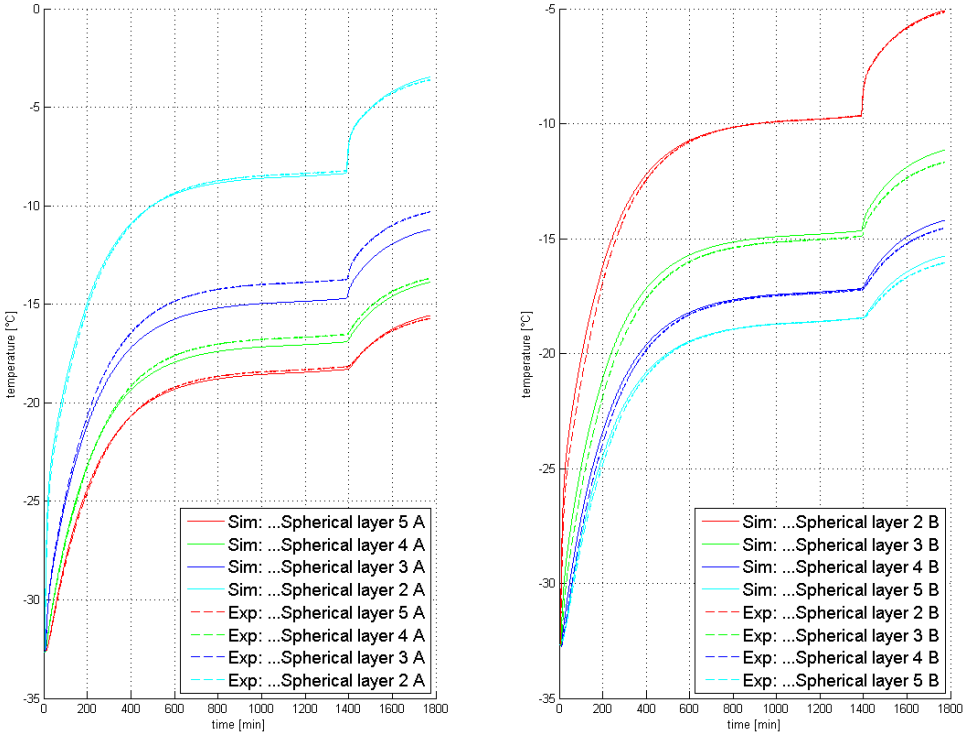

Figure 47 Measured and simulated curves of heat conducting paste cooled down to about 32 [°C] and heated with 4 and 5 Watt

The recording is stopped early by the program during the measurement with a heating power of 5 Watt. The curves fit to the measured temperature profile precisely.

4.3.1.2 10 [wt%] Phase-Change Material and 90 [wt%] Heat Conducting Paste

In contrast to the pure heat conducting paste, it is expected, that the mixture with phase-change material shows a phase change in the operating temperature range. First, the values of heat transfer coefficient and thermal conductivity are determined from the measured data again. The results are listed in the tables below:

P_{el} [W]	T_u [°C]	$T_{surface}$ [°C]	α [W/m²·K]
3.538	-29.862	-21.809	6.125
3.538	-29. 862	-22.287	6.512
3.538	-29. 862	-21.647	6.005
4.430	-29.560	-19.547	6.169
4.430	-29.560	-20.214	6.609
4.430	-29.560	-19.393	6.075
Average:			**6.249**

Table 11 Results of α [W/m²·K] determined from the measured data of the sphere filled with a mixture of 10 [wt%] phase-change material and 90 [wt%] heat conducting paste l, heated with 3.5 and 4.5 [W]

P_{el} [W]	x [m⁻¹]	Temperature difference [K]	λ [W/m·K]
4.430	A 2 to 3: 19.630	11.070	0.625
	A 3 to 4: 7.741	3.736	0.730
	A 4 to 5: 4.178	2.016	0.731
	A 3 to 5: 11.919	5.752	0.730
	A 2 to 4: 27.371	14.805	0.652
	B 2 to 4: 24.484	12.588	0.686
	B 4 to 5: 4.840	1.983	0.686
	B 2 to 5: 29.324	14.571	0.709
Average:			**0.694**

Table 12 Results of λ [W/m·K] determined from the measured data of the sphere with a mixture of 10 [wt%] phase-change material and 90 [wt%] heat conducting paste, heated with 4.5 [W]

The curve fit is started with the measurement data of the sphere, cooled down to -32[°C] without an internal heat source, indicated as experiment I, again. Thereby the values of the specific heat capacity of the solid and the liquid phase, of the melting enthalpy and of the phase transition range are determined by adjusting to the curve of experiment I. The values of the thermal conductivity and of the heat transfer coefficient are set constant and have the initial values determined from the measured data like described in the previous section.

Afterwards the values of c of both phases, of the specific melting enthalpy h_{melt} and of the melting temperature range, T_I and T_{II}, are set constant during fitting to the curve which results from the run heated with 3.5 Watt, experiment II. The thermal conductivity and the heat transfer coefficient are adjusted. If the third decimal point of the values of c, λ and α, the second decimal point of the phase-change temperature range and the value of the melting enthalpy do not change anymore, the parameters λ and α are adjusted to the curve, which results from the experiment heated with 3.5 and 4.5 Watt, indicated as experiment III.

Table 13 shows a list of the performed experiments and the corresponding, adjusted parameters.

	Experiment	Adjusted Parameters
Experiment I	Cooling from 25 [°C] to -32[°C]	c_s, c_l, h_{melt}, T_I, T_{II}
Experiment II	Heating with 3.5 Watt at ambient temperature of -32 [°C]	λ_s, λ_l, α
Experiment III	Heating with 3.5 and 4.5 Watt at ambient temperature of -32 [°C]	λ_s, λ_l, α

Table 13 List of the performed experiments with a mixture of 10 [wt%] phase-change material and 90 [wt%] heat conducting paste and the corresponding, adjusted parameters.

The table below shows the trend of the results. The adjustment is finished if the values do not change at the same decimal points as previously indicated.

Number of fit-iteration	*Experiment*	$c_s / c_l * 10^3$ [J/kg·K]	λ_s / λ_l [W/m·K]	α [W/ m^2·K]	h_{melt} [J/kg]	T_I / T_{II} [°C]
1	I	**1.140 / 1.140**	0.694 / 0.694	6.249	**20000**	**-18.00 / -12.00**
2	II	1.365 / 0.961	**0.694 / 0.694**	**6.249**	13654	-18.00 / -12.47
3	I	**1.365 / 0.961**	0.669 / 0.803	5.332	**13654**	**-18.00 / -12.47**
4	II	1.135 / 0.837	**0.669 / 0.803**	**5.332**	11781	-17.72 / -12.59
5	I	**1.135 / 0.837**	0.722 / 0.769	5.331	**11781**	**-17.72 / -12.59**
6	II	1.134 / 0.830	**0.722 / 0.769**	**5.331**	12007	-17.73 / -12.63
7	I	**1.134 / 0.830**	0.722 / 0.768	5.330	**12007**	**-17.73 / -12.63**
8	II	1.134 / 0.830	**0.722 / 0.768**	**5.330**	12006	-17.73 / -12.63
9	I	**1.134 / 0.830**	0.722 / 0.769	5.330	**12006**	**-17.73 / -12.63**
10	III	1.134 / 0.830	**0.722 / 0.769**	**5.330**	12006	-17.73 / -12.63
11	I	**1.134 / 0.830**	0.729 / 0.732	5.491	**12006**	**-17.73 / -12.63**
12	III	1.183 / 0.850	**0.729 / 0.732**	**5.491**	12388	-17.80 / -12.62
13	I	**1.183 / 0.850**	0.720 / 0.733	5.493	**12388**	**-17.80 / -12.62**
14	III	1.182 / 0.850	**0.720 / 0.733**	**5.493**	12357	-17.80 / -12.62
15	I	**1.182 / 0.850**	0.722 / 0.733	5.493	**12357**	**-17.80 / -12.62**
16	III	1.183 / 0.850	**0.722 / 0.733**	**5.493**	12364	-17.80 / -12.62
17	I	1.183 / 0.850	0.722 / 0.733	5.493	12364	-17.80 / -12.62

Table 14 Resulting values of specific heat capacity, thermal conductivity, heat transfer coefficient, melting enthalpy and phase transition range for the mixture of 10 [wt%] phase-change material and 90 [wt%] heat conducting paste.

The curve fitting, is finished if the second decimal point does not change anymore. The resulted values are a specific heat capacity of 1183 [J/kg·K] of the solid and 850 [J/kg·K] of the liquid phase, a thermal conductivity of 0.72 [W/m·K] of the solid phase and 0.73 [W/m·K]

of the liquid one. The heat transfer coefficient amounts 5.49 [W/m^2·K] and the specific melting enthalpy is 12364 [J/kg]. The phase change occurs between -17.80 and -12.62 [C°].

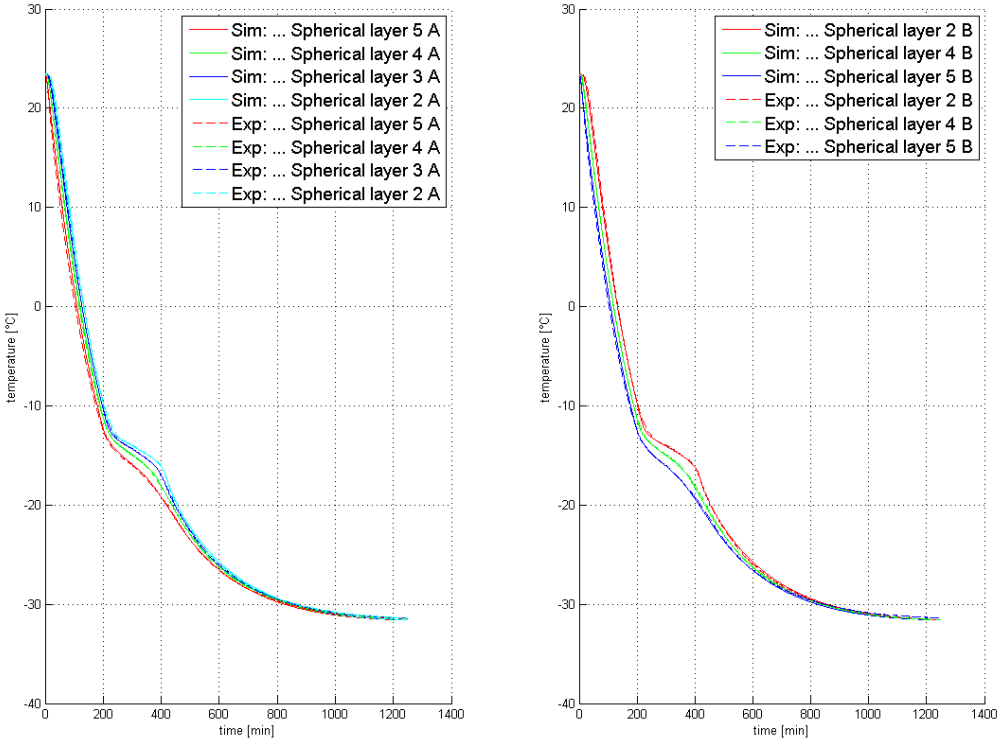

Figure 48 Measured and simulated curves of the mixture of 10 [wt%] phase-change material and [90%] heat conducting paste cooled down to - 32 [°C] without interior heat source

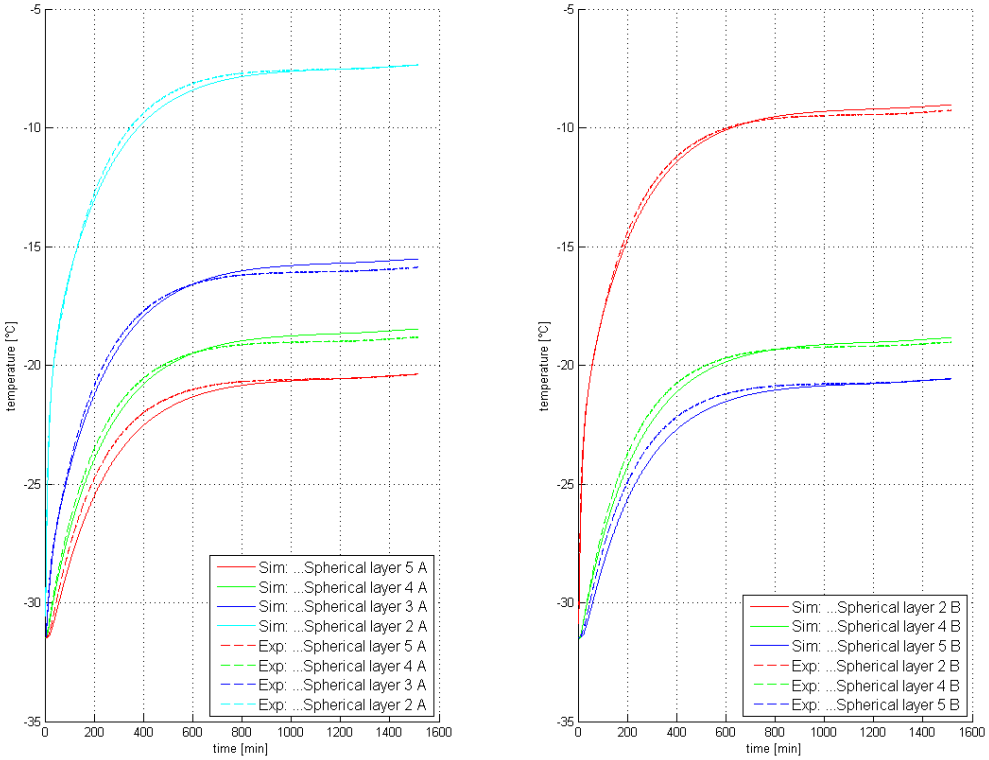

Figure 49 Measured and simulated curves of the mixture of 10 [wt%] phase-change material and [90%] heat conducting paste cooled down to -32 [°C] heated with 3.5 [W]

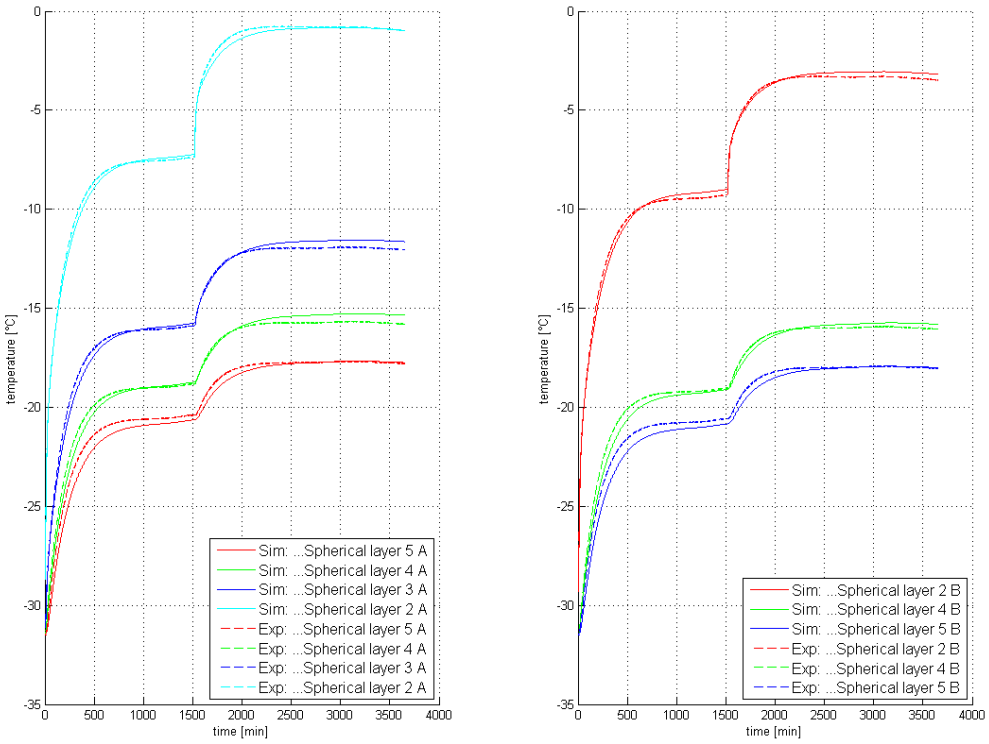

Figure 50 Measured and simulated curves of the mixture of 10 [wt%] phase-change material and 90[wt%] heat conducting paste cooled down to -32 [°C] heated with 3.5 and 4.5 [W]

The simulated temperatures follow the measured temperature profile closely.

Figure 51 shows the measured temperature profile of the mixture cooled down to - 32 [°C] without interior heat source over the thermocouples distances of side A.

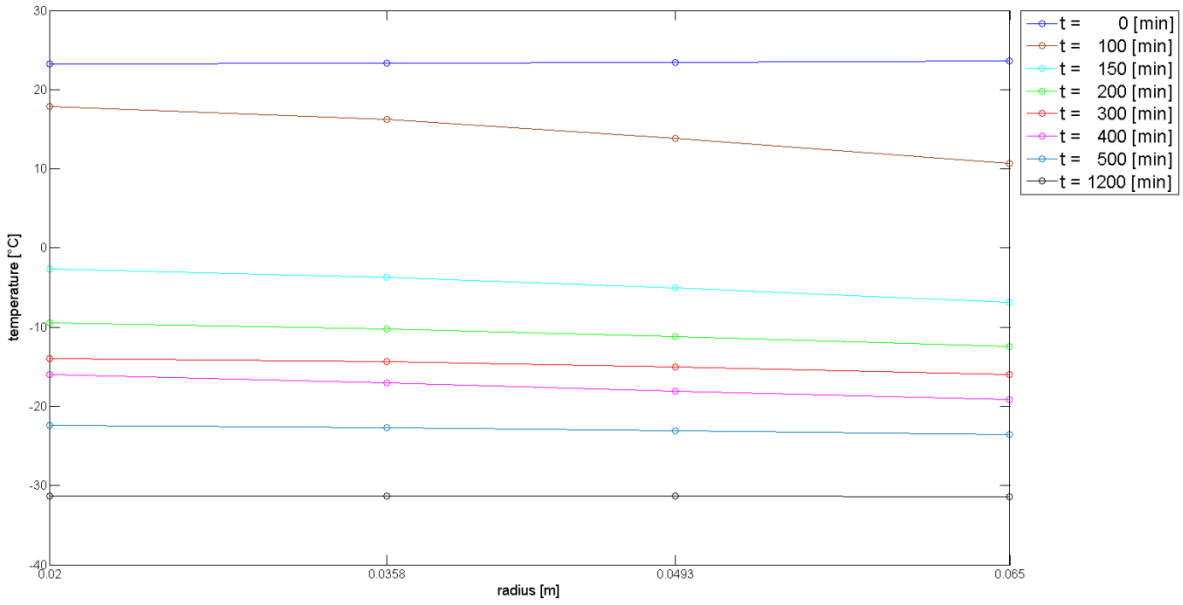

Figure 51 Measured temperature profile of the mixture cooled down to - 32 [°C] without interior heat source over the thermocouples distances (side A)

Phase change occurs in all layers after 300 minutes. The temperature profile is flatter than the curve after 400 minutes.

4.3.2 Oil as Mixing Component

4.3.2.1 55 [wt%] Phase-Change Material and 45 [wt%] Oil

It is expected, that this mixture shows a higher melting enthalpy and a lower thermal conductivity than the mixture with 10 [wt%] phase-change material and 90 [wt%] heat conducting paste. The outer diameter of the sphere amounts 203.5 [mm]. The values of α and of λ are determined from the measured data again. λ is determined from the experiment heated with 4 Watt. The results are listed in the tables below.

P_{el} [W]	T_u [°C]	$T_{surface}$ [°C]	α [W/m²·K]
4.051	-29.074	-24.536	6.861
4.051	-29.074	-23.164	5.268
4.051	-29.074	-22.564	4.783
6.192	-28.211	-21.925	7.572
6.192	-28.211	-18.814	5.065
6.192	-28.211	-19.567	5.506
7.943	-28.046	-20.131	7.713
7.943	-28.046	-17.183	5.620
7.943	-28.046	-16.034	5.083
Average			**5.941**

Table 15 Results of α [W/m²·K] determined from the measured data of the sphere filled with a mixture of 55 [wt%] phase-change material and 45 [wt%] oil, heated with 4, 6 and 8 [W]

P_{el} [W]	x [m⁻¹]	Temperature difference [K]	λ [W/m·K]
4.051	A 2 to 3: 8.332	10.082	0.266
	A 2 to 4: 13.364	13.084	0.329
	A 2 to 5: 16.623	14.926	0.359
	A 2 to 6: 18.818	16.294	0.372
	A 2 to 7: 20.583	17.438	0.381
	A 3 to 4: 5.031	3.002	0.540
	A 3 to 5: 8.291	4.844	0.552
	A 3 to 6: 10.486	6.212	0.544
	A 3 to 7: 12.250	7.356	0.537
	A 4 to 5: 3.260	1.842	0.571
	A 4 to 6: 5.455	3.209	0.548
	A 4 to 7: 7.219	4.354	0.535
	A 5 to 6: 2.195	1.368	0.517
	A 5 to 7: 3.960	2.512	0.508
	A 6 to 7: 1.765	1.145	0.497
	B 2 to 3: 10.878	10.291	0.341
	B 2 to 4: 14.578	12.883	0.365
	B 2 to 6: 19.991	15.951	0.404
	B 2 to 7: 21.691	17.041	0.410
	B 3 to 4: 3.700	2.591	0.460
	B 3 to 6: 9.112	5.659	0.519
	B 3 to 7: 10.813	6.749	0.516
	B 4 to 6: 5.413	3.068	0.569
	B 4 to 7: 7.113	4.158	0.551
	B 6 to 7: 1.700	1.090	0.503
Average:			**0.468**

Table 16 Results of λ [W/m·K] determined from the measured data of the sphere filled with a mixture of 55 [wt%] phase-change material and 45 [wt%] oil, heated with 4 [W]

The values of the thermal conductivity determined from the measured data vary considerably. The curve fit is started with the measurement data of the sphere cooled down to -32[°C] without in internal heat source, indicated as experiment I again. Thereby the values of c of the solid and the liquid phase, of h_{melt} and of the phase transition range are determined by calibration of the one-dimensional model with data from experiment I. The values of λ of both phases and of α are set constant and have the initial values determined from the measured data. Afterwards, the values of c of both phases, of the melting enthalpy h_{melt} and of the melting temperature range, T_I and T_{II}, are set constant during fitting the curve resulted from the run heated with 2.5, experiment II. λ and α are adjusted to the curve resulted from the run heated with 2.5 and 4 Watt, indicated as experiment III, if the values do not change at the same decimals as indicated in the previous experiments. Table 17 shows a list of the performed experiment and the corresponding, adjusted parameters.

	Experiment	**Adjusted Parameters**
Experiment I	Cooling from 25 [°C] to -32[°C]	c_s, c_l, h_{melt}, T_I, T_{II}
Experiment II	Heating with 2.5 Watt at ambient temperature of -32 [°C]	λ_s, λ_l, α
Experiment III	Heating with 2.5 and 4 Watt at ambient temperature of -32 [°C]	λ_s, λ_l, α

Table 17 List of the performed experiments with a mixture of 55 [wt%] phase-change material and 45 [wt%] oil and the corresponding, adjusted parameters.

The table below shows the results. The adjustment is finished if the values do not change at the same decimals as indicated in the previous experiments.

Number of fit-iteration	***Experiment***	$c_s / c_l * 10^3$ **[J/kg·K]**	λ_s / λ_l **[W/m·K]**	α **[W/ m²·K]**	h_{melt} **[J/kg]**	T_I / T_{II} **[°C]**
1	I	**1.700 / 1.700**	0.470 / 0.470	5.941	**70000**	**-17.80 / -12.62**
2	II	3.751 / 2.913	**0.470 / 0.470**	**5.941**	95921	-21.43 / -9.09
3	I	**3.751 / 2.913**	0.210 / 0.450	3.227	**95921**	**-21.43 / -9.09**
4	II	1.789 / 1.755	**0.210 / 0.450**	**3.227**	49996	-20.89 / -8.87
5	I	**1.789 / 1.755**	0.308 / 0.256	4.896	**49996**	**-20.89 / -8.87**
6	II	2.873 / 1.961	**0.308 / 0.256**	**4.896**	73321	-21.30 / -9.48
7	I	**2.873 / 1.961**	0.249 / 0.389	4.162	**73321**	**-21.30 / -9.48**
8	II	2.374 / 2.05	**0.249 / 0.389**	**4.162**	62360	-21.21 / -8.98
9	I	**2.374 / 2.050**	0.275 / 0.346	4.508	**62360**	**-21.21 / -8.98**
10	II	2.206 / 2.081	**0.275 / 0.346**	**4.508**	67624	-21.32 / -9.09
11	I	**2.206 / 2.081**	0.279 / 0.332	4.540	**67624**	**-21.32 / -9.09**
12	II	2.263 / 2.055	**0.279 / 0.332**	**4.540**	68237	-21.37 / -9.10

Number of fit-iteration	*Experiment*	$c_s / c_l * 10^3$ [J/kg·K]	λ_s / λ_l [W/m·K]	α [W/ m^2·K]	h_{melt} [J/kg]	T_I / T_{II} [°C]
13	I	**2.263 / 2.055**	0.276 / 0.338	4.511	**68237**	**-21.37 / -9.10**
14	II	2.608 / 2.061	**0.276 / 0.338**	**4.511**	67726	-21.35 / -9.09
15	I	**2.608 / 2.061**	0.262 / 0.370	4.356	**67726**	**-21.35 / -9.09**
16	II	2.504 / 2.085	**0.262 / 0.370**	**4.356**	65107	-21.23 / -9.07
17	I	**2.504 / 2.085**	0.268 / 0.360	4.433	**65107**	**-21.23 / -9.07**
18	II	2.555 / 2.090	**0.268 / 0.360**	**4.433**	66341	-21.28 / -9.07
19	I	**2.555 / 2.090**	0.265 / 0.365	4.398	**66341**	**-21.28 / -9.07**
20	II	2.585 / 2.126	**0.265 / 0.365**	**4.398**	66765	-21.24 / -9.09
21	I	**2.585 / 2.126**	0.264 / 0.367	4.379	**66765**	**-21.24 / -9.09**
22	II	2.520 / 2.087	**0.264 / 0.367**	**4.379**	65483	-21.25 / -9.07
23	I	**2.520 / 2.087**	0.267 / 0.361	4.420	**65483**	**-21.25 / -9.07**
24	II	2.546 / 2.087	**0.267 / 0.361**	**4.420**	66127	-21.27 / -9.07
25	I	**2.546 / 2.087**	0.265 / 0.364	4.403	**66127**	**-21.27 / -9.07**
26	II	2.534 / 2.089	**0.265 / 0.364**	**4.403**	65779	-21.25 / -9.08
27	I	**2.534 / 2.089**	0.266 / 0.363	4.412	**65779**	**-21.25 / -9.08**
28	II	2.541 / 2.090	**0.266 / 0.363**	**4.412**	65953	-21.26 / -9.08
29	I	**2.541 / 2.090**	0.266 / 0.363	4.406	**65953**	**-21.26 / -9.08**
30	II	2.538 / 2.088	**0.266 / 0.363**	**4.406**	65885	-21.26 / -9.08
31	I	**2.538 / 2.088**	0.266 / 0.363	4.408	**65885**	**-21.26 / -9.08**
32	II	2.539 / 2.088	**0.266 / 0.363**	**4.408**	65907	-21.26 / -9.08
33	III	2.539 / 2.088	**0.266 / 0.363**	**4.408**	65907	-21.26 / -9.08
34	I	**2.539 / 2.088**	0.284 / 0.430	5.195	**65907**	**-21.26 / -9.08**
35	III	2.990 / 2.544	**0.284 / 0.430**	**5.195**	75334	-21.10 / -9.12
36	I	**2.990 / 2.544**	0.275 / 0.432	5.039	**75334**	**-21.10 / -9.12**
37	III	2.892 / 2.490	**0.275 / 0.432**	**5.039**	73058	-21.08 / -9.11
38	I	**2.892 / 2.490**	0.278 / 0.432	5.079	**73058**	**-21.08 / -9.11**
39	III	2.920 / 2.506	**0.278 / 0.432**	**5.079**	73691	-21.08 / -9.11

Number of fit-iteration	*Experiment*	$c_s / c_l * 10^3$ [J/kg·K]	λ_s / λ_l [W/m·K]	α [W/ m^2·K]	h_{melt} [J/kg]	T_I / T_{II} [°C]
40	I	**2.920 / 2.506**	0.278 / 0.432	5.070	**73691**	**-21.08 / -9.11**
41	III	2.915 / 2.502	**0.278 / 0.432**	**5.070**	73599	-21.08 / -9.11
42	I	**2.915 / 2.502**	0.277 / 0.432	5.071	**73599**	**-21.08 / -9.11**
43	III	2.913 / 2.503	**0.277 / 0.432**	**5.071**	73530	-21.08 / -9.11
44	I	2.913 / 2.503	0.277 / 0.432	5.071	73530	-21.08 / -9.11

Table 18 Resulting values of specific heat capacity, of thermal conductivity, of heat transfer coefficient, of melting enthalpy and of phase transition range of the mixture of 55 [wt%] phase-change material and 45 [wt%] oil.

The resulted value of specific heat capacity amounts 2913 [J/kg·K] of the solid and 2503 [J/kg·K] of the liquid phase. The thermal conductivity is 0.28 [W/m·K] of the solid phase and 0.43 [W/m·K] of the liquid one. The heat transfer coefficient amounts 5.07 [W/m^2·K] and the melting enthalpy is 73530 [J/kg]. The phase change occurs between -21.08 and -9.11 [C°].

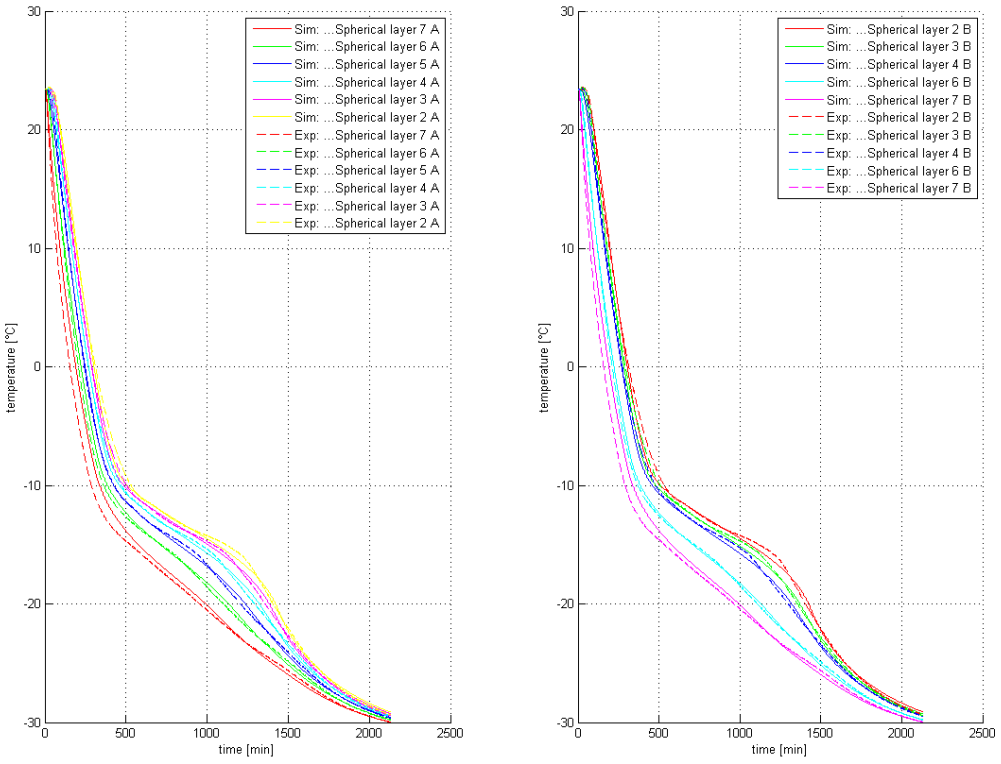

Figure 52 Measured and simulated curves of the mixture of 55 [wt%] phase-change material and 45[wt%] oil cooled down to about -32 [°C] without interior heat source

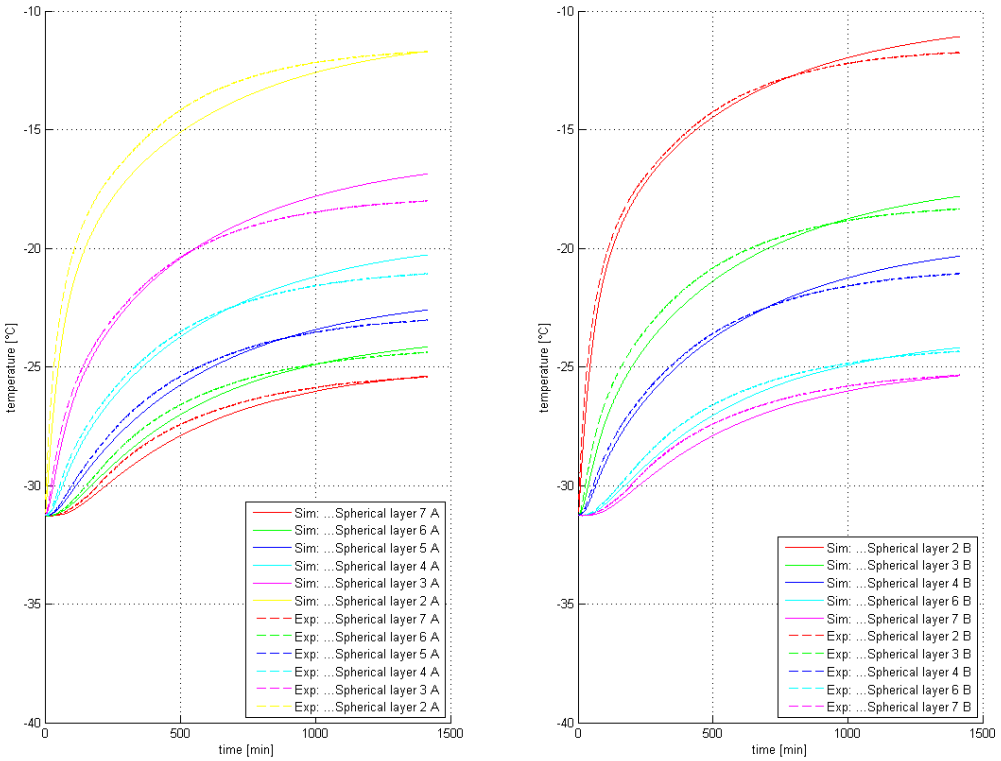

Figure 53 Measured and simulated curves of the mixture of 55 [wt%] phase-change material and 45[wt%] oil cooled down to about -32 [°C] and heated with 2.5 [W]

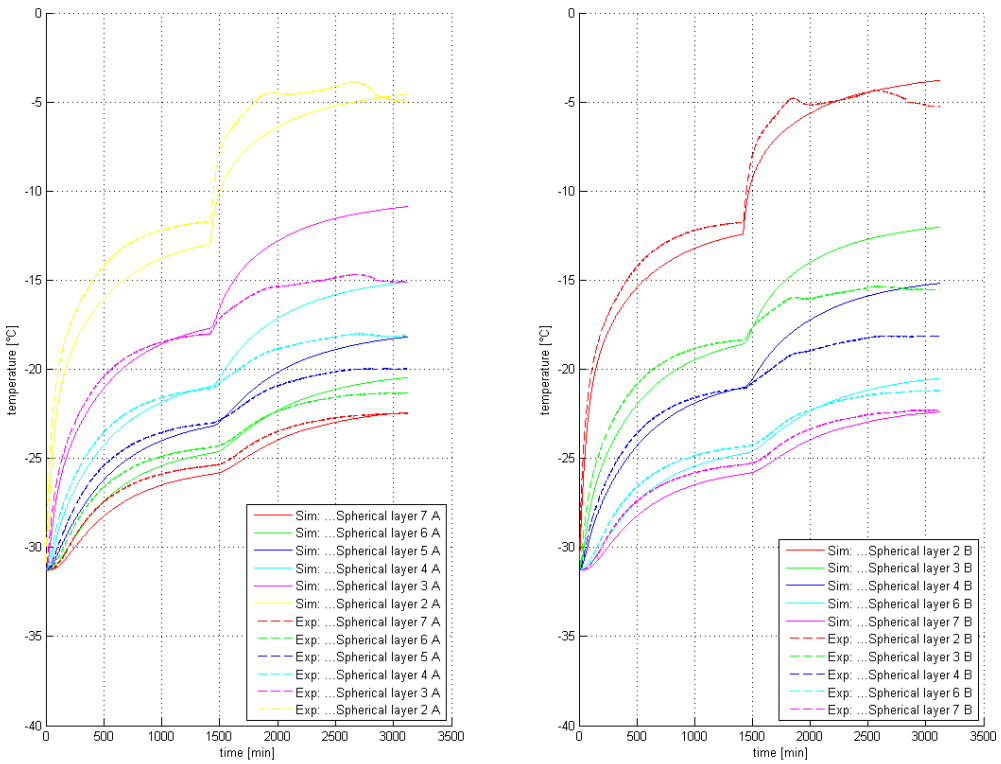

Figure 54 Measured and simulated curves of the mixture of 55 [wt%] phase-change material and 45[wt%] oil cooled down to about -32 [°C] and heated with 2.5 and 4 [W]

The simulated temperatures don´t follow the measured temperature profile precisely. It may be caused by the convection that possibly occurred through large temperature differences and thermal expansion of the oil. Effects like convection are not describable with the model used in this study.

4.3.2.2 44 [wt%] Phase-Change Material, 36 [wt%] Oil and 20 [wt%] Aluminium Powder

It is expected, that the mixture with 20 [wt%] aluminium powder shows a higher thermal conductivity than the previous examined mixtures. The outer diameter of the sphere amounts 203.5 [mm]. The values of the heat transfer coefficient and of the thermal conductivity are determined from the measured data one more time. λ is determined from the run heated with 10 Watt. The results are listed in the tables below.

P_{el} [W]	T_u [°C]	$T_{surface}$ [°C]	α [W/m²·K]
1.039	-28.628	-27.355	6.273
1.039	-28.628	-27.207	5.620
1.039	-28.628	-27.198	5.585
7.804	-27.023	-17.948	6.610
7.804	-27.023	-18.200	6.799
7.804	-27.023	-17.476	6.283
9.964	-25.465	-14.411	6.928
9.964	-25.465	-14.884	7.238
9.964	-25.465	-13.905	6.625
Average			**6.440**

Table 19 Results of the α [W/m²·K] determined from the measured data of the sphere filled with a mixture of 44 [wt%] phase change material, 36 [wt%] oil and 20 [wt%] aluminium powder, heated with 1, 8 and 10 [W]

P_{el} [W]	Layer distance [m⁻¹]	Temperature difference [K]	λ [W/m·K]
7.804	A 2 to 4: 12.487	25.706	0.302
	A 2 to 5: 15.589	29.772	0.325
	A 2 to 6: 17.665	32.581	0.337
	A 2 to 7: 19.527	34.985	0.347
	A 4 to 5: 3.102	4.066	0.474
	A 4 to 6: 5.178	6.875	0.468
	A 4 to 7: 7.040	9.279	0.471
	A 5 to 6: 2.075	2.810	0.459
	A 5 to 7: 3.937	5.213	0.469
	A 6 to 7: 1.862	2.403	0.481
	B 2 to 3: 10.974	21.105	0.323
	B 2 to 4: 15.010	27.911	0.334
	B 2 to 6: 20.367	34.835	0.363
	B 2 to 7: 22.075	37.288	0.368
	B 3 to 4: 4.037	6.807	0.368
	B 3 to 6: 9.393	13.730	0.425
	B 3 to 7: 11.101	16.183	0.426
	B 4 to 6: 5.356	6.924	0.480
	B 4 to 7: 7.065	9.377	0.468
	B 6 to 7: 1.708	2.453	0.433
Average:			**0.413**

Table 20 Results of λ [W/m·K] determined from the measured data of the sphere filled with a mixture of 44 [wt%] phase change material, 36 [wt%] oil and 20 [wt%] aluminium powder, heated with 8 [W]

The curve fit is started with the measurement data of the sphere cooled down to -32 [°C] without in internal heat source, indicated as experiment I, again. Thereby, the values of c of the solid and the liquid phase, of h_{melt} and of the phase transition range are determined by calibration of the 1d-model with data from experiment I. The values of λ of both phases and of α are set constant and have the initial values determined from the measured data. Afterwards the values of c of both phases, of the melting enthalpy h_{melt} and of T_I and T_{II}, are set constant during fitting the curve resulted from the run heated with 8 Watt, experiment II. The adjustment is finished if the values do not change at the same decimal point as indicated in the previous experiments. Table 21 shows a list of the performed experiment and the corresponding, adjusted parameters.

	Experiment	**Adjusted Parameters**
Experiment I	Cooling from 25 [°C] to -32[°C]	c_s, c_l, h_{melt}, T_I, T_{II}
Experiment II	Heating with 8 Watt at ambient temperature of -32 [°C]	λ_s, λ_l, α

Table 21 List of the performed experiments with a mixture of 44 [wt%] phase change material, 36 [wt%] oil and 20 [wt%] aluminium powder and the corresponding, adjusted parameters.

The table below shows the trend of the results, whereby the parameters that are adjusted, are set to bold.

Number of fit-iteration	***Experiment***	$c_s / c_l * 10^3$ **[J/kg·K]**	λ_s / λ_l **[W/m·K]**	α **[W/ m²·K]**	h_{melt} **[J/kg]**	T_I / T_{II} **[°C]**
1	I	**1.700 / 1.700**	0.413 / 0.413	6.440	**60000**	**-21.00 / -9.00**
2	II	3.412 / 2.558	**0.413 / 0.413**	**6.440**	85465	-21.53 / -9.16
3	I	**3.412 / 2.558**	0.461 / 0.334	5.049	**85465**	**-21.53 / -9.16**
4	II	2.841 / 1.957	**0.461 / 0.334**	**5.049**	73462	-21.37 / -9.28
5	I	**2.841 / 1.957**	0.561 / 0.332	5.222	**73462**	**-21.37 / -9.28**
6	II	3.047 / 2.001	**0.561 / 0.332**	**5.222**	79491	-21.46 / -9.23
7	I	**3.047 / 2.001**	0.521 / 0.332	5.186	**79491**	**-21.46 / -9.23**
8	II	2.986 / 1.990	**0.521 / 0.332**	**5.186**	77519	-21.43 / -9.26
9	I	**2.986 / 1.990**	0.532 / 0.332	5.205	**77519**	**-21.43 /-9.26**
10	II	3.008 / 1.996	**0.532 / 0.332**	**5.205**	78167	-21.44 / -9.25
11	I	**3.008 / 1.996**	0.528 / 0.332	5.198	**78167**	**-21.44 / -9.25**
12	II	3.000 / 1.994	**0.528 / 0.332**	**5.198**	77930	-21.43 / -9.26
13	I	**3.000 / 1.994**	0.529 / 0.332	5.198	**77930**	**-21.43 / -9.26**
14	II	3.001 / 1.994	**0.529 / 0.332**	**5.198**	77978	-21.43 / -9.26

Number of fit-iteration	*Experiment*	$c_s / c_l * 10^3$ [J/kg·K]	λ_s / λ_l [W/m·K]	α [W/ m^2·K]	h_{melt} [J/kg]	T_I / T_{II} [°C]
15	I	**3.001 / 1.994**	0.529 / 0.332	5.201	**77978**	**-21.43 / -9.26**
16	II	3.002 / 1.995	**0.529 / 0.332**	**5.201**	78004	-21.43 / -9.26
17	I	**3.002 / 1.995**	0.529 / 0.332	5.200	**78004**	**-21.43 / -9.26**
18	II	3.002 / 1.995	**0.529 / 0.332**	**5.200**	77992	-21.43 / -9.26
19	I	3.002 / 1.995	0.529 / 0.332	5.200	77992	-21.43 / -9.26

Table 22 Values of specific heat capacity, of thermal conductivity, of heat transfer coefficient, of melting enthalpy and of phase transition range of the mixture of 44 [wt%] phase change material, 36 [wt%] oil and 20 [wt%] aluminium powder.

The specific heat capacity amounts 3002 [J/kg·K] of the solid and 1995 [J/kg·K] of the liquid phase. The thermal conductivity amounts 0.53 [W/m·K] of the solid phase and 0.33 [W/m·K] of the liquid one. The heat transfer coefficient amounts 5.20 [W/m^2·K] and the melting enthalpy is 77992 [J/kg]. The phase change occurs between -21.43 and -9.26 [C°].

Figure 55 and Figure 56 show the measured and fitted temperature profile of the sphere cooled down to about -32 [°C] and then heated with 8 Watt.

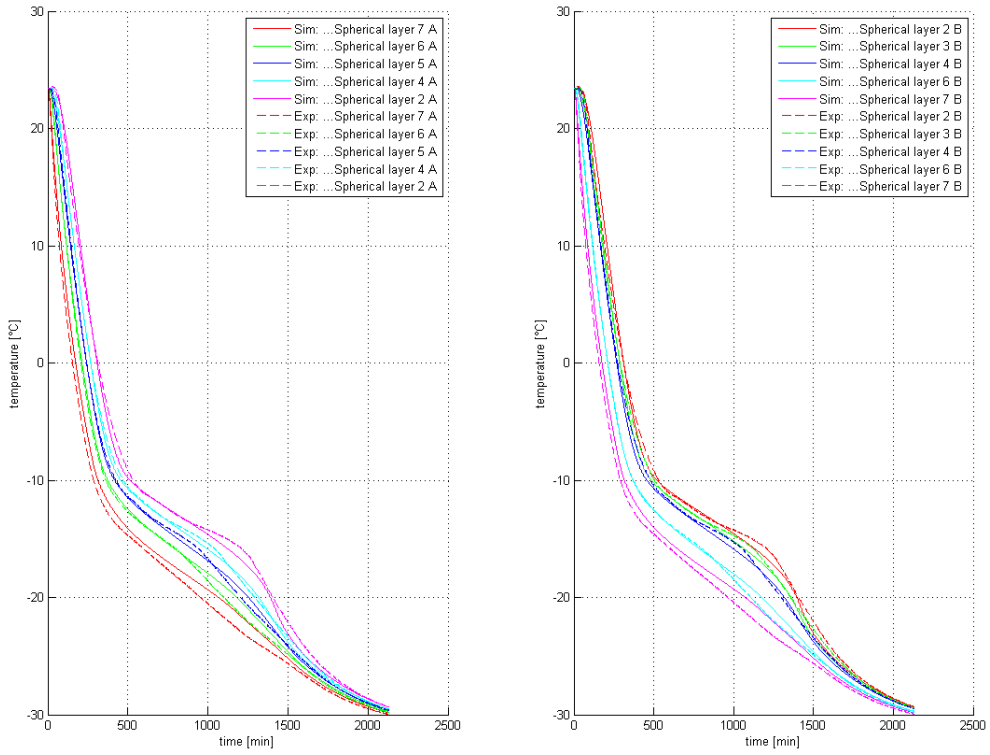

Figure 55 Measured and simulated curves of the mixture of 44 [wt%] phase-change material, 36 [wt%] oil and 20 [wt%] aluminium powder cooled down to about -32 [°C]

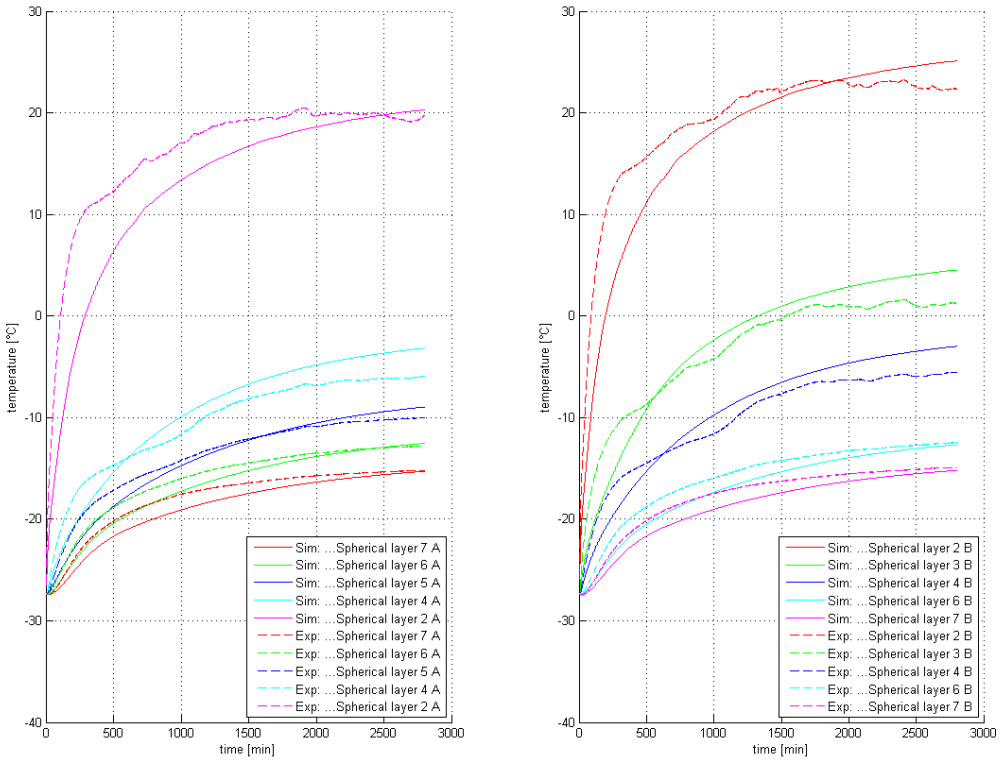

Figure 56 Measured and simulated curves of the mixture of 44 [wt%] phase-change material, 36 [wt%] oil and 20 [wt%] aluminium powder cooled down to about -32 [°C] and heated with 8 [W]

The simulated temperatures don´t follow the measured temperature profile well. The model cannot fit the curves to the fluctuation of the measured data. It may be caused by natural convection again.

4.4 Summary of the Results and Discussion

Since the manufacturer does not provide any data about the specific heat capacity, thermal conductivity and melting enthalpy of the phase-change material, a validation of the calculation model is not possible. However, the specific melting enthalpy of the mixture of 10 [wt%] phase-change material and 90 [wt%] heat conducting paste was measured additional by differential scanning calorimeter. All results are discussed in the current chapter.

The table below, shows the final values of the specific heat capacity, of the thermal conductivity, of the heat transfer coefficient, of the specific melting enthalpy and of the phase transition temperature range of the examined mixtures. D_{Sphere} is the outer diameter of the steel sphere.

Components	**D_{Sphere} [m]**	**Results**							
		$c_s * 10^3$ [J/kg·K]	$c_{l*} 10^3$ [J/kg·K]	λ_s [W/m·K]	λ_l [W/m·K]	α [W/m²·K]	h_{melt} [J/kg]	T_I [°C]	T_{II} [°C]
Heat-conducting paste	0.150	1.026		1.139		4.883	-	-	-
10 [wt%] phase-change material & 90 [wt%] heat-conducting paste	0.150	1.183	0.850	0.722	0.733	5.493	12364	-17.80	-12.62
55 [wt%] phase-change material & 45 [wt%] oil	0.200	2.913	2.503	0.277	0.432	5.071	73530	-21.08	-9.11
44 [wt%] phase-change material & 36 [wt%] oil & 20 [wt%] aluminium powder	0.200	3.002	1.995	0.529	0.332	5.200	77992	-21.43	-9.26

Table 23 Summary of all results of the performed experiments

4.4.1 Specific Heat Capacity

The results of all measurements show that the specific heat capacity of the solid phase is greater than of the liquid phase.

According to the literature an approximate value of 1800 [J/kg·K] is acceptable for alkanes having a melting point at about – 10 [°C]. The value decreases with descending number of C atoms [20]. Considering the *c* of the pure heat conducting paste of 1026 [J/kg·K] and the approximate value for alkanes, a *c* of 1103 [J/kg·K] results for the mixture of 10 [wt%] phase-

change material and 90 [wt%] heat conducting paste. The values of *c* resulting from the calibrated sphere model, are in the same range.

Considering the results from the mixtures with oil, it has to be mentioned again, that free convection may have occurred during the measurements. The material properties of the engine oil SAE 0W30, determined with KULI software [21], are available and yield a *c* of about 1783 [J/kg·K] between a temperature range of 0 [°C] and -20 [°C]. Considering the approximate value of *c* for alkanes and the *c* value of oil, a specific heat capacity of 1792 [J/kg·K] results for the mixture of 55 [wt%] phase-change material and 45 [wt%] oil. The values of *c* resulting from the calibrated sphere model, are not in the same range. The specific heat capacity of aluminium at 0 [°C] amounts 837 [J/kg·K] [15]. Hence, the values of *c* should be smaller than of the mixtures with 55 [wt%] phase-change material and 45 [wt%] oil. This is only the case for the liquid phase.

4.4.2 Thermal Conductivity

As already mentioned, paraffins have a low conductivity. The measurements performed with heat conducting paste, show as expected a lower λ after adding 10 [wt%] phase change material.

According to the available data determined with the KULI software [21], the thermal conductivity of the oil is very low and amounts about 0.138 [W/m·K] between a temperature range of 0 [°C] and -20 [°C]. The measurement results show a poor thermal conductivity of the mixture with 55 [wt%] phase-change material and 45 [wt%] oil compared with the measurements performed with heat conducting paste. However, the measurements results of the mixtures with oil are not as expected. Although the thermal conductivity of the solid phase of the mixture including aluminium is higher than of the mixture without one, but regarding the liquid phase it is reversed. The question, if λ of the solid phase or of the liquid phase is higher, cannot be answered with reference to the present results. Furthermore, the values of λ_s and λ_l resulted from the mixture with 10 [wt%] phase-change material and 90 [wt%] heat-conducting paste are close together. The examination of the measurement uncertainties, described in the next chapter, shows, that a deviation of the distance of the thermocouples may have greater impacts on the thermal conductivity of the liquid phase than of the solid one.

4.4.3 Phase Change Temperature Range, Subcooling and Hysteresis

The phase change temperature range of the mixture with heat conducting paste is narrower than of the mixture with engine oil, although it was expected to be the same. However, the average temperature is approximately the same and amounts -15 [°C]. The difference on both sides amounts about 3.4 [°C]. The reason for that could be that the curves don´t fit the measured temperature profile of the mixtures precisely. Another reason could be the size of the sphere. If there is no thermal equilibrium in the spherical layer, the calculation model may provide erroneous results. As already mentioned, free convection may have occurred during the measurements of the mixtures with oil, which also can lead to faulty results.

The measured cooling curve of all phase change material mixtures shows no subcooling during crystallisation. Subcooling is the effect that a material is not solidified although the melting temperature is already reached. A temperature significantly below the melting temperature must be reached or a nucleating agent must be added to start crystallisation [4].

Hysteresis is usually understood as a property of the sample. It may be caused by subcooling or slow heat release during cooling because the crystal lattice forms very slowly [4]. The heating curve of the mixture with 10 [wt%] phase change material and 90 [wt%] heat conducting paste measured with the differential scanning calorimetry, results an onset temperature of -12.5 [°C]. The offset temperature is defined as -8.8 [°C]. The cooling curve of the mixture measured with the spherical model results a phase change temperature range of -17.8 [°C] and -12.6 [°C]. However, in order to exclude apparent hysteresis, which is caused by non-isothermal conditions in the sample [4], several measurements with varying heating rates should be performed with DSC. Furthermore, the size of the sphere might be varied and compared to ensure isothermal conditions inside the sample or the spherical layers as well.

However, the cooling curve and the heating curve of the phase change material and oil mixtures are measured with the spherical measurement setup and show a hysteresis as well. Figure 57 shows the cooling and the heating curve of the mixture with 44 [wt%] phase-change material, 36 [wt%] oil and 20 [wt%] aluminium powder:

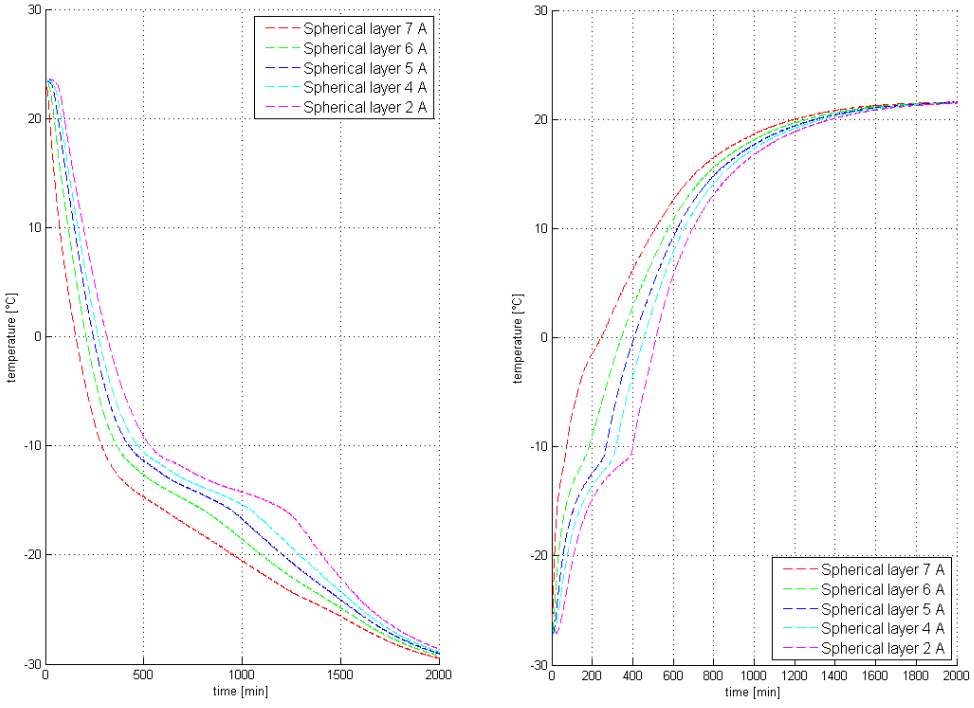

Figure 57 Cooling (left) and warming (right) curves of the mixture with 44 [wt%] phase-change material, 36 [wt%] oil and 20 [wt%] aluminium powder of side A.

In addition to the comparison of the measurements with the sphere model and DSC of the mixture with heat conducting paste and phase-change material, this diagram also shows a hysteresis. It can be seen that the heat release during cooling is slower than the heat supply

during heating. As already mentioned it may be caused by slow forming of the crystal lattice. By means of simulations with the calculation model, a phase-change temperature range of -14 [°C] and -5 [°C] is estimated, which is a broader range again, than measured with heat conducting paste, resulting a temperature range of -12.5 [°C] and -8.8 [°C].

4.4.4 Melting Enthalpy

Figure 58 shows the relation of the resulted melting enthalpy and the percentage of phase-change material measured with the calibrated sphere model. The diagram also includes the measurement results of the differential scanning calorimeter. In the course of this measurement, heat conducting paste is mixed with 5 [wt%], 10 [wt%] and 15 [wt%] phase-change material.

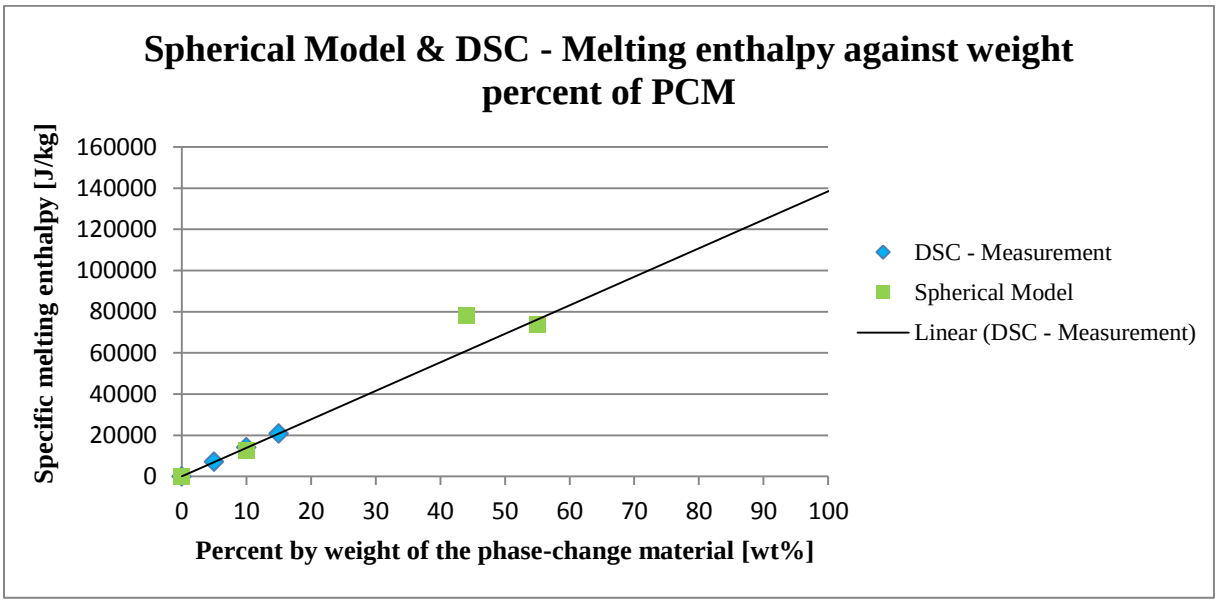

Figure 58 Relationship between the stored energy and the amount of phase-change material measured with spherical model and differential scanning calorimeter

As already mentioned, the stored energy per mass has to be increased with increasing share of phase-change material. However, the value of the specific melting enthalpy of the mixture with 44 [wt%] phase change material is higher than of the mixture with 55 [wt%]. That can be caused by errors during measuring of the weight of the components. Furthermore, the curves don´t fit to the measured temperature profile precisely.

The specific melting enthalpy of the mixture of 10 [wt%] phase-change material and 90 [wt%] heat conducting paste is measured additional by a differential scanning calorimeter, which results in a h_{melt} of 14070 [J/kg]. The difference of the results of the DSC-measurement and of the calibrated sphere model amounts 1706 [J/kg]. It should be noted, that not the same sample was used. Therefore, this deviation of the measurement results can be caused by mixing errors.

4.4.5 Heat Transfer Coefficient

The results of α determined from the Nusselt-number for free convection, based on the correlations from the VDI Wärmeatlas [15] and from measured surface temperature and heating power are compared with the outputs of α by the curve fit. The heat transfer coefficient based on the correlations from the VDI Wärmeatlas [15] is determined at an ambient temperature of -29 [°C] and a sphere surface temperature of 23 [°C]. The substance properties of dry air at 1 [bar] are used. Table 24 shows the summarized values of the heat transfer coefficient determined from the Nusselt-number, from the measured surface and ambient temperature and from the curve fit to the measured temperature profile of the sphere. D_{Sphere} is the outer diameter of the steel sphere.

Components	**D_{Sphere} [m]**	**α [W/m²·K]**		
		VDI Wärme Atlas	**Surface Thermocouples**	**Curve Fit**
Heat-conducting paste	0.150	5.602	5.733	4.911
10 [wt%] phase-change material & 90 [wt%] heat-conducting paste	0.150	5.602	6.249	5.530
55 [wt%] phase-change material & 45 [wt%] oil	0.200	5.141	5.941	5.071
44 [wt%] phase-change material & 36 [wt%] oil & 20 [wt%] aluminium powder	0.200	5.141	6.440	5.200

Table 24 Summary of the values of α determined in three ways.

The values of the heat transfer coefficient are similar. The largest difference of the results of the sphere with a diameter of 0.15 [m] amounts 1.338 [W/m²·K], in the comparison of the values from the curve fit to the other calculation methods. The largest difference of the heat transfer coefficient of the sphere with a diameter of 0.2 [m] is 1.369 [W/m²·K].

The Biot number determined with the largest value of α of 6.249 [W/m²·K], a λ_{Sphere} of 50 [W/m·K] and a thickness of 0.003 [m] amounts $3.486 * 10^{-4}$. Thus the temperature gradient in the steel sphere is negligible compared to the temperature difference between surface and ambient temperature.

4.5 Measurement Uncertainties

Mistakes or inaccuracies during the measurements result in deviations of the obtained values of the fitted parameters. The deviations in heat capacity, melting enthalpy and phase transition range are investigated exemplarily by using the curve resulted from the sphere filled with 10 [wt%] phase-change material and 90 [wt%] heat conducting paste cooled to -32 [°C]. The deviations of the values for the thermal conductivity are examined with the curve resulted from the same sphere heated inside with 3.5 and 4.5 Watt.

First, the maximal measurement errors of the density, the thermocouples, the distance of the measurement point, the heating power and the volume of the sphere are determined. Then the impact on the calibrated parameters is determined. Furthermore, the influence of the deviation of the heat transfer coefficient is examined.

4.5.1 Density Measurements

The density is determined by five measured parameters, four masses and one density, according to equation 41. For the mass measurement, a balance of the company Sartorius is used. A maximal error of the mass of ± 0.025 [g] is the result of a readability of 0.010 [g], a standard deviation of ±0.010 and a maximal linearity of ± 0.010 [g]. The deviation of the density of water is assumed between 17 and 19 [°C] and amounts ± 0.370 [kg/m^3].

The total deviation of the parameters is determined using the following formula [22]:

$$\Delta\rho_{mix} = \left|\frac{\partial\rho_{mix}}{\partial m_0} * \Delta m_0\right| + \left|\frac{\partial\rho_{mix}}{\partial m_1} * \Delta m_1\right| + \left|\frac{\partial\rho_{mix}}{\partial m_2} * \Delta m_2\right| + \left|\frac{\partial\rho_{mix}}{\partial m_3} * \Delta m_3\right| + \left|\frac{\partial\rho_{mix}}{\partial\rho_{aq}} * \Delta\rho_{aq}\right| \quad \text{(Eq. 44)}$$

The formula is solved numerically, whereby an additional measurement error of ± 0.018 [g] is added to m_3. m_3 is the weight of the beaker and the mixture filled up with water till the marking. The additional error results under the assumption of the development of air bubbles with a diameter of 1.5 [mm]. A maximal error of the density of ± 23.054 [kg/m^3] results. The table below shows the maximal determined error of the density and its impact on the parameters.

Varied value	Impact on parameters		
		Add	**Subtract**
ϑ ± 23.054	$c_{,s}$ [J/kg·K]	- 16 (1.35%)	+ 16 (1.35 %)
	$c_{,l}$ [J/kg·K]	- 12 (1.41%)	+ 12 (1.41 %)
	$\lambda_{,s}$ [W/m·K]	- 0.0023 (0.32%)	+ 0.0023 (0.32 %)
	$\lambda_{,l}$ [W/m·K]	+ 0.0005 (0.07%)	- 0.0005 (0.07%)
	Δh [J/kg]	- 167 (1.35%)	+ 172 (1.39%)
	$T_{I,II}$ [°C]	0	0

Table 25 Impact of the density on the parameters *c*, *λ*, h_{melt} and phase change temperature

The density indicates a high influence in terms of the melting enthalpy. A lower density results in a higher value of specific heat capacity. The impact on the thermal conductivity and on the transition temperature is low.

4.5.2 Temperature in the Sphere and Ambient Temperature

For the maximal error of the measured temperature the measurements uncertainty of the thermometer and the maximal temperature difference of the thermocouples during calibration are added. The measurements uncertainty of the thermometer amounts 0.03 [K] and the maximal temperature difference of the thermocouples amounts 0.08 [K]. This results in a maximal error of 0.11 [K].

First the ambient temperature was changed, which is shown in the table below.

Varied value	Impact on parameters		
		Add	**Subtract**
$T_u \pm 0.11$ [K]	$c_{,s}$ [J/kg·K]	- 50 (4.23%)	+ 45 (3.80%)
	$c_{,l}$ [J/kg·K]	- 11 (1.30%)	- 3 (0.35%)
	$\lambda_{,s}$ [W/m·K]	+ 0.0164 (2.27%)	- 0.0162 (2.24%)
	$\lambda_{,l}$ [W/m·K]	+ 0.0013 (0.18%)	- 0.0011 (0.15%)
	Δh [J/kg]	+ 232 (1.88%)	- 49 (0.40%)
	$T_{I,II}$ [°C]	+ 0.09 (0.51%) / - 0.05 (0.40%)	- 0.06 (0.34%) / - 0.006 (0.05%)

Table 26 Impact of the ambient temperature on the parameters c, λ, h_{melt} and phase change temperature

The ambient temperature shows a strong influence especially on the melting enthalpy and on the specific heat capacity. The thermal conductivity of the solid phase is also affected vastly by the ambient temperature. Increasing and decreasing of the ambient temperature has not the same amount of impact on the parameters. The melting enthalpy is more affected by an increase of the ambient temperature.

In order to determine the influence of the measured temperature inside the sphere, four cases are examined. All four temperatures are increased and decreased by the maximum error, indicated as case I and case II. In case III the second and fourth temperature are decreased and the third and fifth are increased. In the last case it is reversed. Table 27 shows the impact of the measured temperatures inside the sphere on the parameters.

Varied value		Impact on parameters
Case I		
		Add
T_{Sphere} ± 0.11 [K]	$c_{,s}$ [J/kg·K]	+ 45 (3.80%)
	$c_{,l}$ [J/kg·K]	+ 4 (0.47%)
	$\lambda_{,s}$ [W/m·K]	- 0.018 (2.49%)
	$\lambda_{,l}$ [W/m·K]	- 0.0008 (0.11%)
	Δh [J/kg]	- 114 (0.92%)
	$T_{I,II}$ [°C]	- 0.17 (0.96%) / - 0.095 (0.75%)
Case II		
		Subtract
T_{Sphere} ± 0.11 [K]	$c_{,s}$ [J/kg·K]	- 50 (4.23%)
	$c_{,l}$ [J/kg·K]	- 4 (0.47%)
	$\lambda_{,s}$ [W/m·K]	+0.018 (2.49%)
	$\lambda_{,l}$ [W/m·K]	+ 0.0008 (0.11%)
	Δh [J/kg]	+ 158 (1.28%)
	$T_{I,II}$ [°C]	+ 0.19 (1.07%) / + 0.089 (0.71%)
Case III		
		Add (3 & 5) / Subtract (2 & 4)
T_{Sphere} ± 0.11 [K]	$c_{,s}$ [J/kg·K]	- 20 (1.69%)
	$c_{,l}$ [J/kg·K]	- 3 (0.35%)
	$\lambda_{,s}$ [W/m·K]	- 0.0002 (0.03%)
	$\lambda_{,l}$ [W/m·K]	+ 0.006 (0.82%)
	Δh [J/kg]	+ 118 (0.95%)
	$T_{I,II}$ [°C]	- 0.14 (0.79%) / - 0.075 (0.59%)
Case IV		
		Add (2 & 4) / Subtract (3& 5)
T_u ± 0.11 [K]	$c_{,s}$ [J/kg·K]	+ 14 (1.18%)
	$c_{,l}$ [J/kg·K]	+ 1 (0.12%)
	$\lambda_{,s}$ [W/m·K]	- 0.002 (0.28%)
	$\lambda_{,l}$ [W/m·K]	- 0.005 (0.68%)
	Δh [J/kg]	- 108 (0.87%)
	$T_{I,II}$ [°C]	- 0.027 (0.15%) / - 0.13 (1.03%)

Table 27 Impact of the temperature inside the sphere on the parameters c, λ, h_{melt} and phase change temperature

In contrast to the ambient temperature, the temperature inside the sphere shows a similar amount of impact on the parameters regarding increasing and decreasing. An increasing of the temperature of all thermocouples results in an increased specific heat capacity and a decreased melting enthalpy. It also has a considerable impact on the thermal conductivity of the solid phase. However, there is no great change of λ and c of the liquid phase concerning this experiment. Case III and IV show lower impact on the parameters than the other two cases with the exception of the melting enthalpy.

4.5.3 Distance of the Measurement Points

The error of the distance of the thermocouples is assumed with 2 [mm]. This assumption arose from the distance measurement before and after the experiment. The width of the measuring tip amounts 0.065 [mm]. This results in a maximum error of ± 2.065 [mm]. In order to determine the influence of the position of the thermocouples four cases are examined. All four thermocouples distances are increased and decreased by the maximum error, indicated as case I and case II. In case III the second and fourth thermocouple distances is decreased and the third and fifth on is increased. In the last case it is reversed. Table below shows its impact on the parameters.

Varied value	**Impact on parameters**	
Case I		
		Add
Distance ± 2.065*10^{-3} [m]	$c_{,s}$ [J/kg·K]	+ 0.3 (0.03%)
	$c_{,l}$ [J/kg·K]	+ 9 (1.06%)
	$\lambda_{,s}$ [W/m·K]	- 0.093 (12.88%)
	$\lambda_{,l}$ [W/m·K]	- 0.094 (12.82%)
	Δh [J/kg]	+ 85 (0.69%)
	$T_{I,II}$ [°C]	- 0.043 (0.24%) / - 0.06 (0.48%)
Case II		
		Subtract
Distance ± 2.065*10^{-3} [m]	$c_{,s}$ [J/kg·K]	- 0.6 (0.05%)
	$c_{,l}$ [J/kg·K]	- 11 (1.29%)
	$\lambda_{,s}$ [W/m·K]	+ 0.105 (14.54%)
	$\lambda_{,l}$ [W/m·K]	+ 0.121 (16.51%)
	Δh [J/kg]	- 39 (0.32%)
	$T_{I,II}$ [°C]	+ 0.08 (0.45%) / + 0.01 (0.79%)
Case III		
		Add (3 & 5) / Subtract (2 & 4)
Distance ± 2.065*10^{-3} [m]	$c_{,s}$ [J/kg·K]	+ 3 (0.25%)
	$c_{,l}$ [J/kg·K]	- 4 (0.47%)
	$\lambda_{,s}$ [W/m·K]	+ 0.090 (12.47%)
	$\lambda_{,l}$ [W/m·K]	+ 0.125 (17.05%)
	Δh [J/kg]	+ 25 (0.20%)
	$T_{I,II}$ [°C]	+ 0.04 (0.22%) / - 0.08 (0.63%)
Case IV		
		Add (2 & 4) / Subtract (3& 5)
Distance ± 2.065*10^{-3} [m]	$c_{,s}$ [J/kg·K]	+ 0.4 (0.03%)
	$c_{,l}$ [J/kg·K]	+ 7 (0.82%)
	$\lambda_{,s}$ [W/m·K]	- 0.059 (8.17%)
	$\lambda_{,l}$ [W/m·K]	- 0.104 (14.19%)
	Δh [J/kg]	- 136 (1.10%)
	$T_{I,II}$ [°C]	- 0.056 (0.31) / - 0.048 (0.28%)

Table 28 Impact of the distance of the thermocouple on the parameters c, λ, h_{melt} and phase change temperature

The distance of the thermocouples shows an appreciable effect on the thermal conductivity of both phases. The values of the thermal conductivity and the phase change temperatures increase if the thermocouples are closer to the small sphere inside, as case II shows. The other parameters decrease. In case I the impacts are reversed.

4.5.4 Heating Power

The uncertainty of the introduced heating power is determined with ± (0.1 % of reading + 0.2 % range) of voltage and current. The measurement range amounts 15 [V] and 1 [A]. Table 29 shows the influence of the deviations of the heating power on the parameters. The values indicated for the heating power are mean values because of the reading fluctuation.

Varied value	Impact on parameters		
		Add	**Subtract**
P_{el} ± (0.1 % of reading + 0.2 % range) of voltage and current 3.537 ± 0.036 4.471 ± 0.042	$c_{,s}$ [J/kg·K]	---	---
	$c_{,l}$ [J/kg·K]	---	---
	$\lambda_{,s}$ [W/m·K]	+ 0.022 (3.05%)	- 0.022 (3.05%)
	$\lambda_{,l}$ [W/m·K]	+ 0.008 (1.09%)	+ 0.008 (1.09%)
	Δh [J/kg]	---	---
	$T_{I,II}$ [°C]	---	---

Table 29 Impact of the heating power on the parameters *c, λ, h_{melt}* and phase change temperature

A higher heating power leads to higher values of the thermal conductivity and a lower one results in a lower value.

4.5.5 Diameter of the Sphere

The outer diameter of the sphere is measured at several points. A maximum error of ± 0.15 [mm] is detected.

Varied value	Impact on parameters		
		Add	**Subtract**
$D_{sphere} \pm 0.15*10^{-3}$ [m]	$c_{,s}$ [J/kg·K]	- 1.4 (0.12%)	+ 1.4 (0.12%)
	$c_{,l}$ [J/kg·K]	-1.2 (0.14%)	+ 1.2 (0.14%)
	$\lambda_{,s}$ [W/m·K]	- 0.0024 (0.33%)	+ 0.0024 (0.33%)
	$\lambda_{,l}$ [W/m·K]	- 0.00006 (0.01%)	+ 0.00004 (0.01%)
	Δh [J/kg]	- 17.8 (0.14%)	+ 17.8 (0.14%)
	$T_{I,II}$ [°C]	+ 0.001 (0.01%) / + 0.0009 (0.01%)	- 0.002 (0.01%) / - 0.0005 (0.00%)

Table 30 Impact of the volume of the outer sphere on the parameters *c, λ, h_{melt}* and phase change temperature

A larger volume results in a decrease of all parameters with the exception of the phase change temperature range. A smaller volume shows the opposite case.

4.5.6 Heat Transfer Coefficient

In order to investigate the influence of the deviation of the heat transfer coefficient, the largest difference in comparison of the values from the curve fit to the other calculation methods is used. Considering the experiment performed with 10 [wt%] phase-change material and 90 [wt%] heat conducting paste, the difference amounts ± 0.719 [W/m^2·K]

Varied value	Impact on parameters		
		Add	**Subtract**
α ± 0.719 [W/m^2·K]	$c_{,s}$ [J/kg·K]	+ 188 (15.89%)	- 169 (14.29%)
	$c_{,l}$ [J/kg·K]	+ 124 (14.59%)	- 119 (14.00%)
	$\lambda_{,s}$ [W/m·K]	-0.137 (18.98%)	+ 0.153 (21.19%)
	$\lambda_{,l}$ [W/m·K]	- 0.009 (1.23%)	+ 0.047 (6.41%)
	Δh [J/kg]	+ 1337 (10.81%)	- 1403 (11.35%)
	$T_{I,II}$ [°C]	+ 0.14 (0.79%) / - 0.09 (0.71%)	- 0.17 (0.96%) / + 0.03 (0.24%)

Table 31 Impact of the heat transfer coefficient on the parameters c, λ, h_{melt} and phase change temperature

The change of the value of the heat transfer coefficient shows its large influence on the parameters. A higher value of α results in an increase of the specific heat capacity, of the melting enthalpy and of the phase change temperature range. Furthermore, the values of λ decrease. A smaller value of α shows the opposite case. However, the absolute values are not the same.

4.6 Optimization of the Measurement Procedure

Due to the gained knowledge of the dependence of the results on boundary conditions, several processes should be improved. Furthermore, the occurrence of convection inside the sphere must be avoided.

A pycnometer might be used instead of a simple beaker to enhance the precision of the density measurement.

After the first measurement performed with pure heat conducting paste, the construction of the temperature sensors were improved. They were fixed with hard plastic and the positions before and after measurement show a difference little less than 2 [mm]. However, this uncertainty should be always included in the measurement evaluation.

To compare the heat transfer coefficient determined from the measured surface and ambient temperature with α determined from the curve fit to the measured temperature profile of the sphere the surface thermocouples should be positioned always at the same place. Furthermore, they should be equally distributed on the surface of the sphere. The number of the surface thermocouples should not be increased, because of its influences on the α and surface conditions.

Due to the influence of the ambient temperature on the values of the parameters, more than one thermocouple should be used to measure it.

Moreover, to create a better statement about the correctness of the results the measurements of the mixture should be repeated with differently sized spheres. It is important to use the same mixture to exclude mixing error and inhomogeneity. In addition, smaller spheres should be used to avoid non isothermal condition inside the layers.

4.7 Effects on Refrigeration Circuit

The obtained data from the measurements are finally incorporated into an existing refrigeration circuit simulation. It is a transient one-dimensional circuit simulation programmed in VBA. The simulation program was validated with a freezer assigned to the efficiency class A+++ and with an energy consumption of 127 [kWh/year].

In addition to the measured mixtures with phase-change material, four hypothetical compounds are integrated. All hypothetical cases consist of pure phase-change material with various thermal conductivities of 0.2, 0.5, 1.0 and 1.5 [W/m·K]. The density amounts 770 [kg/m^3] and the specific heat capacity is 1800 [J/kg·K]. The melting enthalpy amounts 150010 [J/kg]. The phase change temperature range is set between -19 and -17 [°C].

Figure 59 shows the calculated, averaged energy consumption over a period of 24 hours of the freezer.

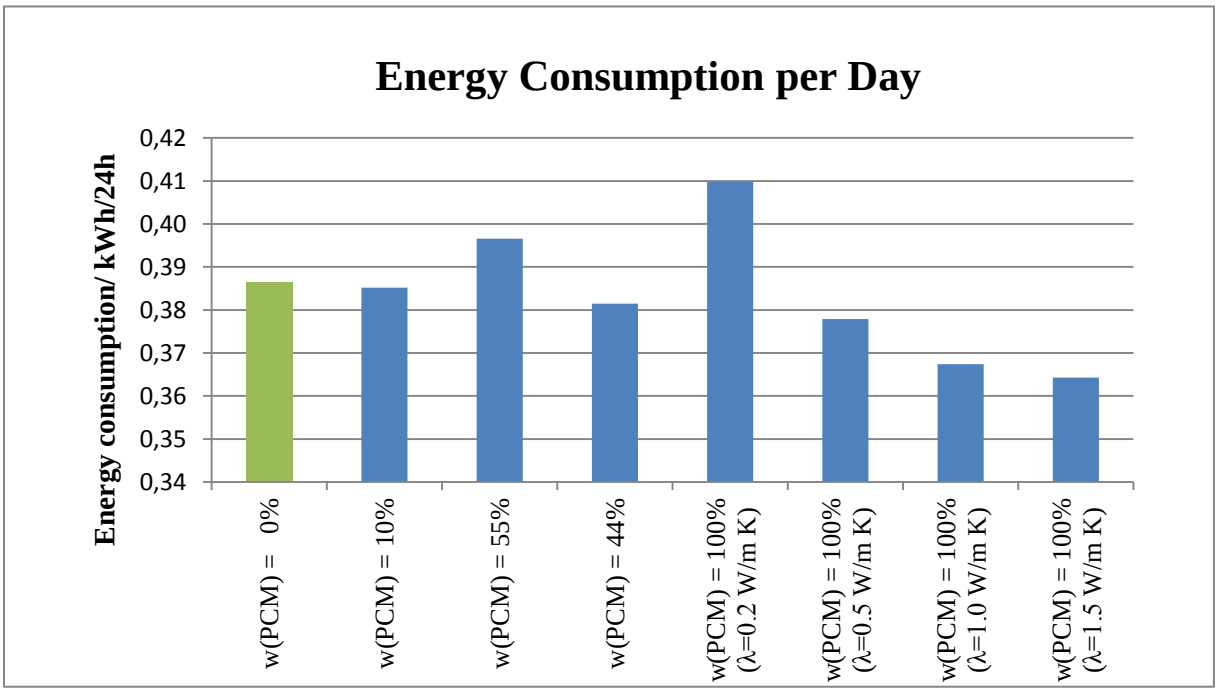

Figure 59 Energy consumption per day calculated with an available refrigeration circuit simulation

The pure heat conducting paste serves as reference to identify the effect of the phase-change material on the averaged energy consumption of the freezer. The blend containing 10 [wt%] phase-change material and 90 [wt%] heat conducting paste shows an improvement of 0.34 [%] in terms of energy consumption per day.

An appropriate statement about the effect of the blends containing oil is not possible. The mixture with 55 [wt%] phase-change material shows a deterioration in terms of energy consumption. However, the mixture with 44 [wt%] phase-change material and 20 [wt%] aluminium powder shows an enhancement. This may be due to the higher averaged thermal conductivity or to the higher melting enthalpy of the mixture containing 44 [wt%]. As already mentioned, the stored energy per mass of the mixture increases with an increasing amount of phase-change material. In this case the amount of phase-change material is smaller, therefore the melting enthalpy should be smaller.

Considering the hypothetical substances consisting of pure phase-change materials with various thermal conductivities, it can be seen that the thermal conductivity influences the energy consumption strongly. The phase-change material with a thermal conductivity of 0.2 [W/m·K] shows a deterioration of 6.03 [%] in comparison with the reference. However, an enhancement of 0.3 [W/m·K] results in an improvement of 2.22 [%]. The simulations with a pure phase-change material having a thermal conductivity of 1.0 and 1.5 [W/m·K] result in an improvement of 4.93 and 5.74 [%]. The melting enthalpy is equal for all compounds and amounts 150010 [J/kg].

The duration of the on– and off-cycles is also determined by the simulation program and is shown in Figure 60.

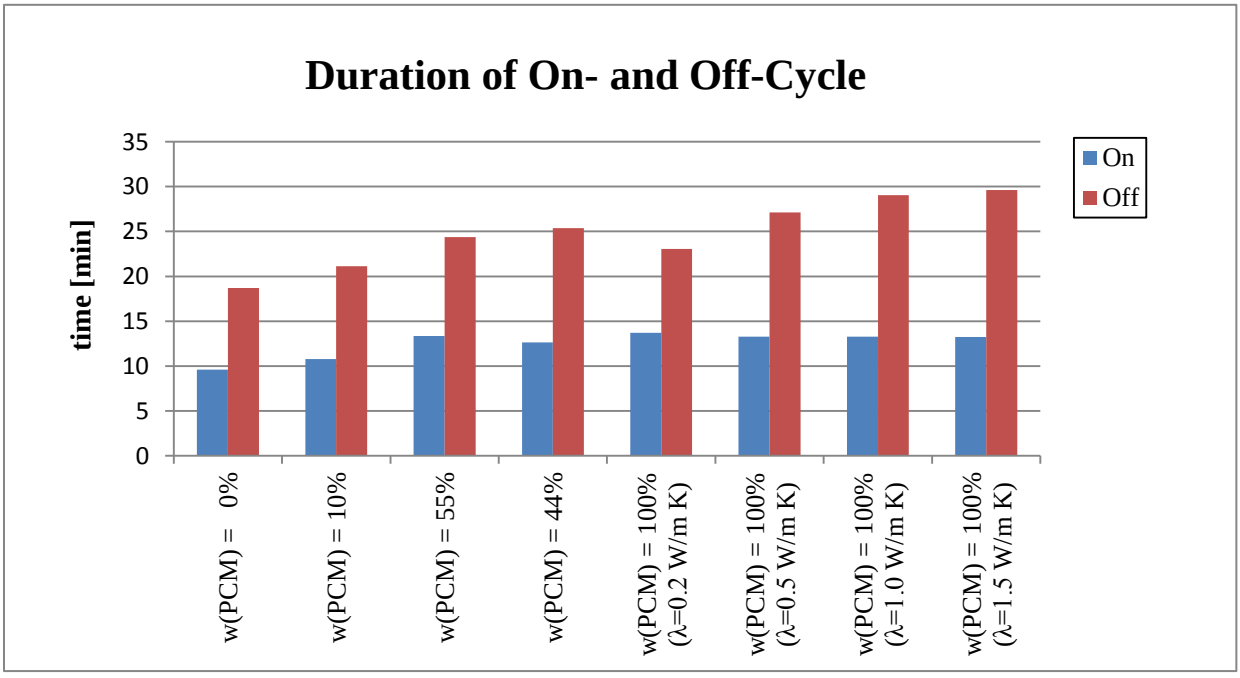

Figure 60 Duration of on- and off-cycles calculated with an available refrigeration circuit simulation

The mixture containing 10 [wt%] phase-change material and 90 [wt%] heat conducting paste shows an increase of both modes. However, the on-cycle takes 1.18 [min] and the off-cycle 2.43 [min] longer than the modes of the reference.

A properly evaluation of the results of the simulation performed with oil is here too, not possible.

All simulations performed with pure phase-change material show an increase of both modes. However, the on-modes take equally long for all four cases and amounts on average 13.37 [min]. That is an increase of 3.78 minutes compared to the reference. The off-modes increase with an enhancement of the thermal conductivity. In comparison with the reference, the simulations with a pure phase-change material having a thermal conductivity of 0.2, 0.5 1.0 and 1.5 [W/m·K] result in an extension of the duration of the off-mode of 4.35, 8.43, 10.33 and 10.90 minutes.

5 Conclusion

Thermal energy storage is a significant option to save energy in various applications. The phase-change material, which was examined in the course of this work, stores energy in the form of latent heat. The paraffin blend might be used to enhance the energy efficiency of refrigerating systems, whereby it is located on the evaporator.

The knowledge of several parameters of the material is essential to investigate its impact on the energy efficiency of refrigerating systems. The study of these parameters was the task of this work.

The phase-change material was mixed on the one hand with heat conducting paste and on the other hand with engine oil. It was investigated on thermal conductivity and specific heat capacity. Furthermore, the energy stored per mass and the phase-change temperature ranges were determined. The measuring construction comprises a hollow steel sphere and a smaller one in the middle serving as a heat source. At certain distances, thermocouples are attached to measure the temperature profile. In order to determine the necessary parameters, a model in MATLAB was created, whereby transient one-dimensional heat conduction is considered.

Four experiments were conducted. The first one was performed with pure heat conducting paste. Then an amount of 10 [wt%] phase change material was added. The third experiment was performed with 55 [wt%] phase change material and 45 [wt%] oil. After that 20 [wt%] of aluminium powder was added to enhance heat conduction.

During and after the measurement performed with oil as mixing components, leakage and separation of the ingredients could be observed. It is assumed, that a part of heat transfer occurs through free convection which is not describable by the calculation model. This is shown in the resulting diagrams. The simulated curves don´t fit to the measured temperature profile well.

This phenomenon is not observed during the measurements performed with heat conducting paste. The calculation model fits the curves precisely to the measured temperature profiles. The resulted values of the parameters show the expected trend and can be partly well matched with data from the literature. However, to create a better statement about the correctness of the results, the measurements should be repeated with different sizes of spheres. In addition, the evaluation of the results shows, that they are strongly influenced by boundary conditions. For this reason the measurement uncertainties in term of maximum error and their influences were specified. Furthermore, some processes during the measurements should be improved like the density measurement, which might be improved by using a pycnometer instead of a simple beaker. Due to the influence of the ambient temperature on the results it might be used more than one thermocouple to measure it.

Finally, the resulted values of thermal conductivity, specific heat capacity and melting enthalpy are feeded into a refrigeration circuit simulation. It is shown that the thermal conductivity has a major influence on the average energy consumption and on the duration of the on- and off-modes of a refrigerating appliance.

6 References

[1] Pielichowska, K.; Pielichowski, K. (2014): Phase change materials for thermal energy storage, *Progress in Materials Science* 65, 67-123

[2] Sharma, A., Tyagi, V., Chen C., Buddhi, D. (2009): Review on thermal energy storage with phase change materials and applications, *Renewable and Sustainable Energy Reviews 13*, 318–345

[3] Mondal, S. (2008): Phase change materials for smart textiles – An overview, *Applied Thermal Engineering 28*, 1536–1550

[4] Mehling, H.; Cabeza, L.F. (2008): Heat and cold storage with PCM, An up to date introduction into basics and applications, Springer-Verlag, Berlin, Germany

[5] Castell, A., Solé, C. (2015): An overview on design methodologies for liquid–solid PCM storage systems, *Renewable and Sustainable Energy Reviews 52,* 289–307

[6] Farid M., Khudhair A., Razack S., Al-Hallaj S. (2004): A review on phase change energy storage: materials and applications, *Energy Conversion and Management 45,* 1597–1615

[7] Oró, E.; Gracia, A.; Castell, A.; Farid, M.M.; Cabeza, L.F. (2012): Review on phase change materials (PCMs) for cold thermal energy storage applications, *Applied Energy 99,* 513–533

[8] http://www.microteklabs.com/technical-overview.html, 21. January 2016, 12:50

[9] Sonnenrein, G.; Elsner, A.; Fieback, K.; Lessmann, K.; Morbach, A.; Vrabec, J (2015): Effizienzsteigerung von Haushaltskühlgeräten durch polymergebundene Phasenwechselmaterialien, DKV-Tagung, Dresden, Germany

[10] Eichlseder, H. (2010): Thermodynamik (Vorlesungsskript), Graz, Technische Universität, Institut für Verbrennungskraftmaschinen und Thermodynamik

[11] Cheng, W.; Yuan, X. (2013): Numerical analysis of a novel household refrigerator with shape-stabilized PCM (phase change material) heat storage condensers, *Energy 59,* 265-276

[12] Azzouz, K.; Leducq, D.; Gobin, D. (2008): Performance enhancement of a household refrigerator by addition of latent heat storage, *International Journal of Refrigeration 31,* 892-901

[13] Brenn, G.; Meile, W. (2005): Strömungslehre und Wärmeübertragung I (Vorlesungsskript), Graz, Technische Universität, Institut für Strömungslehre und Wärmeübertragung

[14] Böckh, P.; Wetzel, T. (2011): Wärmeübertragung, Grundlagen und Praxis, 4. Auflage, Springer-Verlag, Berlin, Germany

[15] Verein Deutscher Ingenieure, VDI-Wärmeatlas, 11. Auflage, Springer-Verlag, Berlin, Germany

[16] Höhne, G.W.H.; Hemminger, W.F.; Flammersheim, H.-J. (2003): Differential Scanning Calorimetry, Second Edition, Springer-Verlag, Berlin, Germany

[17] http://www.hitachi-hightech.com/file/global/pdf/products/science/appli/ana/thermal/application_TA_064e.pdf, 01st June 2016, 12:55

[18] Schaber, S.; Mayinger, S.: Thermodynamik, Band 1: Einstoffsysteme, 18. Auflage, Springer-Verlag, Berlin, Germany

[19] Wittenberger, W. (2005): Rechnen in der Chemie, Grundoperationen, Stöchiometrie, 15. Auflage, Springer-Verlag, Vienna, Austria

[20] Freund, M.; Csikos. R.; Keszthelyi, S.; Mozes. GY. (1982): Paraffin Products: Properties, Technologies, Applications, Elsevier Science

[21] KULI Energy Management Simulation Software, Version 8.0-1.02

[22] http://public.rz.fh-wolfenbuettel.de/~harrieha/vl/mathe/2/arbeitsblaetter/fehlerfortv3.pdf, 31. March 2016, 13:58

7 Appendix

7.1 List of Equipment

Equipment	Company	Type
Cooling thermostat	Lauda	RE 1225 G
Thermometer	WIKA Alexander Wiegand SE & Co. KG	CTH 6500
Analog output	National Instruments	NI 9263
Analog input	National Instruments	NI 9205
Terminal block	National Instruments	NI 9214
Ethernet-chassis	National Instruments	NI cDAQ-9188
Electronic precision balances	Sartorius	E 2000 D
Differential scanning calorimeter	Netzsch	DSC 204 F1 Phoenix
Power supply	Xantrex	HPD 60-5
Digital power meter	Yokogawa	WT330

Table 32 List of equipment

7.2 Differential Scanning Calorimetry Heat Capacity Measurement Results

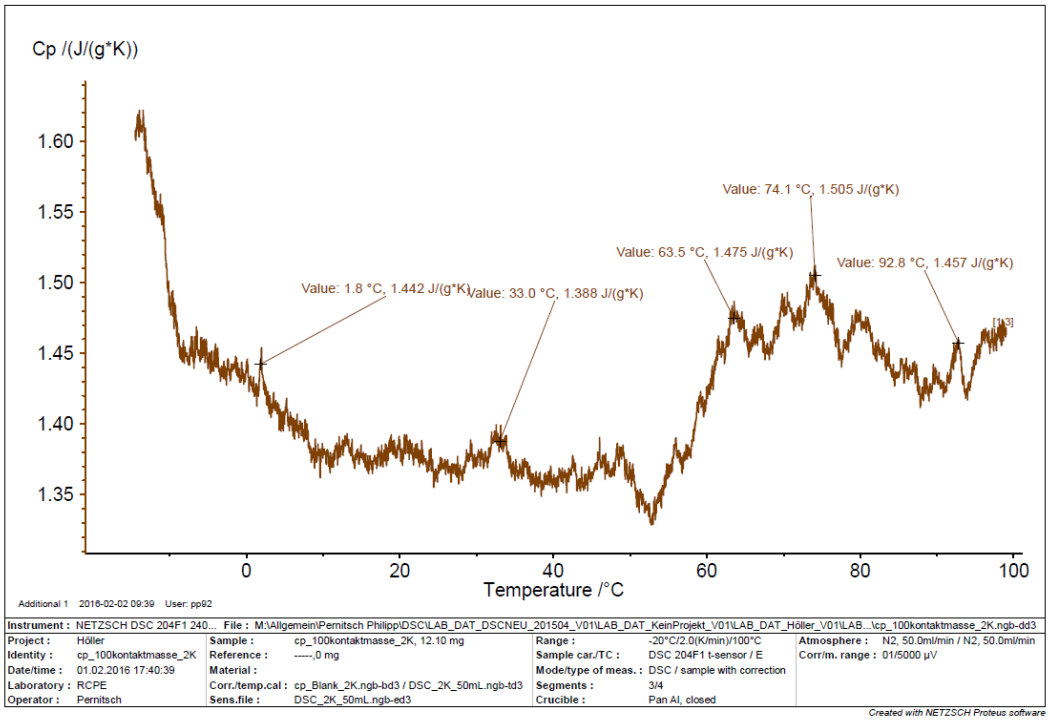

Figure 61 Specific heat capacity of pure heat conducting paste performed with DSC

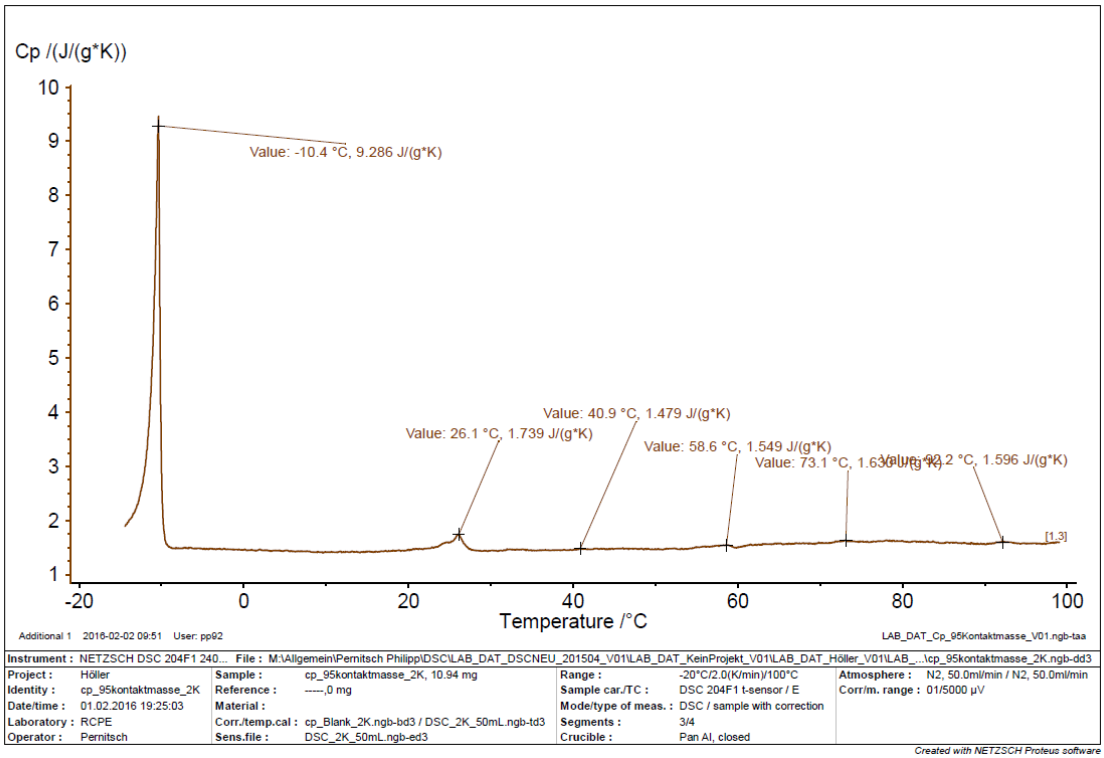

Figure 62 Specific heat capacity of a mixture of 5 [wt%] phase change material and 95 [wt%] heat conducting paste performed with DSC

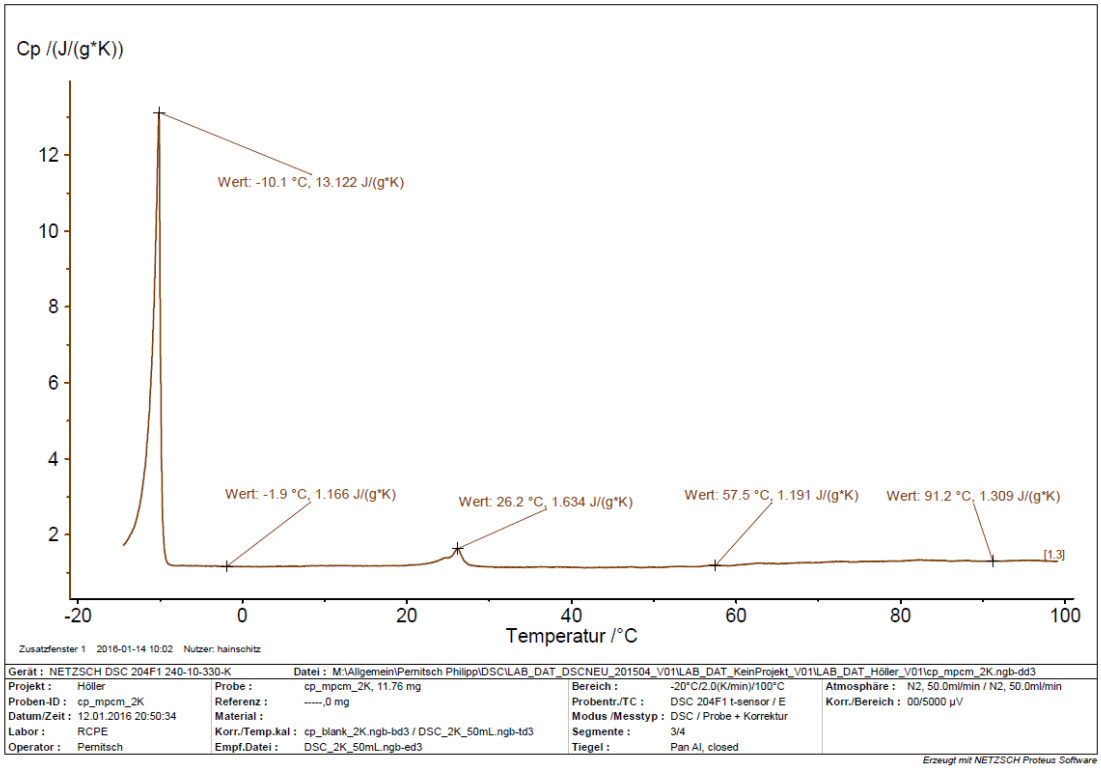

Figure 63 Specific heat capacity of a mixture of 10 [wt%] phase change material and 90 [wt%] heat conducting paste performed with DSC

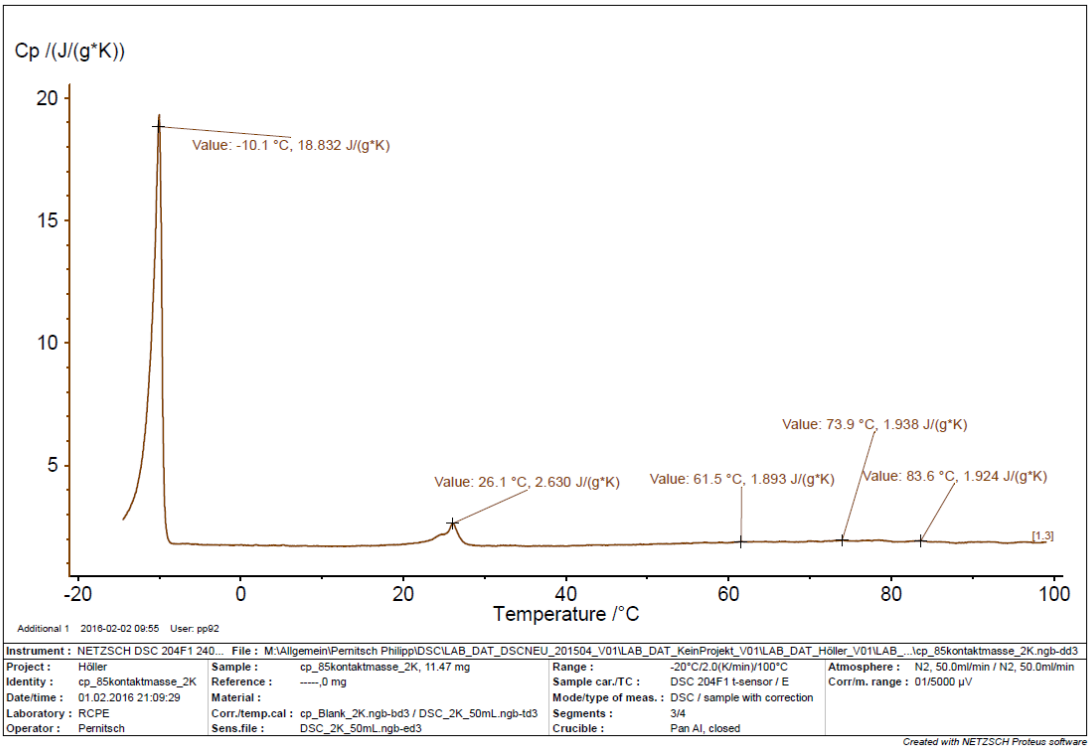

Figure 64 Specific heat capacity of a mixture of 15 [wt%] phase change material and 85 [wt%] heat conducting paste performed with DSC

7.3 List of Figures

Figure 1 T,s-digram of a simplified refrigerant cycle. T_u = ambient temperature, T_K = temperature of cold store; Unterkühlung = subcooling, überhitztes Verfahren = superheated process 6

Figure 2 Sketch of the spherical model 8

Figure 3 Sketch of the spherical model including $\boldsymbol{Q}_{\text{right}}$ and $\boldsymbol{Q}_{\text{left}}$ 9

Figure 4 Relationship between thermal conductivity & specific heat capacity and temperature during a melting process [6]. Right: simplification in the model 12

Figure 5 Heat-exchanging calorimeter. 1 disk-support, 2 oven, 3 cover, 4 thermocouples, 5 temperature controller and programming device 15

Figure 6 Simple model of the DSC to describe its functional principle 16

Figure 7 Transient temperatures at six positions cooled down from 25 [°C] to -30 [°C] 20

Figure 8 Temperature profile over the averaged radii of all six layers cooled down from 25 [°C] to -30 [°C] 21

Figure 9 Transient temperatures at third position cooled down from 25 [°C] to -30 [°C] with varied specific heat capacity of the solid phase 22

Figure 10 Zoom of the transient temperatures at third position cooled down from 25 [°C] to -30 [°C] with varied specific heat capacity for the solid phase 23

Figure 11 Transient temperatures at third position cooled down from 25 [°C] to -30 [°C] with varied specific heat capacity for the liquid phase 24

Figure 12 Transient temperatures at third position cooled down from 25 [°C] to -30 [°C] with varied thermal conductivity for the solid phase 25

Figure 13 Magnification of the transient temperatures at third position cooled down from 25 [°C] to -30 [°C] with varied thermal conductivity for the solid phase 25

Figure 14 Transient temperatures at third position cooled down from 25 [°C] to -30 [°C] with varied thermal conductivity for the liquid phase 26

Figure 15 Transient temperatures at third position cooled down from 25 [°C] to -30 [°C] with varied specific melting enthalpy 27

Figure 16 Transient temperatures at six positions cooled down from 25 [°C] to -30 [°C] with a specific melting enthalpy of 20000 [J/kg] 28

Figure 17 Transient temperatures at third position cooled down from 25 [°C] to -30 [°C] with varied heat transfer coefficient 29

Figure 18 Transient temperatures at third position cooled down from 25 [°C] to -30 [°C] with varied density 30

Figure 19 Transient temperatures at third position cooled down from 25 [°C] to -30 [°C] with varied specific heat capacity of the steel sphere 31

Figure 20 Temperatures at twenty-seven positions heated with 6 Watt from the inside at an ambient temperature of -30 [°C] 32

Figure 21 Temperature profile over the averaged radii of all twenty-seven layers heated with 6 Watt from the inside at an ambient temperature of -30 [°C] 33

Figure 22 Temperatures at third, seventh and twentieth position heated with 6 Watt from the inside at an ambient temperature of -30 [°C] with varied specific heat capacity for the solid phase 34

Figure 23 Temperatures at third, seventh and twentieth position heated with 6 Watt from the inside at an ambient temperature of -30 [°C] with varied specific heat capacity for the liquid phase. 35

Figure 24 Temperatures at third, seventh and twentieth position heated with 6 Watt from the inside at an ambient temperature of -30 [°C] with varied thermal conductivity for the solid phase. 36

Figure 25 Temperatures at third, seventh and twentieth position heated with 2 Watt from the inside at an ambient temperature of -30 [°C] with varied thermal conductivity for the solid phase. 37

Figure 26 Temperatures at third, seventh and twentieth position heated with 6 Watt from the inside at an ambient temperature of -30 [°C] with varied thermal conductivity for the liquid phase. 38

Figure 27 Temperatures at twenty-seventh position (outer steel sphere) heated with 6 Watt from the inside at an ambient temperature of -30 [°C] with varied thermal conductivity for the liquid phase. 39

Figure 28 Temperatures at third, seventh and twentieth position heated with 6 Watt from the inside at an ambient temperature of -30 [°C] with varied specific melting enthalpy..... 40

Figure 29 Temperatures at third, seventh and twentieth position heated with 6 Watt from the inside at an ambient temperature of -30 [°C] with varied heat transfer coefficient. 41

Figure 30 Temperatures at twenty-seventh position (outer steel sphere) heated with 6 Watt from the inside at an ambient temperature of -30 [°C] with varied heat transfer coefficient. . 42

Figure 31 Temperatures at third, seventh and twentieth position heated with 6 Watt from the inside at an ambient temperature of -30 [°C] with density. 43

Figure 32 Temperatures at eleventh positions heated with varied heating power from the inside at an ambient temperature of -30 [°C] 45

Figure 33 Mass distribution of the content of the sphere divided into 20 layers 46

Figure 34 Temperatures at twenty-two positions heated with 9 Watt from the inside at an ambient temperature of -30 [°C] 46

Figure 35 Left: Complete setup of the calibration. Right: Thermocouples fixed at the tip of the reference thermometer..... 50

Figure 36 Measured temperatures of thirty-two thermocouples at 15 °C. 50

Figure 37 Measured temperatures of thirty-two thermocouples at 15°C automatic corrected by LabVIEW 51

Figure 38 Setup of the lower hemisphere for the determination of the thermal conductivity and specific heat capacity..... 53

Figure 39 Lower hemisphere filled with heat conducting paste 53

Figure 40 Filled sphere put into the refrigerator and the additional thermocouple to measure the ambient temperature 54

Figure 41 Lower hemisphere filled with a mixture of 55 [wt%] phase-change material and 45 [wt%] oil after the experiments 56

Figure 42 Temperature-modulated DSC traces at 2 [K/min] of a mixture with 10 wt% phase-change material and 90 wt% heat-conducting paste. 59

Figure 43 Temperature-modulated DSC traces at 2 [K/min] of mixtures with 0 [wt%], 5 [wt%] and 15 [wt%] phase-change material and 100 [wt%], 95 [wt%] and 85 [wt%] heat-conducting paste. 60

Figure 44 Relationship between the stored energy and the amount of phase-change material measured with DSC. 61

Figure 45 Measured and simulated curves of heat conducting paste cooled down to 32 [°C] without interior heat source 64

Figure 46 Measured and simulated curves of heat conducting paste cooled down to about 32 [°C] and heated with 4 Watt 65

Figure 47 Measured and simulated curves of heat conducting paste cooled down to about 32 [°C] and heated with 4 and 5 Watt 65

Figure 48 Measured and simulated curves of the mixture of 10 [wt%] phase-change material and [90%] heat conducting paste cooled down to - 32 [°C] without interior heat source 68

Figure 49 Measured and simulated curves of the mixture of 10 [wt%] phase-change material and [90%] heat conducting paste cooled down to -32 [°C] heated with 3.5 [W] 68

Figure 50 Measured and simulated curves of the mixture of 10 [wt%] phase-change material and 90[wt%] heat conducting paste cooled down to -32 [°C] heated with 3.5 and 4.5 [W] 69

Figure 51 Measured temperature profile of the mixture cooled down to - 32 [°C] without interior heat source over the thermocouples distances (side A) 69

Figure 52 Measured and simulated curves of the mixture of 55 [wt%] phase-change material and 45[wt%] oil cooled down to about -32 [°C] without interior heat source 73

Figure 53 Measured and simulated curves of the mixture of 55 [wt%] phase-change material and 45[wt%] oil cooled down to about -32 [°C] and heated with 2.5 [W] 74

Figure 54 Measured and simulated curves of the mixture of 55 [wt%] phase-change material and 45[wt%] oil cooled down to about -32 [°C] and heated with 2.5 and 4 [W] 74

Figure 55 Measured and simulated curves of the mixture of 44 [wt%] phase-change material, 36 [wt%] oil and 20 [wt%] aluminium powder cooled down to about -32 [°C] 77

Figure 56 Measured and simulated curves of the mixture of 44 [wt%] phase-change material, 36 [wt%] oil and 20 [wt%] aluminium powder cooled down to about -32 [°C] and heated with 8 [W] 78

Figure 57 Cooling (left) and warming (right) curves of the mixture with 44 [wt%] phase-change material, 36 [wt%] oil and 20 [wt%] aluminium powder of side A 81

Figure 58 Relationship between the stored energy and the amount of phase-change material measured with spherical model and differential scanning calorimeter 82

Figure 59 Energy consumption per day calculated with an available refrigeration circuit simulation 90

Figure 60 Duration of on- and off-cycles calculated with an available refrigeration circuit simulation 91

Figure 61 Specific heat capacity of pure heat conducting paste performed with DSC 96

Figure 62 Specific heat capacity of a mixture of 5 [wt%] phase change material and 95 [wt%] heat conducting paste performed with DSC 96

Figure 63 Specific heat capacity of a mixture of 10 [wt%] phase change material and 90 [wt%] heat conducting paste performed with DSC 97

Figure 64 Specific heat capacity of a mixture of 15 [wt%] phase change material and 85 [wt%] heat conducting paste performed with DSC 97

7.4 List of Tables

Table 1 Values of the parameters during the plausibility check of the sphere cooled down without interior heat source 19

Table 2 Values of the parameters during the plausibility check of the sphere heated from the inside at an ambient temperature of -30 [°C] 31

Table 3 Results of the heat transferred to the ambient with varied calculation time and heating power 44

Table 4 Results of the heat transferred to the ambient with varied heating power 44

Table 5 Overview of the performed experiments 57

Table 6 Values of the density of the mixtures 58

Table 7 Results of the α [W/m^2·K] determined from the measured data of the sphere filled with heat conducting paste, heated with 4 and 5 [W] 62

Table 8 Results of λ [W/m·K] determined from the measured data of the sphere filled with pure heat conducting paste, heated with 4 [W] 63

Table 9 List of the performed experiments with pure heat conducting paste and the corresponding, adjusted parameters. 63

Table 10 Resulting values of specific heat capacity, thermal conductivity and of heat transfer coefficient of heat conducting paste. 64

Table 11 Results of α [W/m^2·K] determined from the measured data of the sphere filled with a mixture of 10 [wt%] phase-change material and 90 [wt%] heat conducting paste l, heated with 3.5 and 4.5 [W] 66

Table 12 Results of λ [W/m·K] determined from the measured data of the sphere with a mixture of 10 [wt%] phase-change material and 90 [wt%] heat conducting paste, heated with 4.5 [W] 66

Table 13 List of the performed experiments with a mixture of 10 [wt%] phase-change material and 90 [wt%] heat conducting paste and the corresponding, adjusted parameters. ... 67

Table 14 Resulting values of specific heat capacity, thermal conductivity, heat transfer coefficient, melting enthalpy and phase transition range for the mixture of 10 [wt%] phase-change material and 90 [wt%] heat conducting paste. 67

Table 15 Results of α [W/m^2·K] determined from the measured data of the sphere filled with a mixture of 55 [wt%] phase-change material and 45 [wt%] oil, heated with 4, 6 and 8 [W].... 70

Table 16 Results of λ [W/m·K] determined from the measured data of the sphere filled with a mixture of 55 [wt%] phase-change material and 45 [wt%] oil, heated with 4 [W] 70

Table 17 List of the performed experiments with a mixture of 55 [wt%] phase-change material and 45 [wt%] oil and the corresponding, adjusted parameters. 71

Table 18 Resulting values of specific heat capacity, of thermal conductivity, of heat transfer coefficient, of melting enthalpy and of phase transition range of the mixture of 55 [wt%] phase-change material and 45 [wt%] oil. 73

Table 19 Results of the α [W/m^2·K] determined from the measured data of the sphere filled with a mixture of 44 [wt%] phase change material, 36 [wt%] oil and 20 [wt%] aluminium powder, heated with 1, 8 and 10 [W] 75

Table 20 Results of λ [W/m·K] determined from the measured data of the sphere filled with a mixture of 44 [wt%] phase change material, 36 [wt%] oil and 20 [wt%] aluminium powder, heated with 8 [W] 75

Table 21 List of the performed experiments with a mixture of 44 [wt%] phase change material, 36 [wt%] oil and 20 [wt%] aluminium powder and the corresponding, adjusted parameters. 76

Table 22 Values of specific heat capacity, of thermal conductivity, of heat transfer coefficient, of melting enthalpy and of phase transition range of the mixture of 44 [wt%] phase change material, 36 [wt%] oil and 20 [wt%] aluminium powder. 77

Table 23 Summary of all results of the performed experiments 79

Table 24 Summary of the values of α determined in three ways. 83

Table 25 Impact of the density on the parameters c, λ, h_{melt} and phase change temperature .. 84

Table 26 Impact of the ambient temperature on the parameters c, λ, h_{melt} and phase change temperature 85

Table 27 Impact of the temperature inside the sphere on the parameters c, λ, h_{melt} and phase change temperature 86

Table 28 Impact of the distance of the thermocouple on the parameters c, λ, h_{melt} and phase change temperature 87

Table 29 Impact of the heating power on the parameters c, λ, h_{melt} and phase change temperature 88

Table 30 Impact of the volume of the outer sphere on the parameters c, λ, h_{melt} and phase change temperature 88

Table 31 Impact of the heat transfer coefficient on the parameters c, λ, h_{melt} and phase change temperature 89

Table 32 List of equipment 95